University of California
Santa Barbara

Semiclassical methods for high frequency wave propagation in periodic media.

A dissertation submitted in partial satisfaction
of the requirements for the degree

Doctor of Philosophy
in
Mathematics

by

Ricardo A. Delgadillo

Committee in charge:

    Professor Xu Yang, Chair
    Professor Hector Ceniceros
    Professor Carlos Garcia Cervera

June 2016

The Dissertation of Ricardo A. Delgadillo is approved.

_____

Professor Hector Ceniceros

_____

Professor Carlos Garcia Cervera

_____

Professor Xu Yang, Committee Chair

May 2016

Semiclassical methods for high frequency wave propagation in periodic media.

Copyright © 2016

by

Ricardo A. Delgadillo

Acknowledgements

I would like to thank my adviser Xu Yang for all his helpful advise and efforts in teaching me about mathematics research. I am grateful to my collaborator Jianfeng Lu for our discussions and for his support.

Curriculum Vitæ
Ricardo A. Delgadillo

Education

2016	Ph.D. in Mathematics (Expected), University of California, Santa Barbara.
2012	M.A. in Mathematics, University of California, Santa Barbara.
2010	B.A. in Mathematics, University of California, San Diego.

Publications

(1) Frozen Gaussian approximation for high frequency wave propagation in periodic media (2015) with Jianfeng Lu (Duke) and Xu Yang(UCSB), available at arXiv:1504.08051 [math.NA]

(2) Gauge-invariant frozen Gaussian approximation method for the Schrödinger equation with periodic potentials with Jianfeng Lu (Duke) and Xu Yang (UCSB), accepted to SISC, and available at arXiv:1509.05552 [math.NA]

(3) Frozen Gaussian approximation-based artificial boundary conditions for one-dimensional nonlinear Schrödinger equation in the semiclassical regime with Jiwei Zhang and Xu Yang (UCSB) (Preprint)

Abstract

Semiclassical methods for high frequency wave propagation in periodic media.

by

Ricardo A. Delgadillo

We will study high-frequency wave propagation in periodic media. A typical example is given by the Schrödinger equation in the semiclassical regime with a highly oscillatory periodic potential and external smooth potential. This problem presents a numerical challenge when in the semiclassical regime. For example, conventional methods such as finite differences and spectral methods leads to high numerical cost, especially in higher dimensions. For this reason, asymptotic methods like the frozen Gaussian approximation (FGA) was developed to provide an efficient computational tool. Prior to the development of the FGA, the geometric optics and Gaussian beam methods provided an alternative asymptotic approach to solving the Schrödinger equation efficiently. Unlike the geometric optics and Gaussian beam methods, the FGA does not lose accuracy due to caustics or beam spreading.

In this thesis, we will briefly review the geometric optics, Gaussian beam, and FGA methods. The mathematical techniques used by these methods will aid us in formulating the Bloch-decomposition based FGA. The Bloch-decomposition FGA generalizes the FGA to wave propagation in periodic media. We will establish the convergence of the Bloch-decomposition based FGA to the true solution for Schrödinger equation and develop a gauge-invariant algorithm for the Bloch-decomposition based FGA. This algorithm will avoid the numerical difficulty of computing the gauge-dependent Berry phase. We will show the numerical performance of our algorithm by several one-dimensional examples.

Lastly, we will propose a time-splitting FGA-based artificial boundary conditions for solving the one-dimensional nonlinear Schrödinger equation (NLS) on an unbounded domain. The NLS will be split into two parts, the linear and nonlinear parts. For the linear part we will use the following absorbing boundary strategy: eliminate Gaussian functions whose centers are too distant to a fixed domain.

Contents

Chapter 1

Introduction

In this chapter we will introduce the semiclassical Schrödinger equation and some of its early asymptotic solutions. We also include a direct numerical method for solving the semiclassical Schrödinger equation, the Strang-splitting spectral method. The Strang-splitting spectral method will be used throughout our thesis to obtain the exact numerical solution to the semiclassical Schrödinger equation.

1.1   The semiclassical Schrödinger equation and its approximate solutions

We begin by introducing the Schrödinger equation in physical units,

$$i\hbar\frac{\partial\psi}{\partial t} = -\frac{\hbar^2}{2m}\Delta\psi + U_0(\boldsymbol{x})\psi, \tag{1.1}$$

where m is the atomic mass and $\hbar$ is the reduced Plank constant. $U_0(\boldsymbol{x})$ represents an external potential, for example, a quadratic function such as

$$U_0(\boldsymbol{x}) = \frac{m\omega_0^2}{2}|\boldsymbol{x}|^2, \qquad \omega_0 \in \mathbb{R}, \boldsymbol{x} \in \mathbb{R}^3. \tag{1.2}$$

Such potential is used to confine electrons about the origin.

We will nondimensionalize this equation by performing the substitutions,

$$\widetilde{t} = \omega_x t, \qquad \widetilde{\boldsymbol{x}} = \frac{\boldsymbol{x}}{x_s}, \qquad \widetilde{\psi}(\widetilde{\boldsymbol{x}}, \widetilde{t}) = x_s^{3/2} \psi(\boldsymbol{x}, t). \tag{1.3}$$

Inserting this into equation (1.1), multiplying by $1/(m\omega_0^2 x_s^{1/2})$, and dropping tildes we obtain,

$$i\varepsilon \frac{\partial \psi}{\partial t} = -\frac{\varepsilon^2}{2} \Delta \psi + U(\boldsymbol{x})\psi. \tag{1.4}$$

The parameter ε is defined by,

$$\varepsilon := \frac{\hbar}{\omega_0 m x_s^2} \tag{1.5}$$

and the potential $U(\boldsymbol{x})$ is given by,

$$U(\boldsymbol{x}) := \frac{|\boldsymbol{x}|^2}{2}. \tag{1.6}$$

In many physical applications, such as modeling the dynamics of electrons in crystals, equation (1.4) contains a periodic lattice potential. For example, the potential

$$V(\boldsymbol{x}) = \sum_{i=1}^{3} \frac{\hbar^2 \xi_l^2}{2m} \sin^2(\xi_l x_l) \tag{1.7}$$

with $\boldsymbol{\xi} = (\xi_1, \xi_2, \xi_3)$ and $\xi_l \in \mathbb{R}$ is commonly used when studying Bose-Einstein condensate [1]. To incorporate this potential, we modify equation (1.1) by,

$$i\hbar \frac{\partial \psi}{\partial t} = -\frac{\hbar^2}{2m} \Delta \psi + V(\boldsymbol{x})\psi + U_0(\boldsymbol{x})\psi. \tag{1.8}$$

Using the same substitutions as in equation (1.3), multiplying by $1/(m\omega_0^2 x_s^2)$, and omitting the tildes we obtain,

$$i\varepsilon \frac{\partial \psi}{\partial t} = -\frac{\varepsilon^2}{2} \Delta \psi + V_\Gamma(\frac{\boldsymbol{x}}{\varepsilon})\psi + U(\boldsymbol{x})\psi, \tag{1.9}$$

2

where the potential $V_\Gamma(\boldsymbol{x})$ is given by,

$$V_\Gamma(\boldsymbol{x}) := \frac{V(x_s \varepsilon \boldsymbol{x})}{m\omega_0^2 x_s^2}. \tag{1.10}$$

The parameter ε is called the semiclassical parameter. Our goal is to study values of ε that lie within $0 < \varepsilon \ll 1$. The spatial dimension will be denoted by d, it is a positive integer, and we will take as initial condition for equations (1.4) or (1.9), $\psi_0^\varepsilon(\boldsymbol{x})$ in $L^2(\mathbb{R}^d)$. $\psi^\varepsilon(t, \boldsymbol{x})$ will denote a complex-valued solution to equations (1.4) or (1.9). In our study, the potentials will not be restricted to the forms given by equations (1.10) and (1.6), but will also include a class of general smooth potentials. In particular, we will let $V_\Gamma(\boldsymbol{x})$ be a function in $\mathcal{C}(\mathbb{R}^d)$, periodic with respect to the lattice $\Gamma := [0, 1)^d$. $U(\boldsymbol{x})$ will also be assumed to be a smooth function in $\mathcal{C}(\mathbb{R}^d)$.

Direct numerical approximation to equation (1.4) such as finite differences or spectral methods are computationally more expensive compared to asymptotic methods. For example, the Crank-Nicolson scheme or the Dufort-Frankel requires a mesh size of $o(\varepsilon)$ [2, 3] while the time-splitting spectral method requires a mesh size of $\mathcal{O}(\varepsilon)$ [4]. In the presence of a highly oscillatory potential, as in equation (1.9), we must further restrict the mesh size of the time-splitting spectral method to $o(\varepsilon)$ in order to capture its dynamics. Because of this, there has been many attempts to find solutions to equation (1.4) and (1.9) asymptotically. One of the earliest attempt to solve equation (1.4) asymptotically is the WKB method. Although this method is highly efficient, it suffers from the formation of caustics [5, 6, 7] for which the solution becomes undefined.

The Gaussian beam method (GBM) [8] was then introduced by Popov to overcome the problem at caustics and decrease the computational cost of conventional methods. One draw back of the GBM is that it looses accuracy from the spreading of the beams. It was only until recently, that the frozen Gaussian approximation (FGA) [9, 10] was developed to deal with the loss of accuracy of the GBM by using Gaussian functions of

fixed width in phase space.

In this thesis we generalize the frozen Gaussian approximation for computation of the Schrödinger equation (1.9) with periodic potentials.

1.2   Strang-splitting spectral method

This section is devoted to solving the Schrödinger equation exactly by using the time-splitting spectral approximation. This non-asymptotic method for solving equation (1.4) (or (1.9)) will be used later to numerically compute the exact solution to equation (1.4) and (1.9). For more details, we refer the reader to [4].

First-order time-splitting spectral method

Suppose we are interested in the solution to equation (1.4) at time t_{final}. Suppose also that we have a discretization of time, $0 = t_0 < t_1 < t_2 < \cdots < t_N = t_{final}$, so that $\delta t = t_{final}/N$. We split equation (1.4) in two parts,

$$i\varepsilon \partial_t \psi^\varepsilon = -\frac{\varepsilon^2}{2}\Delta \psi^\varepsilon, \qquad (1.11)$$

and

$$i\varepsilon \partial_t \psi^\varepsilon = U(\boldsymbol{x})\psi^\varepsilon. \qquad (1.12)$$

Equation (1.11) will be solved exactly for one time step, starting at t_0, using the Fourier transform. The solution to equation (1.12) is given by,

$$\psi^\varepsilon(t_{n+1}, \boldsymbol{x}) = \exp\left(-\frac{i}{\varepsilon}U(\boldsymbol{x})\delta t\right)\psi^*(t_{n+1}, \boldsymbol{x}), \qquad (1.13)$$

where $\psi^*(t_{n+1}, \boldsymbol{x})$ is the solution to equation (1.11) at time t_{n+1} with initial condition $\psi^\varepsilon(t_n, \boldsymbol{x})$.

Strang-splitting spectral method

We can improve the order of accuracy in time by using the Strang-splitting spectral method. This method splits the equation (1.4) into 3 parts,

$$i\varepsilon\partial_t\psi^\varepsilon = U(\boldsymbol{x})\psi^\varepsilon, \tag{1.14}$$

$$i\varepsilon\partial_t\psi^\varepsilon = -\frac{\varepsilon^2}{2}\Delta\psi^\varepsilon, \tag{1.15}$$

$$i\varepsilon\partial_t\psi^\varepsilon = U(\boldsymbol{x})\psi^\varepsilon, \tag{1.16}$$

where equation (1.14) and (1.16) are solved on half a time step and equation (1.15) on one time step. More explicitly, the solution at time t_n is given by,

$$\psi^\varepsilon(t_{n+1}, \boldsymbol{x}) = \exp\left(-\frac{i}{2\varepsilon}U(\boldsymbol{x})\delta t\right)\psi^*(t_{n+1}, \boldsymbol{x}), \tag{1.17}$$

where $\psi^*(t_{n+1}, \boldsymbol{x})$ solves equation (1.15) with initial condition $\exp\left(-\frac{i}{2\varepsilon}U(\boldsymbol{x})\delta t\right)\psi^\varepsilon(t_n, \boldsymbol{x})$.

Equation (1.9) can also be solved exactly using the Strang-splitting spectral method by replacing the potential $U(\boldsymbol{x})$ with $V_\Gamma(\boldsymbol{x}/\varepsilon) + U(\boldsymbol{x})$. Typically, the Strang-splitting spectral method requires a spatial meshing of size $\mathcal{O}(\varepsilon)$ and a time step of size $o(\varepsilon)$; this is proved in [4].

1.3   WKB approximation

We now discuss several asymptotic solutions of equation (1.4). The first asymptotic solution we will introduce is known as the *WKB method.*

This ansatz is one of the earliest attempts for obtaining an asymptotic solution to the Schrödinger equation and is also known as the *geometric optics ansatz.*

The ansatz is given by,

$$\psi(x,t) = (a_0(t,x) + \varepsilon a_1(t,x) + \varepsilon^2 a_2(t,x) + \cdots)e^{\frac{i}{\varepsilon}S(t,x)}. \tag{1.18}$$

The motivation for using this ansatz is to understand the highly oscillatory structure of the solution to equation (1.4). $S(t, \boldsymbol{x})$ is real valued and is called the phase. $a^{\varepsilon} := a_0(t,x) + \varepsilon a_1(t,x) + \varepsilon^2 a_2(t,x) + \cdots$ is possibly complexed valued and is called the amplitude. Substituting this equation into (1.4) and grouping terms of $\mathcal{O}(1)$ and $\mathcal{O}(\varepsilon)$ gives us,

$$\partial_t S + \frac{1}{2}|\nabla S|^2 + U(\boldsymbol{x}) = 0, \tag{1.19}$$

and

$$\partial_t a_0 + \nabla S \cdot \nabla a_0 + \frac{a_0}{2}\Delta S = 0, \tag{1.20}$$

with initial conditions $S(0,x) = S_{in}(x)$ and $a_0(0,x) = a_{in}(x)$. Equation (1.19) can be solved analytically using the method of characteristics. The characteristic $X_t : \boldsymbol{s} \to \boldsymbol{x}(t, \boldsymbol{s})$ satisfies the following Hamiltonian flow:

$$\begin{cases} \dfrac{d\boldsymbol{x}}{dt} = \boldsymbol{p}(t, \boldsymbol{s}), & \boldsymbol{x}(0, \boldsymbol{s}) = \boldsymbol{s}, \\[2mm] \dfrac{d\boldsymbol{p}}{dt} = -\nabla_{\boldsymbol{x}} U(\boldsymbol{x}(t, \boldsymbol{s})), & \boldsymbol{p}(0, \boldsymbol{s}) = \nabla_{\boldsymbol{s}} S_{in}(\boldsymbol{s}). \end{cases} \tag{1.21}$$

The solution $S(t, x)$ is given by,

$$S(t, \boldsymbol{x}) = S(0, \boldsymbol{x}) + \int_0^t \frac{1}{2}|\nabla S(\tau, \boldsymbol{s}(t, \boldsymbol{x}))|^2 - U(\boldsymbol{s}(\tau, \boldsymbol{x}))d\tau. \tag{1.22}$$

This is only defined up to some (possibly) finite time $T > 0$ due to the crossing of characteristic curves. Furthermore, a_0 satisfies

$$a_0(t, \boldsymbol{x}) = \frac{a_{in}(\boldsymbol{x})}{\sqrt{J_t(\boldsymbol{s}(t, \boldsymbol{x}))}}, \tag{1.23}$$

where J_t denotes the Jacobian determinant of the Hamiltonian flow. The equation of $a_0(t, \boldsymbol{x})$ is also defined up to some (possibly) finite time $T > 0$. When characteristic

6

curves cross, the Jacobian determinant J_t is no longer defined. This is problematic as we are seeking solutions in $L^2(\mathbb{R}^d)$. We also note that the equations for $a_0(t, \boldsymbol{x})$ and $S(t, \boldsymbol{x})$ are independent of ε. This independence of ε makes the WKB method computationally efficient compared to conventional numerical methods.

1.4 Gaussian Beam method

The Gaussian beam method will improve upon the WKB method by removing the problem of caustics. We will present material found in [11] throughout this section. The Gaussian beam ansatz has the form

$$\phi(t, \boldsymbol{x}, \boldsymbol{y}_0) = A(t, \boldsymbol{y})e^{iT(t,\boldsymbol{x},\boldsymbol{y})/\varepsilon}, \tag{1.24}$$

where

$$T(t, \boldsymbol{x}, \boldsymbol{y}) = S(t, \boldsymbol{x}) + \boldsymbol{p}(t, \boldsymbol{y}) \cdot (\boldsymbol{x} - \boldsymbol{y}) + \frac{1}{2}(\boldsymbol{x} - \boldsymbol{y})^T M(t, \boldsymbol{y})(\boldsymbol{x} - \boldsymbol{y}), \tag{1.25}$$

where $S \in \mathbb{R}$, $\boldsymbol{p} \in \mathbb{R}^d$, and $M \in \mathbb{C}^{d \times d}$, and $\boldsymbol{y} = \boldsymbol{y}(t, \boldsymbol{y}_0)$ is the center of the beam. The Gaussian profile is maintained by keeping the imaginary part of $M = \nabla^2 S$ positive definite (see theorem 1.4.1). This differs from the WKB ansatz in that the GBM uses a complex phase, and we now use a Taylor expansion of the phase function to second order about $\boldsymbol{y}$. If one substitutes this ansatz into equation (1.4) we obtain the set of ordinary differential equations,

$$\frac{d\boldsymbol{y}}{dt} = \boldsymbol{p}, \tag{1.26}$$

$$\frac{d\boldsymbol{p}}{dt} = -\nabla_{\boldsymbol{y}}U, \tag{1.27}$$

$$\frac{dS}{dt} = \frac{1}{2}|\boldsymbol{p}|^2 - U, \tag{1.28}$$

$$\frac{dM}{dt} = -M^2 - \nabla_{\boldsymbol{y}}^2 U, \tag{1.29}$$

$$\frac{dA}{dt} = \frac{1}{2}\left(\mathrm{tr}(M)\right)A, , \tag{1.30}$$

where $\boldsymbol{p}$, U, S, M, and A are functions of $(t, \boldsymbol{y}(t, \boldsymbol{y}_0))$. Equations (1.26) and (1.27) describe the associated Hamiltonian flow $(\boldsymbol{y}(t, \boldsymbol{y}), \boldsymbol{p}(t, \boldsymbol{y}))$ to (1.4). Part 3 of the next theorem justifies the claim that $\phi(t, \boldsymbol{x}, \boldsymbol{y}_0)$ retains a Gaussian profile for all time.

Theorem 1.4.1. *Let $P(t, \boldsymbol{y}(t, \boldsymbol{y}_0))$ and $R(t, \boldsymbol{y}(t, \boldsymbol{y}_0))$ be the (global) solutions of the equations*

$$\frac{dP}{dt} = R, \qquad \frac{dR}{dt} = -(\nabla_{\boldsymbol{y}}^2 U)P, \tag{1.31}$$

with initial conditions

$$P(0, \boldsymbol{y}_0) = I, R(0, \boldsymbol{y}_0) = M(0, \boldsymbol{y}_0), \tag{1.32}$$

where the matrix I is the identity matrix and $\mathfrak{Im}(M(0, \boldsymbol{y}_0))$ is positive definite. Assume $M(0, \boldsymbol{y}_0)$ is symmetric. Then, for each initial position y_0, we have the following.

1. $P(t, \boldsymbol{y}(t, \boldsymbol{y}_0))$ is invertible for all $t > 0$.

2. The solution to equation (1.28) is given by

$$M(t, \boldsymbol{y}(t, \boldsymbol{y}_0)) = R(t, \boldsymbol{y}(t, \boldsymbol{y}_0))P^{-1}(t, \boldsymbol{y}(t, \boldsymbol{y}_0)). \tag{1.33}$$

3. $M(t, \boldsymbol{y}(t, \boldsymbol{y}_0))$ is symmetric and $\mathfrak{Im}(M(t, \boldsymbol{y}(t, \boldsymbol{y}_0)))$ is positive definite for all $t > 0$.

4. Not only is the Hamiltonian $U + \frac{1}{2}|\boldsymbol{p}|^2$ conserved along the $\boldsymbol{y}$-trajectory, another quantity $A^2 \det P$ is also conserved, which means $A(t, \boldsymbol{y}(t, \boldsymbol{y}_0))$ can also be computed by

$$A(t, \boldsymbol{y}(t, \boldsymbol{y}_0)) = [(\det P(t, \boldsymbol{y}(t, \boldsymbol{y}_0)))^{-2}A^2(0, \boldsymbol{y}_0)]^{1/2}, \tag{1.34}$$

where the square root is taken as the principal value.

For details on the proof of Theorem 1.4.1 see [11] and [12].

Beam summation.

By construction, $\phi(t, \boldsymbol{x}, \boldsymbol{y}_0)$ is a solution to equation (1.4) for each $\boldsymbol{y}_0 \in \mathbb{R}$ and thus so is the sum of finitely many such expressions. The next theorem, found in [11], summarizes

this observation at time $t = 0$. A formulation for higher order Gaussian beams can also be found in [13].

Theorem 1.4.2. *Let $A_0 \in \mathcal{C}^1(\mathbb{R}^d) \cap l^2(\mathbb{R}^d)$ and $S_0 \in \mathcal{C}^3(\mathbb{R}^d)$, define*

$$\psi_0^\varepsilon(\boldsymbol{x}) = A_0(\boldsymbol{x})e^{iS_0(\boldsymbol{x})/\varepsilon}, \tag{1.35}$$

$$\phi_0^\varepsilon(\boldsymbol{x}, \boldsymbol{y}_0) = A_0(\boldsymbol{y}_0)e^{iT_0(\boldsymbol{x},\boldsymbol{y}_0)/\varepsilon}, \tag{1.36}$$

where

$$T_0(\boldsymbol{x}, \boldsymbol{y}_0) = T_{\alpha 0}(\boldsymbol{y}_0) + T_{\beta 0} \cdot (\boldsymbol{x} - \boldsymbol{y}_0) + \frac{1}{2}(\boldsymbol{x} - \boldsymbol{y}_0)^T T_{\gamma 0}(\boldsymbol{x} - \boldsymbol{y}_0), \tag{1.37}$$

$$T_{\alpha 0}(\boldsymbol{y}_0) = S_0(\boldsymbol{y}_0), T_{\beta 0}(\boldsymbol{y}_0) = \nabla_{\boldsymbol{x}}S_0(\boldsymbol{y}_0), T_{\gamma 0}(\boldsymbol{y}_0) = \nabla_{\boldsymbol{x}}^2 S_0(\boldsymbol{y}_0) + iI. \tag{1.38}$$

Then

$$\left\| \int_{\mathbb{R}^n} \left(\frac{1}{2\pi\varepsilon}\right)^{\frac{d}{2}} r_\theta(\boldsymbol{x} - \boldsymbol{y}_0)\phi_0^\varepsilon(\boldsymbol{x}, \boldsymbol{y}_0)d\boldsymbol{y}_0 - \psi_0^\varepsilon(\boldsymbol{x}) \right\|_{l^2} \leqslant C\varepsilon^{\frac{1}{2}}. \tag{1.39}$$

where $r_\theta \in \mathcal{C}_0^\infty(\mathbb{R}^d)$, $r_\theta \geqslant 0$ is a truncation function with $r_\theta := 1$ in a ball of radius $\theta > 0$ about the origin and C is a constant related to θ.

At a later time $t > 0$, the Gaussian beam summation approximates the solution to the Schrödinger equation (1.4) by,

$$\phi_{la}^\varepsilon(t, \boldsymbol{x}) = \int_{\mathbb{R}^d} \left(\frac{1}{2\pi\varepsilon}\right)^{\frac{d}{2}} r_\theta(\boldsymbol{x} - \boldsymbol{y}(t, \boldsymbol{y}_0))\phi^\varepsilon(t, \boldsymbol{x}, \boldsymbol{y}_0)d\boldsymbol{y}_0. \tag{1.40}$$

In discretized form $\phi_{la}^\varepsilon(t, \boldsymbol{x})$ is approximated by,

$$\phi_{la}^\varepsilon(t, \boldsymbol{x}) \approx \sum_{j=1}^\infty \left(\frac{1}{2\pi\varepsilon}\right)^{d/2} r_\theta(\boldsymbol{x} - \boldsymbol{y}(t, \boldsymbol{y}_0^j))\phi_{la}^\varepsilon(t, \boldsymbol{x}, \boldsymbol{y}_0^j)\Delta\boldsymbol{y}_0. \tag{1.41}$$

Remark. The approximation of $\phi_{la}^\varepsilon(t, \boldsymbol{x})$ given by (1.41) made use of the Taylor expansion about $\boldsymbol{y}_0^j$, hence it looses accuracy when the width of the Gaussian function ϕ_{la}^ε becomes too large. We call this phenomena *beam spreading*.

9

Remark. In view of theorem 1.4.1 part 4, we see that we no longer have the problem of caustics.

1.5   Frozen Gaussian approximation

Because of the problem of beam spreading suffered by $\phi_{la}^{\varepsilon}(t, \boldsymbol{x})$, the frozen Gaussian approximation (FGA) was developed [14]. The FGA method removes the inaccuracy introduced in the Taylor expansion of $\phi_{la}^{\varepsilon}(t, \boldsymbol{x})$ by using a superposition of Gaussian functions of fixed widths in phase space. One may also draw motivation for decomposing the solution in terms of Gaussian functions of fixed by the work of M. Herman and E. Kluk, [34]. In quantum chemistry, the FGA method is also known as the Herman-Kluk propagator. We begin the construction of the FGA by decomposing the initial data into several Gaussian functions in phase space.

Theorem 1.5.1. *For any* $\psi_0^{\varepsilon}(\boldsymbol{x}) \in L^2(\mathbb{R}^d)$,

$$\psi_0^{\varepsilon}(\boldsymbol{x}) = \frac{2^{d/2}}{(2\pi\varepsilon)^{3d/2}} \int_{\mathbb{R}^{2d}} G_{\boldsymbol{q},\boldsymbol{p}}^{\varepsilon}(\boldsymbol{x}) \left(\int_{\mathbb{R}^d} \bar{G}_{\boldsymbol{q},\boldsymbol{p}}^{\varepsilon} \psi_0^{\varepsilon}(\boldsymbol{y}) d\boldsymbol{y} \right) d\boldsymbol{q} d\boldsymbol{p}, \tag{1.42}$$

where

$$G_{\boldsymbol{q},\boldsymbol{p}}^{\varepsilon}(\boldsymbol{x}) = \exp\left(-\frac{1}{2\varepsilon} |\boldsymbol{x} - \boldsymbol{q}|^2 + \frac{\mathrm{i}}{\varepsilon} \boldsymbol{p} \cdot (\boldsymbol{x} - \boldsymbol{q}) \right). \tag{1.43}$$

Proof: Fix a $f \in L^2(\mathbb{R})$, by definition, we have

$$\frac{2^{d/2}}{(2\pi\varepsilon)^{3d/2}} \int_{\mathbb{R}^{2d}} G_{\boldsymbol{q},\boldsymbol{p}}^{\varepsilon}(\boldsymbol{x}) \int_{\mathbb{R}^d} \bar{G}_{\boldsymbol{q},\boldsymbol{p}}^{\varepsilon}(\boldsymbol{y}) f(\boldsymbol{y}) d\boldsymbol{y} d\boldsymbol{q} d\boldsymbol{p} \tag{1.44}$$

$$= \frac{2^{d/2}}{(2\pi\varepsilon)^{3d/2}} \int_{\mathbb{R}^{3d}} G_{\boldsymbol{q},\boldsymbol{p}}^{\varepsilon}(\boldsymbol{x}) \bar{G}_{\boldsymbol{q},\boldsymbol{p}}^{\varepsilon}(\boldsymbol{y}) f(\boldsymbol{y}) d\boldsymbol{y} d\boldsymbol{q} d\boldsymbol{p}. \tag{1.45}$$

Integrating in $\boldsymbol{q}$ first,

$$\int_{\mathbb{R}^d} G_{\boldsymbol{q},\boldsymbol{p}}(\boldsymbol{x})\bar{G}_{\boldsymbol{q},\boldsymbol{p}}(\boldsymbol{y})d\boldsymbol{q} = e^{\mathrm{i}\boldsymbol{p}\cdot(\boldsymbol{x}-\boldsymbol{y})/\varepsilon}\int_{\mathbb{R}^d} e^{-|\boldsymbol{x}-\boldsymbol{q}|^2/(2\varepsilon)-|\boldsymbol{y}-\boldsymbol{q}|^2/(2\varepsilon)}d\boldsymbol{q} \tag{1.46}$$

$$= e^{\mathrm{i}\boldsymbol{p}\cdot(\boldsymbol{x}-\boldsymbol{y})/\varepsilon}e^{-|\boldsymbol{x}-\boldsymbol{y}|^2/(4\varepsilon)}\int_{\mathbb{R}^d} e^{-\frac{1}{\varepsilon}\left|\boldsymbol{q}-\frac{\boldsymbol{x}+\boldsymbol{y}}{2}\right|^2}d\boldsymbol{q} \tag{1.47}$$

$$= (\pi\varepsilon)^{d/2}e^{\mathrm{i}\boldsymbol{p}\cdot(\boldsymbol{x}-\boldsymbol{y})/\varepsilon}e^{-|\boldsymbol{x}-\boldsymbol{y}|^2/(4\varepsilon)} \tag{1.48}$$

Denoting $\widetilde{f}^\varepsilon(\boldsymbol{x},\boldsymbol{y}) = e^{-|\boldsymbol{x}-\boldsymbol{y}|^2/(4\varepsilon)}f(\boldsymbol{y})$, the right hand side of 1.42 becomes

$$\frac{1}{(2\pi\varepsilon)}\iint_{\mathbb{R}^{2d}} e^{\mathrm{i}\boldsymbol{p}\cdot(\boldsymbol{x}-\boldsymbol{y})/\varepsilon}e^{-|\boldsymbol{x}-\boldsymbol{y}|^2/(4\varepsilon)}f(\boldsymbol{y})d\boldsymbol{y}d\boldsymbol{p} = \frac{1}{(2\pi\varepsilon)^d}\iint_{\mathbb{R}^{2d}} e^{\mathrm{i}\boldsymbol{p}\cdot(\boldsymbol{x}-\boldsymbol{y})/\varepsilon}\widetilde{f}^\varepsilon(\boldsymbol{x},\boldsymbol{y})d\boldsymbol{y}d\boldsymbol{p} \tag{1.49}$$

$$= \frac{1}{(2\pi)^d}\iint_{\mathbb{R}^{2d}} e^{\mathrm{i}\boldsymbol{p}\cdot(\boldsymbol{x}-\boldsymbol{y})}\widetilde{f}^\varepsilon(\boldsymbol{x},\boldsymbol{y})d\boldsymbol{y}d\boldsymbol{p} \tag{1.50}$$

$$= \widetilde{f}^\varepsilon(\boldsymbol{x},\boldsymbol{x}) \quad \text{(by Fourier inversion formula)} \tag{1.51}$$

$$= e^{-|\boldsymbol{x}-\boldsymbol{x}|^2/(4\varepsilon)}f(\boldsymbol{x}) = f(\boldsymbol{x}) \tag{1.52}$$

Now that we legitimized the decomposition of any $L^2(\mathbb{R}^d)$ data in terms of Gaussian functions in phase space, we propagate the center of the Gaussian functions using the Hamiltonian flow of equation (1.26) and (1.27). This leads to the FGA ansatz for solving (1.4) asymptotically,

$$\psi_{FGA}^\varepsilon(t,\boldsymbol{x}) = \frac{2^{d/2}}{(2\pi\varepsilon)^{3d/2}}\int_{\mathbb{R}^{2d}} a(t,\boldsymbol{q},\boldsymbol{p})G_{\boldsymbol{Q},\boldsymbol{P}}^\varepsilon(\boldsymbol{x})e^{\mathrm{i}S(t,\boldsymbol{q},\boldsymbol{p})/\varepsilon}\left(\int_{\mathbb{R}^d}\bar{G}_{\boldsymbol{q},\boldsymbol{p}}^\varepsilon\psi_0^\varepsilon(\boldsymbol{y})d\boldsymbol{y}\right)d\boldsymbol{q}d\boldsymbol{p}, \tag{1.53}$$

where $\boldsymbol{Q}(t,\boldsymbol{q},\boldsymbol{p})$ and $\boldsymbol{P}(t,\boldsymbol{q},\boldsymbol{p})$ satisfy the evolution equation

$$\frac{d\boldsymbol{Q}}{dt} = \boldsymbol{P} \tag{1.54}$$

$$\frac{d\boldsymbol{P}}{dt} = -\nabla_{\boldsymbol{Q}}U(\boldsymbol{Q}). \tag{1.55}$$

As in the WKB and Gaussian beam methods, we include $ae^{\mathrm{i}S/\varepsilon}$ to capture amplitude and highly oscillatory nature of the solutions to equation (1.4). Because we are working in

phase space, both a and S now depend on $(t, \boldsymbol{q}, \boldsymbol{p})$. It remains to be specified the phase $S(t, \boldsymbol{q}, \boldsymbol{p})$ and the amplitude $a(t, \boldsymbol{q}, \boldsymbol{p})$. The evolution for these terms can be determined by substituting the ansatz into the Schrödinger equation (1.4). Upon grouping orders of ε and simplifying we obtain,

$$\frac{dS}{dt} = \frac{|\boldsymbol{P}|^2}{2} - U(\boldsymbol{Q}),$$ (1.56)

$$\frac{da}{dt} = \frac{1}{2} a \operatorname{tr} \left(Z^{-1}(\partial_{\boldsymbol{z}} \boldsymbol{P} - \mathrm{i} \partial_{\boldsymbol{z}} \boldsymbol{Q} \partial_{\boldsymbol{Q}}^2 U) \right),$$ (1.57)

where $Z := \partial_{\boldsymbol{z}}(\boldsymbol{Q} + \mathrm{i} \boldsymbol{P})$ and $\partial_{\boldsymbol{z}} := \partial_q - \mathrm{i} \partial_p$.

The frozen Gaussian approximation can be applied to solve the problem with periodic potentials, equation (1.9), by replacing $U(\boldsymbol{x})$ with $V_\Gamma(\boldsymbol{x}) + U(\boldsymbol{x})$. However, many others have taken advantage of the fact that equation (1.9) with $U(\boldsymbol{x}) = 0$ can be solved exactly by diagonalizing the Hamiltonian operator using the corresponding eigenfunctions, known as Bloch waves. We will discuss Bloch waves in the next chapter. For the Bloch decomposition-based time-splitting method see [15]. For Bloch-based WKB and Gaussian beam methods see [16, 17].

a collaboration with Alice and Bob, and has previously appeared in

Chapter 2

Preliminaries

2.1   Notations

Let us start with fixing some notations. We will switch between physical domain and phase space in the FGA formulation. For clarity, we will use $\boldsymbol{x}, \boldsymbol{y} \in \mathbb{R}^d$ as spatial variables, $(\boldsymbol{q}, \boldsymbol{p}) \in \mathbb{R}^{2d}$ as phase space variables. The capital letters $\boldsymbol{X}$ and $\boldsymbol{Y}$ are shorthand notations for $\boldsymbol{X} = \boldsymbol{x}/\varepsilon$ and $\boldsymbol{Y} = \boldsymbol{y}/\varepsilon$. At times we will use subscripts and superscripts to denote dependence of a quantity on a variable such as, $E_n := E(n)$. $\mathcal{S}$ will denote the space of Schwartz functions.

2.2   Bloch-decomposition

Denote a unit cell in $\mathbb{R}^d$ by $\Gamma = [0, 1)^d$ and its reciprocal lattice by $\Gamma^* = [-\pi, \pi)^d$. The periodic part of the Schrödinger operator (in atomic units) is given by

$$H_{Per} := -\frac{1}{2}\Delta + V(\boldsymbol{x}) \tag{2.1}$$

13

By the theory of compact operators, the spectrum is given by

$$\mathrm{spec}(H_{Per}) = \bigcup_{n=1}^{\infty} \bigcup_{\boldsymbol{\xi} \in \Gamma*} E_n(\boldsymbol{\xi}) \tag{2.2}$$

where $E_n(\boldsymbol{\xi})$, for $\boldsymbol{\xi} \in \Gamma^*$, are the eigenvalues (in ascending order) of the operator

$$H_{\boldsymbol{\xi}} = \frac{1}{2}(-\mathrm{i}\nabla_{\boldsymbol{x}} + \boldsymbol{\xi})^2 + V(\boldsymbol{x}) \tag{2.3}$$

with periodic boundary conditions on Γ. The set $\{E_n(\boldsymbol{\xi}) : \boldsymbol{\xi} \in \Gamma^*\} \subset \mathbb{R}$ is called the nth energy band. E_n is also called the nth adiabatic surface.

The Bloch waves, also known as adiabatic states, $u_n(\boldsymbol{\xi})$ (for each $n \in 1, 2, \cdots$ and $\boldsymbol{\xi} \in \Gamma^*$) are the associated eigenfunctions:

$$H_{\boldsymbol{\xi}} u_n(\boldsymbol{\xi}, \boldsymbol{x}) = E_n(\boldsymbol{\xi}) u_n(\boldsymbol{\xi}, \boldsymbol{x}) \tag{2.4}$$

with periodic boundary conditions on Γ. We also normalize u_n with respect to $\boldsymbol{x}$ so that

$$\int_{\Gamma} |u_n(\boldsymbol{\xi}, \boldsymbol{x})|^2 d\boldsymbol{x} = 1. \tag{2.5}$$

The eigenfunctions for (2.3) and normalization are defined up to a unit complex number, in particular, for any function ϕ periodic in Γ^*, $\tilde{u}_n(\boldsymbol{\xi}, \boldsymbol{x}) = e^{\mathrm{i}\phi(\boldsymbol{\xi})} u_n(\boldsymbol{\xi}, \boldsymbol{x})$ also provides a set of Bloch waves. It is known that the gauge ϕ can be chosen so that $\tilde{u}_n(\boldsymbol{\xi}, \boldsymbol{x})$ is continuous with respect to $\boldsymbol{\xi}$. We also define the berry phase:

$$\mathcal{A}_n(\boldsymbol{\xi}) := \mathrm{i} \int_{\Gamma} \overline{u}_n(\boldsymbol{\xi}, \boldsymbol{x}) \nabla_{\boldsymbol{\xi}} u_n(\boldsymbol{\xi}, \boldsymbol{x}) d\boldsymbol{x} \tag{2.6}$$

for each $\boldsymbol{\xi} \in \Gamma^*$ and $n \in 1, 2, \cdots$. This makes sense as long as we choose a gauge for which u_n is smooth.

Bloch waves allows us to decompose the Hilbert space $L^2(\mathbb{R}^d)$ into a direct sum of Band spaces. For any $f \in L^2(\mathbb{R}^d)$, we have the Bloch decomposition

$$f(\boldsymbol{x}) = \frac{1}{(2\pi)^{d/2}} \sum_{n=1}^{\infty} \int_{\Gamma*} u_n(\boldsymbol{\xi}, \boldsymbol{x}) e^{\mathrm{i}\boldsymbol{\xi}\cdot\boldsymbol{x}} (\mathcal{B}f)_n(\boldsymbol{\xi}) \, d\boldsymbol{\xi}. \tag{2.7}$$

14

In the above equation, the Bloch transform $\mathcal{B} : L^2(\mathbb{R}^d) \to L^2(\Gamma^*)^{\mathbb{N}}$ is given by

$$(\mathcal{B}f)_n(\boldsymbol{\xi}) = \frac{1}{(2\pi)^{d/2}} \int_{\mathbb{R}^d} \bar{u}_n(\boldsymbol{\xi}, \boldsymbol{y}) e^{-\mathrm{i}\boldsymbol{\xi} \cdot \boldsymbol{y}} f(\boldsymbol{y}) \, \mathrm{d}\boldsymbol{y}. \tag{2.8}$$

As an analog of the Parseval's identity, we have

$$\int_{\mathbb{R}^d} |f(\boldsymbol{x})|^2 \, \mathrm{d}\boldsymbol{x} = \sum_{n=1}^{\infty} \int_{\Gamma^*} |(\mathcal{B}f)_n(\boldsymbol{\xi})|^2 \, \mathrm{d}\boldsymbol{\xi}. \tag{2.9}$$

As suggested by (2.7) and (2.8), we introduce the notation Ω to denote the phase space corresponding to one band

$$\Omega := \mathbb{R}^d \times \Gamma^* = \left\{ (\boldsymbol{x}, \boldsymbol{\xi}) \mid \boldsymbol{x} \in \mathbb{R}^d, \, \boldsymbol{\xi} \in \Gamma^* \right\}. \tag{2.10}$$

Correspondingly, we will use the notation $(\boldsymbol{q}, \boldsymbol{p})$ for a point in Ω. For more analysis concerning Bloch waves see [18]

2.3   Windowed Bloch transform

We shall now introduce the windowed Bloch transform. This is an analog of the windowed Fourier transform (also known as the short time Fourier transform) widely used in time-frequency signal analysis.

Definition 2.3.1. The windowed Bloch transform $\mathcal{W} : L^2(\mathbb{R}^d) \to L^2(\Omega)^{\mathbb{N}}$ is defined as

$$(\mathcal{W}f)_n(\boldsymbol{q}, \boldsymbol{p}) = \frac{2^{d/4}}{(2\pi)^{3d/4}} \langle u_n(\boldsymbol{p}, \cdot) G_{\boldsymbol{q}, \boldsymbol{p}}, f \rangle = \frac{2^{d/4}}{(2\pi)^{3d/4}} \int_{\mathbb{R}^d} \bar{u}_n(\boldsymbol{p}, \boldsymbol{x}) \bar{G}_{\boldsymbol{q}, \boldsymbol{p}}(\boldsymbol{x}) f(\boldsymbol{x}) \, \mathrm{d}\boldsymbol{x}, \tag{2.11}$$

where $G_{\boldsymbol{q}, \boldsymbol{p}}$ is a Gaussian centered at $(\boldsymbol{q}, \boldsymbol{p}) \in \Omega$, given by

$$G_{\boldsymbol{q}, \boldsymbol{p}}(\boldsymbol{x}) = \exp\left(-\frac{1}{2} |\boldsymbol{x} - \boldsymbol{q}|^2 + \mathrm{i}\boldsymbol{p} \cdot (\boldsymbol{x} - \boldsymbol{q})\right). \tag{2.12}$$

The adjoint operator $\mathcal{W}^* : L^2(\Omega)^{\mathbb{N}} \to L^2(\mathbb{R}^d)$ is then

$$(\mathcal{W}^* g)(\boldsymbol{x}) = \frac{2^{d/4}}{(2\pi)^{3d/4}} \sum_{n=1}^{\infty} \iint_{\Omega} u_n(\boldsymbol{p}, \boldsymbol{x}) G_{\boldsymbol{q}, \boldsymbol{p}}(\boldsymbol{x}) g_n(\boldsymbol{q}, \boldsymbol{p}) \, \mathrm{d}\boldsymbol{q} \, \mathrm{d}\boldsymbol{p}. \tag{2.13}$$

Proposition 2.3.2. *The windowed Bloch transform and its adjoint satisfies*

$$\mathcal{W}^*\mathcal{W} = \mathrm{Id}_{L^2(\mathbb{R}^d)}. \tag{2.14}$$

Remark. Similar to the windowed Fourier transform, the representation given by the windowed Bloch transform is redundant, so that $\mathcal{W}\mathcal{W}^* \neq \mathrm{Id}_{L^2(\Omega)^\mathbb{N}}$. The normalization constant in the definition of $\mathcal{W}$ is also due to this redundancy.

Proof: Fix a $f \in L^2(\mathbb{R}^d)$, by definition, we have

$$(\mathcal{W}^*\mathcal{W}f)(\boldsymbol{x}) = \frac{2^{d/2}}{(2\pi)^{3d/2}} \sum_{n=1}^{\infty} \iint_{\Omega} u_n(\boldsymbol{p}, \boldsymbol{x}) G_{\boldsymbol{q},\boldsymbol{p}}(\boldsymbol{x}) \langle G_{\boldsymbol{q},\boldsymbol{p}} u_n(\boldsymbol{p}, \cdot), f \rangle \, \mathrm{d}\boldsymbol{q} \, \mathrm{d}\boldsymbol{p}$$

$$= \frac{2^{d/2}}{(2\pi)^{3d/2}} \sum_{n=1}^{\infty} \iint_{\Omega} \int_{\mathbb{R}^d} u_n(\boldsymbol{p}, \boldsymbol{x}) G_{\boldsymbol{q},\boldsymbol{p}}(\boldsymbol{x}) \bar{G}_{\boldsymbol{q},\boldsymbol{p}}(\boldsymbol{y}) \bar{u}_n(\boldsymbol{p}, \boldsymbol{y}) f(\boldsymbol{y}) \, \mathrm{d}\boldsymbol{y} \, \mathrm{d}\boldsymbol{q} \, \mathrm{d}\boldsymbol{p}.$$

Let us integrate in $\boldsymbol{q}$ first.

$$\int_{\mathbb{R}^d} G_{\boldsymbol{q},\boldsymbol{p}}(\boldsymbol{x}) \bar{G}_{\boldsymbol{q},\boldsymbol{p}}(\boldsymbol{y}) \, \mathrm{d}\boldsymbol{q} = e^{\mathrm{i}\boldsymbol{p}\cdot(\boldsymbol{x}-\boldsymbol{y})} \int_{\mathbb{R}^d} e^{-|\boldsymbol{x}-\boldsymbol{q}|^2/2 - |\boldsymbol{y}-\boldsymbol{q}|^2/2} \, \mathrm{d}\boldsymbol{q}$$

$$= e^{\mathrm{i}\boldsymbol{p}\cdot(\boldsymbol{x}-\boldsymbol{y})} e^{-|\boldsymbol{x}-\boldsymbol{y}|^2/4} \int_{\mathbb{R}^d} \exp\left(-\left|\boldsymbol{q} - \frac{\boldsymbol{x}+\boldsymbol{y}}{2}\right|^2\right) \, \mathrm{d}\boldsymbol{q}$$

$$= \pi^{d/2} e^{\mathrm{i}\boldsymbol{p}\cdot(\boldsymbol{x}-\boldsymbol{y})} e^{-|\boldsymbol{x}-\boldsymbol{y}|^2/4}.$$

Hence, denoting $\widetilde{f}_{\boldsymbol{x}}(\boldsymbol{y}) = e^{-|\boldsymbol{x}-\boldsymbol{y}|^2/4} f(\boldsymbol{y})$, we have

$$(\mathcal{W}^*\mathcal{W}f)(\boldsymbol{x}) = \frac{1}{(2\pi)^d} \sum_{n=1}^{\infty} \int_{\Gamma^*} \int_{\mathbb{R}^d} u_n(\boldsymbol{p}, \boldsymbol{x}) e^{\mathrm{i}\boldsymbol{p}\cdot(\boldsymbol{x}-\boldsymbol{y})} e^{-|\boldsymbol{x}-\boldsymbol{y}|^2/4} \bar{u}_n(\boldsymbol{p}, \boldsymbol{y}) f(\boldsymbol{y}) \, \mathrm{d}\boldsymbol{y} \, \mathrm{d}\boldsymbol{p}$$

$$= \frac{1}{(2\pi)^d} \sum_{n=1}^{\infty} \int_{\Gamma^*} \int_{\mathbb{R}^d} u_n(\boldsymbol{p}, \boldsymbol{x}) e^{\mathrm{i}\boldsymbol{p}\cdot(\boldsymbol{x}-\boldsymbol{y})} \bar{u}_n(\boldsymbol{p}, \boldsymbol{y}) \widetilde{f}_{\boldsymbol{x}}(\boldsymbol{y}) \, \mathrm{d}\boldsymbol{y} \, \mathrm{d}\boldsymbol{p}$$

$$\overset{(2.7)}{=} \widetilde{f}_{\boldsymbol{x}}(\boldsymbol{x}) = e^{-|\boldsymbol{x}-\boldsymbol{x}|^2/4} f(\boldsymbol{x}) = f(\boldsymbol{x}).$$

The previous proposition motivates us to consider the contribution of each band to the reconstruction formulae (2.14). We define the projection operator $\Pi_n^{\mathcal{W}} : L^2(\mathbb{R}^d) \to L^2(\mathbb{R}^d)$ for each $n \in \mathbb{N}$ onto the *nth* band space as:

16

Definition 2.3.3. The projection of $f \in L^2(\mathbb{R}^d)$ onto the nth band space is given by,

$$(\Pi_n^{\mathcal{W}} f)(\boldsymbol{x}) = \frac{2^{d/4}}{(2\pi)^{3d/4}} \iint_{\Omega} u_n(\boldsymbol{p}, \boldsymbol{x}) G_{\boldsymbol{q},\boldsymbol{p}}(\boldsymbol{x})(\mathcal{W}f)_n(\boldsymbol{q}, \boldsymbol{p}) \, \mathrm{d}\boldsymbol{q} \, \mathrm{d}\boldsymbol{p}. \tag{2.15}$$

It follows from (2.14) that $\sum_n \Pi_n^{\mathcal{W}} = \mathrm{Id}_{L^2(\mathbb{R}^d)}$.

2.4 The Fourier integral operator

Given a classical Hamiltonian $h(\boldsymbol{q}, \boldsymbol{p})$ defined for $(\boldsymbol{q}, \boldsymbol{p}) \in \Omega$, the associated Hamiltonian flow governs the dynamics of $(\boldsymbol{Q}(t, \boldsymbol{q}, \boldsymbol{p}), \boldsymbol{P}(t, \boldsymbol{q}, \boldsymbol{p}))$ by:

$$\begin{cases} \dfrac{d\boldsymbol{Q}}{dt} = \nabla_{\boldsymbol{P}} h(\boldsymbol{Q}, \boldsymbol{P}), \\[2mm] \dfrac{d\boldsymbol{P}}{dt} = -\nabla_{\boldsymbol{Q}} h(\boldsymbol{Q}, \boldsymbol{P}), \end{cases} \tag{2.16}$$

on Ω with the initial conditions $\boldsymbol{Q}(0, \boldsymbol{q}, \boldsymbol{p}) = \boldsymbol{q}$ and $\boldsymbol{P}(0, \boldsymbol{q}, \boldsymbol{p}) = \boldsymbol{p}$. We associate to this flow a real-valued *action* function $S(t, \boldsymbol{q}, \boldsymbol{p})$. $S(t, \boldsymbol{q}, \boldsymbol{p})$ satisfies

$$\nabla_{\boldsymbol{q}} S(t, \boldsymbol{q}, \boldsymbol{p}) = -\boldsymbol{p} \cdot \boldsymbol{1} + \nabla_{\boldsymbol{q}} \boldsymbol{Q} \cdot \boldsymbol{P}, \qquad \nabla_{\boldsymbol{p}} S(t, \boldsymbol{q}, \boldsymbol{p}) = \nabla_{\boldsymbol{p}} \boldsymbol{Q} \cdot \boldsymbol{P}. \tag{2.17}$$

The action $S(t, \boldsymbol{q}, \boldsymbol{p})$ can be obtained by solving the evolution equation

$$\frac{dS}{dt} = \boldsymbol{P} \cdot \nabla_{\boldsymbol{P}} h(\boldsymbol{Q}, \boldsymbol{P}) - h(\boldsymbol{Q}, \boldsymbol{P}), \tag{2.18}$$

with initial condition $S(0, \boldsymbol{q}, \boldsymbol{p}) = 0$.

Our asymptotic solution to equation (1.4) will be formulated by the following Fourier integral operator:

Definition 2.4.1. (Fourier Integral Operator) For $u \in \mathcal{S}(\mathbb{R}^{2d} \times \Omega, \mathbb{C})$ and $\varphi \in \mathcal{S}(\mathbb{R}^d, \mathbb{C})$ we define the Fourier Integral Operator with symbol u by the oscillatory integral

$$[\mathcal{I}^\varepsilon(u)\varphi](\boldsymbol{x}) = \frac{1}{(2\pi\varepsilon)^{3d/2}} \iint_{\Omega} \int_{\mathbb{R}^d} e^{\frac{i}{\varepsilon}\Phi(t,\boldsymbol{x},\boldsymbol{y},\boldsymbol{q},\boldsymbol{p})} u(\boldsymbol{x}, \boldsymbol{y}, \boldsymbol{q}, \boldsymbol{p})\varphi(\boldsymbol{y}) \, \mathrm{d}\boldsymbol{y} \, \mathrm{d}\boldsymbol{q} \, \mathrm{d}\boldsymbol{p} \tag{2.19}$$

where the complex valued phase function $\Phi(t, \boldsymbol{x}, \boldsymbol{y}, \boldsymbol{q}, \boldsymbol{p})$ is given by

$$\Phi(t, \boldsymbol{x}, \boldsymbol{y}, \boldsymbol{q}, \boldsymbol{p}) = S(t, \boldsymbol{q}, \boldsymbol{p}) - \boldsymbol{p} \cdot (\boldsymbol{y} - \boldsymbol{q}) + \boldsymbol{P} \cdot (\boldsymbol{x} - \boldsymbol{Q}) + \frac{i}{2}|\boldsymbol{y} - \boldsymbol{q}|^2 + \frac{i}{2}|\boldsymbol{x} - \boldsymbol{Q}|^2. \tag{2.20}$$

2.5   Semiclassical scaling

It will be convenient to rescale our formulas in the last 4 sections.

Definition 2.5.1. The semiclassical Gaussian function is defined by,

$$G_{\boldsymbol{q},\boldsymbol{p}}^{\varepsilon}(\boldsymbol{x}) := \exp\left(-\frac{|\boldsymbol{x}-\boldsymbol{q}|^2}{2\varepsilon} + \mathrm{i}\frac{\boldsymbol{p}\cdot(\boldsymbol{x}-\boldsymbol{q})}{\varepsilon}\right), \tag{2.21}$$

where the subscripts $(\boldsymbol{q},\boldsymbol{p})$ indicate the center of the Gaussian in phase space.

For convenience, we also provide the semiclassical Fourier transform of $G_{\boldsymbol{q},\boldsymbol{p}}^{\varepsilon}$:

$$\widehat{G}_{\boldsymbol{q},\boldsymbol{p}}^{\varepsilon}(\boldsymbol{\xi}) = \frac{1}{(2\pi\varepsilon)^{d/2}}\int_{\mathbb{R}^d} G_{\boldsymbol{q},\boldsymbol{p}}^{\varepsilon}(\boldsymbol{x})e^{-\mathrm{i}\boldsymbol{\xi}\cdot\boldsymbol{x}/\varepsilon}\,\mathrm{d}\boldsymbol{x} = \exp\left(-\frac{|\boldsymbol{\xi}-\boldsymbol{p}|^2}{2\varepsilon} + \mathrm{i}\frac{\boldsymbol{q}\cdot(\boldsymbol{\xi}-\boldsymbol{p})}{\varepsilon}\right). \tag{2.22}$$

We also scale the windowed Bloch transform $\mathcal{W} : L^2(\mathbb{R}^d) \to L^2(\Omega)^{\mathbb{N}}$.

Definition 2.5.2. the semiclassical windowed Bloch transform $\mathcal{W}^{\varepsilon} : L^2(\mathbb{R}^d) \to L^2(\Omega)^{\mathbb{N}}$ is given by,

$$(\mathcal{W}^{\varepsilon}f)_n(\boldsymbol{q},\boldsymbol{p}) = \frac{2^{d/4}}{(2\pi\varepsilon)^{3d/4}}\langle u_n(\boldsymbol{p},\cdot/\varepsilon)G_{\boldsymbol{q},\boldsymbol{p}}^{\varepsilon}, f\rangle = \frac{2^{d/4}}{(2\pi\varepsilon)^{3d/4}}\int_{\mathbb{R}^d}\bar{u}_n(\boldsymbol{p},\boldsymbol{x}/\varepsilon)\bar{G}_{\boldsymbol{q},\boldsymbol{p}}^{\varepsilon}(\boldsymbol{x})f(\boldsymbol{x})\,\mathrm{d}\boldsymbol{x}. \tag{2.23}$$

Similarly we can scale the projection operator $\Pi_n^{\mathcal{W}} : L^2(\mathbb{R}^d) \to L^2(\mathbb{R}^d)$ for each $n \in \mathbb{N}$.

Definition 2.5.3. The projection of $f \in L^2(\mathbb{R}^d)$ onto the nth band space is given by $\Pi_n^{\mathcal{W},\varepsilon} : L^2(\mathbb{R}^d) \to L^2(\mathbb{R}^d)$ for each $n \in \mathbb{N}$ where

$$(\Pi_n^{\mathcal{W},\varepsilon}f)(\boldsymbol{y}) = \frac{2^{d/4}}{(2\pi\varepsilon)^{3d/4}}\iint_{\Omega} u_n(\boldsymbol{\xi},\boldsymbol{y}/\varepsilon)G_{\boldsymbol{x},\boldsymbol{\xi}}^{\varepsilon}(\boldsymbol{y})(\mathcal{W}^{\varepsilon}f)_n(\boldsymbol{x},\boldsymbol{\xi})\,\mathrm{d}\boldsymbol{x}\,\mathrm{d}\boldsymbol{\xi}. \tag{2.24}$$

It follows from (2.14) and a change of variable that $\sum_n \Pi_n^{\mathcal{W},\varepsilon} = \mathrm{Id}_{L^2(\mathbb{R}^d)}$.

18

Chapter 3

Bloch-based frozen Gaussian

approximation

3.1 Bloch-based FGA ansatz

We are now ready to state our ansatz for solving equation (1.9) asymptotically. First, we define the classical Hamiltonian,

$$h_n(\boldsymbol{q}, \boldsymbol{p}) := E_n(\boldsymbol{p}) + U(\boldsymbol{q}) \tag{3.1}$$

for each $n = 1, 2, \cdots$. The corresponding Hamiltonian flow $(\boldsymbol{Q}_n(t, \boldsymbol{q}, \boldsymbol{p}), \boldsymbol{P}_n(\boldsymbol{q}, \boldsymbol{p}))$ and action function $S_n(t, \boldsymbol{q}, \boldsymbol{p})$ satisfy

$$\begin{cases} \dfrac{d\boldsymbol{Q}_n}{dt} = \nabla_{\boldsymbol{P}_n} h_n(\boldsymbol{Q}_n, \boldsymbol{P}_n), \\[2mm] \dfrac{d\boldsymbol{P}_n}{dt} = -\nabla_{\boldsymbol{Q}_n} h_n(\boldsymbol{Q}_n, \boldsymbol{P}_n), \end{cases} \tag{3.2}$$

and

$$\frac{dS_n}{dt} = \boldsymbol{P}_n \cdot \nabla_{\boldsymbol{P}_n} h_n(\boldsymbol{Q}_n, \boldsymbol{P}_n) - h_n(\boldsymbol{Q}_n, \boldsymbol{P}_n), \tag{3.3}$$

on Ω with the initial conditions $\boldsymbol{Q}_n(0, \boldsymbol{q}, \boldsymbol{p}) = \boldsymbol{q}$, $\boldsymbol{P}_n(0, \boldsymbol{q}, \boldsymbol{p}) = \boldsymbol{p}$ and $S_n(0, \boldsymbol{q}, \boldsymbol{p}) = 0$, for each $n = 1, 2, \cdots$.

19

To simplify our equations, we will often omit the parameters $(t, \boldsymbol{q}, \boldsymbol{p})$ in $\boldsymbol{Q}_n(t, \boldsymbol{q}, \boldsymbol{p})$, $\boldsymbol{P}_n(t, \boldsymbol{q}, \boldsymbol{p})$, and $\boldsymbol{S}_n(t, \boldsymbol{q}, \boldsymbol{p})$.

The Bloch-based FGA approximates the solution of the Schrödinger equation (1.9) on the n-th band space to the leading order by

$$\psi_{\mathrm{FGA}}^{\varepsilon,n}(t, \boldsymbol{x}) = [\mathcal{I}^\varepsilon \left(a_{n,0}(t, \boldsymbol{q}, \boldsymbol{p}) u_n(\boldsymbol{P}_n, \boldsymbol{X}) \bar{u}_n(\boldsymbol{p}, \boldsymbol{Y}) \psi_0^\varepsilon\right] (\boldsymbol{x}), \tag{3.4}$$

where ψ_0^ε is the initial condition. More explicitly, at time t, $\psi_{\mathrm{FGA}}^{\varepsilon,n}$ is given by

$$\psi_{\mathrm{FGA}}^\varepsilon(t, \boldsymbol{x}) = \frac{1}{(2\pi\varepsilon)^{3d/2}} \iint_\Omega a_{n,0}(t, \boldsymbol{q}, \boldsymbol{p}) e^{\mathrm{i}S_n(t,\boldsymbol{q},\boldsymbol{p})/\varepsilon} G_{\boldsymbol{Q}_n,\boldsymbol{P}_n}^\varepsilon(\boldsymbol{x}) u_n(\boldsymbol{P}_n, \boldsymbol{x}/\varepsilon)$$

$$\cdot \langle G_{\boldsymbol{q},\boldsymbol{p}}^\varepsilon u_n(\boldsymbol{p}, \cdot/\varepsilon), \psi_0^\varepsilon(\cdot)\rangle \, \mathrm{d}\boldsymbol{q} \, \mathrm{d}\boldsymbol{p}. \tag{3.5}$$

The only term in (3.5) that remains to be specified is the amplitude $a_{n,0}(t, \boldsymbol{q}, \boldsymbol{p})$. It solves the evolution equation

$$\partial_t a_{n,0} = -\mathrm{i}a_{n,0}\mathcal{A}_n(\boldsymbol{P}_n) \cdot \nabla U(\boldsymbol{Q}_n) + \frac{1}{2}a_{n,0} \operatorname{tr}\left(\partial_{\boldsymbol{z}}\boldsymbol{P}_n \, \nabla^2 E(\boldsymbol{P}_n)(Z_n)^{-1}\right)$$

$$- \frac{\mathrm{i}}{2}a_{n,0} \operatorname{tr}\left(\partial_{\boldsymbol{z}}\boldsymbol{Q}_n \, \nabla^2 U(\boldsymbol{Q}_n)(Z_n)^{-1}\right), \tag{3.6}$$

with initial conditions $a_{n,0}(0, \boldsymbol{q}, \boldsymbol{p}) = 2^{d/2}$ for each $(\boldsymbol{q}, \boldsymbol{p})$ and we recall that $\mathcal{A}_n(\boldsymbol{\xi}) = \langle u_n(\boldsymbol{\xi}, \cdot), \mathrm{i}\nabla_{\boldsymbol{\xi}} u_n(\boldsymbol{\xi}, \cdot)\rangle$ is the Berry phase. Here the matrix Z_n associated with the Hamiltonian flow $(\boldsymbol{Q}_n, \boldsymbol{P}_n)$ is defined by

$$Z_n(t, q, p) := \partial_{\boldsymbol{z}}\left(\boldsymbol{Q}_n + \mathrm{i}\boldsymbol{P}_n\right), \tag{3.7}$$

where $\partial_{\boldsymbol{z}} := \partial_{\boldsymbol{q}} - \mathrm{i}\partial_{\boldsymbol{p}}$.

Given any initial condition $\psi_0^\varepsilon \in L^2(\mathbb{R}^2)$, the FGA solution to equation (1.9) is given by

$$\psi_{\mathrm{FGA}}^\varepsilon = \sum_{n=1}^\infty \psi_{\mathrm{FGA}}^{\varepsilon,n}. \tag{3.8}$$

20

The main focus of this thesis is equation (3.8). We will derive and prove that equation (3.8) is a valid asymptotic solution. We will also derive a gauge-invariant algorithm in chapter 8 and apply equation (3.8) to the nonlinear Schrödinger equation with periodic potentials.

3.2 Convergence theorems for the Bloch-based FGA

One of our required assumptions will be that the external potential is subquadratic:

Definition 3.2.1. A potential U is called *subquadratic*, if $\|\partial_{\boldsymbol{x}}^{\alpha} U(\boldsymbol{x})\|_{L^{\infty}}$ is finite for all multi-index $|\alpha| \geqslant 2$.

We now state the main result of this thesis.

Theorem 3.2.1. *Assume that the n-th Bloch band $E_n(\boldsymbol{\xi})$ does not intersect any other Bloch bands for all $\boldsymbol{\xi} \in \Gamma^*$ and the Hamiltonian $h_n(\boldsymbol{x}, \boldsymbol{\xi})$ is subquadratic. Let $\mathscr{U}_t^{\varepsilon}$ be the propagator of the time-dependent Schrödinger equation (1.9) with initial condition $\psi_0^{\varepsilon} \in L^2(\mathbb{R}^d)$. Then for any given T, $0 \leqslant t \leqslant T$ and sufficiently small ε, we have*

$$\sup_{0 \leqslant t \leqslant T} \left\| \mathscr{U}_t^{\varepsilon}\big(\Pi_n^{\mathcal{W},\varepsilon}\psi_0^{\varepsilon}\big) - \mathcal{I}^{\varepsilon}\big(a_{n,0} u_n(\boldsymbol{P}_n, \boldsymbol{x}/\varepsilon)\bar{u}_n(\boldsymbol{p}, \boldsymbol{y}/\varepsilon)\big)\psi_0^{\varepsilon} \right\|_{L^2} \leqslant C_{T,n}\,\varepsilon\,\big\|\psi_0^{\varepsilon}\big\|_{L^2}. \qquad (3.9)$$

Remark. Note that $\psi_{\mathrm{FGA}}^{\varepsilon,n}$ approximates the time evolution of $\Pi_n^{\mathcal{W},\varepsilon}\psi_0^{\varepsilon}$, which is the n-th band contribution to the initial condition in the reconstruction formula (2.14). In particular, if the initial condition is concentrated on the n-th band in the sense that $\psi_0^{\varepsilon} = \Pi_n^{\mathcal{W},\varepsilon}\psi_0^{\varepsilon}$, the theorem states that the solution to (1.9) is approximated by $\psi_{\mathrm{FGA}}^{\varepsilon,n}$ with $\mathcal{O}(\varepsilon)$ error.

Remark. We can also construct higher order approximations by replacing the term $a_{n,0} u_n(\boldsymbol{P}_n, \boldsymbol{x}/\varepsilon)$ with an ε-expansion of the form $b_{n,0} + \varepsilon b_{n,1} + \varepsilon^2 b_{n,2} + \ldots + \varepsilon^{K-1} b_{n,K-1}$ where $b_{n,0} = a_{n,0} u_n(\boldsymbol{P}_n, \boldsymbol{x}/\varepsilon)$. This will give an approximate solution $\psi_{\mathrm{FGA},K}^{\varepsilon,n}$ to $\mathcal{O}(\varepsilon^K)$

21

accuracy. In this thesis we shall focus on the first order approximation and omit the formulation and proof for higher orders.

The proof of Theorem 3.2.1 is given in chapter 7. By linearity of (1.9), we have the following more general statement, as an easy corollary from Theorem 3.2.1.

Theorem 3.2.2. *Assume that the first N Bloch bands $E_n(\boldsymbol{\xi})$, $n = 1, \cdots, N$ do not intersect and are separated from the other bands for all $\boldsymbol{\xi} \in \Gamma^*$; and assume that the Hamiltonian $h_n(\boldsymbol{x}, \boldsymbol{\xi})$ is subquadratic. Let $\mathscr{U}_t^\varepsilon$ be the propagator of the time-dependent Schrödinger equation* (1.9) *with initial condition $\psi_0^\varepsilon \in L^2(\mathbb{R}^d)$. Then for any given T, $0 \leqslant t \leqslant T$ and sufficiently small ε, we have*

$$
\sup_{0 \leqslant t \leqslant T} \left\| \mathscr{U}_t^\varepsilon \psi_0^\varepsilon - \sum_{n=1}^N \mathcal{I}^\varepsilon \big(a_{n,0} u_n(\boldsymbol{P}_n, \boldsymbol{x}/\varepsilon) \bar{u}_n(\boldsymbol{p}, \boldsymbol{y}/\varepsilon) \big) \psi_0^\varepsilon \right\|_{L^2}
$$

$$
\leqslant C_{T,N}\, \varepsilon \big\| \psi_0^\varepsilon \big\|_{L^2} + \left\| \psi_0^\varepsilon - \sum_{n=1}^N \Pi_n^{\mathcal{W},\varepsilon} \psi_0^\varepsilon \right\|_{L^2}. \quad (3.10)
$$

Proof: Taking the short-hand notation $\psi_{0,n}^\varepsilon = \Pi_n^{\mathcal{W},\varepsilon} \psi_0^\varepsilon$ and $\mathscr{V}_{t,n}^\varepsilon = \mathcal{I}^\varepsilon \big(a_{n,0} u_n(\boldsymbol{P}_n, \boldsymbol{x}/\varepsilon) \bar{u}_n(\boldsymbol{p}, \boldsymbol{y}/\varepsilon) \big)$, we have

$$
\left\| \mathscr{U}_t^\varepsilon \psi_0^\varepsilon - \sum_{n=1}^N \mathscr{V}_{t,n}^\varepsilon \psi_0^\varepsilon \right\|_{L^2} = \left\| \mathscr{U}_t^\varepsilon \left(\sum_{n=1}^\infty \psi_{0,n}^\varepsilon \right) - \sum_{n=1}^N \mathscr{V}_{t,n}^\varepsilon \psi_0^\varepsilon \right\|_{L^2}
$$

$$
= \left\| \mathscr{U}_t^\varepsilon \left(\sum_{n=1}^N \psi_{0,n}^\varepsilon \right) + \mathscr{U}_t^\varepsilon \left(\sum_{n=N+1}^\infty \psi_{0,n}^\varepsilon \right) - \sum_{n=1}^N \mathscr{V}_{t,n}^\varepsilon \psi_0^\varepsilon \right\|_{L^2}
$$

$$
\leqslant \left\| \mathscr{U}_t^\varepsilon \left(\sum_{n=1}^N \psi_{0,n}^\varepsilon \right) - \sum_{n=1}^N \mathscr{V}_{t,n}^\varepsilon \psi_0^\varepsilon \right\|_{L^2} + \left\| \mathscr{U}_t^\varepsilon \left(\sum_{n=N+1}^\infty \psi_{0,n}^\varepsilon \right) \right\|_{L^2}
$$

$$
\overset{(3.9)}{\leqslant} \sum_{n=1}^N C_{T,n} \varepsilon \big\| \psi_{n,0}^\varepsilon \big\|_{L^2} + \left\| \sum_{n=N+1}^\infty \psi_0^\varepsilon \right\|_{L^2}
$$

$$
\leqslant C_{T,N} \varepsilon \big\| \psi_0^\varepsilon \big\|_{L^2} + \left\| \psi_0^\varepsilon - \sum_{n=1}^N \Pi_n^{\mathcal{W},\varepsilon} \psi_0^\varepsilon \right\|_{L^2}.
$$

22

3.3 Derivation of the leading order amplitude and higher order corrections

We will now show how to obtain equation (3.6) for $a_{n,0}$. In addition, we will derive an equation for $a_{n,1}$. The calculation techniques used in this section can be used to obtain higher order amplitude corrections.

We will substitute our ansatz and perform matched asymptotic expansion. Let us fix a band $n \in \mathbb{N}$ and consider the ansatz

$$\psi_{\text{FGA},\infty}^{\varepsilon,n} = \frac{1}{(2\pi\varepsilon)^{3d/2}} \iint_{\Omega} b^{\varepsilon}(t, \boldsymbol{X}, \boldsymbol{q}, \boldsymbol{p}) G_{\boldsymbol{Q}_n, \boldsymbol{P}_n}^{\varepsilon} e^{\mathrm{i}S_n/\varepsilon} \langle G_{\boldsymbol{q},\boldsymbol{p}}^{\varepsilon} u_n(\boldsymbol{p}, \cdot/\varepsilon), \psi_0 \rangle \, \mathrm{d}\boldsymbol{q} \, \mathrm{d}\boldsymbol{p}, \qquad (3.11)$$

where the coefficient b^{ε} assumes the asymptotic expansion

$$
\begin{aligned}
b^{\varepsilon}(t, \boldsymbol{X}, \boldsymbol{q}, \boldsymbol{p}) &:= \sum_{j=0}^{\infty} \varepsilon^j b_j(t, \boldsymbol{X}, \boldsymbol{q}, \boldsymbol{p}) \\
&= a_{n,0}(t, \boldsymbol{q}, \boldsymbol{p}) u_n(\boldsymbol{P}_n, \boldsymbol{X}) \\
&\quad + \varepsilon \big(a_{n,1}(t, \boldsymbol{q}, \boldsymbol{p}) u_n(\boldsymbol{P}_n, \boldsymbol{X}) + b_{n,1}^{\perp}(t, \boldsymbol{X}, \boldsymbol{q}, \boldsymbol{p}) \big) \\
&\quad + \varepsilon^2 \big(a_{n,2}(t, \boldsymbol{q}, \boldsymbol{p}) u_n(\boldsymbol{P}_n, \boldsymbol{X}) + b_{n,2}^{\perp}(t, \boldsymbol{X}, \boldsymbol{q}, \boldsymbol{p}) \big) + \sum_{j=3}^{\infty} \varepsilon^j b_j(t, \boldsymbol{X}, \boldsymbol{q}, \boldsymbol{p})
\end{aligned}
$$

$$(3.12)$$

We assume that we are given the classical Hamiltonian $h_n(\boldsymbol{q}, \boldsymbol{p}) = E_n(\boldsymbol{q}, \boldsymbol{p}) + U(\boldsymbol{q})$ and the corresponding flow $(\boldsymbol{Q}_n, \boldsymbol{P}_n)$ and action function S_n.

To make the calculations easier to follow, we will make use of the following Lemma.

Definition 3.3.1. For $f = f(t, \boldsymbol{x}, \boldsymbol{y}, \boldsymbol{q}, \boldsymbol{p})$ and $g = g(t, \boldsymbol{x}, \boldsymbol{y}, \boldsymbol{q}, \boldsymbol{p})$ such that for any t and $\boldsymbol{x}$,

$$f(t, \boldsymbol{x}, \cdot, \cdot, \cdot), g(t, \boldsymbol{x}, \cdot, \cdot, \cdot) \in L^{\infty}(\mathbb{R}^d; \mathcal{S}(\mathbb{R}^d \times \Gamma^*)),$$

we say that f and g are equivalent for the n-th Bloch band, denoted as $f \sim_n g$ if for any

$t \geqslant 0$ and $\Psi_0 \in L^2(\mathbb{R}^d)$

$$\iint_\Omega \int_{\mathbb{R}^d} (f - g)(t, \boldsymbol{x}, \boldsymbol{y}, \boldsymbol{q}, \boldsymbol{p}) G^\varepsilon_{\boldsymbol{Q}_n, \boldsymbol{P}_n} e^{iS_n(t, \boldsymbol{q}, \boldsymbol{p})/\varepsilon} \bar{G}^\varepsilon_{\boldsymbol{q}, \boldsymbol{p}}(\boldsymbol{y}) \Psi_0(\boldsymbol{y}) \, d\boldsymbol{y} \, d\boldsymbol{q} \, d\boldsymbol{p} = 0. \qquad (3.13)$$

Lemma 3.3.2. *For any d-vector function $\boldsymbol{v}(\boldsymbol{y}, \boldsymbol{q}, \boldsymbol{p})$ such that each component is in $L^\infty(\mathbb{R}^d; \mathcal{S}(\mathbb{R}^d \times \Gamma^*))$*

$$\boldsymbol{v}(\boldsymbol{y}, \boldsymbol{q}, \boldsymbol{p}) \cdot (\boldsymbol{x} - \boldsymbol{Q}_n) \sim_n -\varepsilon \partial_{\boldsymbol{z}} \cdot (\boldsymbol{v} Z_n^{-1}), \qquad (3.14)$$

and for any $d \times d$ matrix function $M(\boldsymbol{y}, \boldsymbol{q}, \boldsymbol{p})$ such that each component is in $L^\infty(\mathbb{R}^d; \mathcal{S}(\mathbb{R}^d \times \Gamma^*))$

$$
\begin{aligned}
\operatorname{tr}\left(M(\boldsymbol{y}, \boldsymbol{q}, \boldsymbol{p})(\boldsymbol{x} - \boldsymbol{Q}_n)^2\right) \sim_n & \varepsilon \operatorname{tr}\left(\partial_{\boldsymbol{z}} \boldsymbol{Q}_n M Z_n^{-1}\right) - \varepsilon \operatorname{tr}\left(\partial_{\boldsymbol{z}} M(\boldsymbol{x} - \boldsymbol{Q}_n) Z_n^{-1}\right. \\
& \left. + M(\boldsymbol{x} - \boldsymbol{Q}_n) \partial_{\boldsymbol{z}} Z_n^{-1}\right) \\
= & \varepsilon \operatorname{tr}\left(\partial_{\boldsymbol{z}} \boldsymbol{Q}_n M Z_n^{-1}\right) + \varepsilon^2 \operatorname{tr}\left(\partial_{\boldsymbol{z}}\left(\partial_{\boldsymbol{z}} M (Z_n^{-1})^2\right)\right. \\
& \left. + \partial_{\boldsymbol{z}}\left(M \partial_{\boldsymbol{z}} Z_n^{-1}\right) Z_n^{-1}\right).
\end{aligned}
\qquad (3.15)
$$

Higher order terms can be obtained recursively. In general we have for any multi-index α that $|\alpha| \geqslant 3$,

$$(\boldsymbol{x} - \boldsymbol{Q}_n)^\alpha \sim_n \mathcal{O}\left(\varepsilon^{\lfloor \frac{|\alpha|+1}{2} \rfloor}\right). \qquad (3.16)$$

Proof: The proof of lemma 3.3.2 is similar to [21] Lemma 3.

Computing the partial derivatives of Φ_n (see (2.20)),

$$\partial_{\boldsymbol{q}} \Phi_n = \partial_{\boldsymbol{q}} S_n + (\partial_{\boldsymbol{q}} \boldsymbol{P}_n - i \partial_{\boldsymbol{q}} \boldsymbol{Q}_n) \cdot (\boldsymbol{x} - i \boldsymbol{Q}_n) + \boldsymbol{p} \cdot \mathbf{1} - i(\boldsymbol{y} - \boldsymbol{q}) \cdot \mathbf{1} - \boldsymbol{P}_n \cdot \partial_{\boldsymbol{q}} \boldsymbol{Q}_n \qquad (3.17)$$

$$= (\partial_{\boldsymbol{q}} \boldsymbol{P}_n - i \partial_{\boldsymbol{q}} \boldsymbol{Q}_n) \cdot (\boldsymbol{x} - \boldsymbol{Q}_n) - i(\boldsymbol{y} - \boldsymbol{q}) \cdot \mathbf{1} \qquad \text{(by (2.17))}, \qquad (3.18)$$

$$\partial_{\boldsymbol{p}} \Phi_n = \partial_{\boldsymbol{p}} S_n - \mathbf{1} \cdot (\boldsymbol{y} - \boldsymbol{q}) + (\partial_{\boldsymbol{p}} \boldsymbol{P}_n - \partial_{\boldsymbol{q}} \boldsymbol{Q}_n) \cdot (\boldsymbol{x} - \boldsymbol{Q}_n) - \boldsymbol{P}_n \cdot \partial_{\boldsymbol{q}} \boldsymbol{Q}_n \qquad (3.19)$$

$$= -\mathbf{1} \cdot (\boldsymbol{y} - \boldsymbol{q}) + (\partial_{\boldsymbol{p}} \boldsymbol{P}_n - \partial_{\boldsymbol{q}} \boldsymbol{Q}_n) \cdot (\boldsymbol{x} - \boldsymbol{Q}_n) \qquad \text{(by (2.17))}. \qquad (3.20)$$

24

This implies,

$$i\partial_z \Phi_n = \boldsymbol{Z}_n(\boldsymbol{x} - \boldsymbol{Q}_n). \tag{3.21}$$

$\boldsymbol{Z}_n$ is invertible, this will be shown later in chapter 7 (see proposition 4.2.3). Thus,

$$i\boldsymbol{Z}_n^{-1}\partial_z \Phi_n = (\boldsymbol{x} - \boldsymbol{Q}_n) \tag{3.22}$$

From our previous calculations and integration by parts,

$$\iint_\Omega \int_{\mathbb{R}^d} v \cdot (\boldsymbol{x} - \boldsymbol{Q}_n) e^{\frac{i}{\varepsilon}\Phi_n} d\boldsymbol{y} d\boldsymbol{p} d\boldsymbol{q} = \varepsilon \iint_\Omega \int_{\mathbb{R}^d} v_j Z_{n,j,k}^{-1} \left(\frac{i}{\varepsilon}\partial_{\boldsymbol{z}_k}\Phi_n\right) e^{\frac{i}{\varepsilon}\Phi_n} d\boldsymbol{y} d\boldsymbol{p} d\boldsymbol{q} \tag{3.23}$$

$$= -\varepsilon \iint_\Omega \int_{\mathbb{R}^d} \partial_{\boldsymbol{z}_k}(v_j Z_{n,j,k}^{-1}) e^{\frac{i}{\varepsilon}\Phi_n} d\boldsymbol{y} d\boldsymbol{p} d\boldsymbol{q}. \tag{3.24}$$

This proves (3.14). Equation (3.15) can be proved by using (3.14). Higher order terms can be obtained by recursion.

We digress to compute some derivatives of $H_{\boldsymbol{\xi}}$. Recall the operator $H_{\boldsymbol{\xi}}$,

$$H_{\boldsymbol{\xi}} = \frac{1}{2}(-i\nabla_{\boldsymbol{x}} + \boldsymbol{\xi})^2 + V(\boldsymbol{x}). \tag{3.25}$$

This operator defines $E_n(\boldsymbol{\xi})$ and $u_n(\boldsymbol{\xi}, \boldsymbol{x})$ through

$$H_{\boldsymbol{\xi}} u_n(\boldsymbol{\xi}, \cdot) = E_n(\boldsymbol{\xi}) u_n(\boldsymbol{\xi}, \cdot), \tag{3.26}$$

for each $n = 1, 2, \cdots$.

Differentiating (3.26) with respect to $\boldsymbol{\xi}$ produces

$$H_{\boldsymbol{\xi}} \nabla_{\boldsymbol{\xi}} u_n(\boldsymbol{\xi}, \boldsymbol{x}) + (-i\nabla_{\boldsymbol{x}} + \boldsymbol{\xi}) u_n(\boldsymbol{\xi}, \boldsymbol{x}) = E_n(\boldsymbol{\xi}) \nabla_{\boldsymbol{\xi}} u_n(\boldsymbol{\xi}, \boldsymbol{x}) + \nabla_{\boldsymbol{\xi}} E_n(\boldsymbol{\xi}) u_n(\boldsymbol{\xi}, \boldsymbol{x}). \tag{3.27}$$

Taking inner product with $u_n(\boldsymbol{\xi}, \cdot)$ yields

$$\nabla_{\boldsymbol{\xi}} E_n(\boldsymbol{\xi}) = -i\langle u_n(\boldsymbol{\xi}, \cdot), \nabla_{\boldsymbol{x}} u_n(\boldsymbol{\xi}, \cdot) \rangle + \boldsymbol{\xi}. \tag{3.28}$$

Differentiate (3.27) with respect to $\boldsymbol{\xi}$ again gives

$$H_{\boldsymbol{\xi}} \nabla_{\boldsymbol{\xi}}^2 u_n(\boldsymbol{\xi}, \boldsymbol{x}) + 2(-i\nabla_{\boldsymbol{x}} + \boldsymbol{\xi})\nabla_{\boldsymbol{\xi}} u_n(\boldsymbol{\xi}, \boldsymbol{x}) + u_n(\boldsymbol{\xi}, \boldsymbol{x})I$$

$$= E_n(\boldsymbol{\xi})\nabla_{\boldsymbol{\xi}}^2 u_n(\boldsymbol{\xi}, \boldsymbol{x}) + 2\nabla_{\boldsymbol{\xi}} E_n(\boldsymbol{\xi})\nabla_{\boldsymbol{\xi}} u_n(\boldsymbol{\xi}, \boldsymbol{x}) + E_n(\boldsymbol{\xi})\nabla_{\boldsymbol{\xi}}^2 u_n(\boldsymbol{\xi}, \boldsymbol{x}). \tag{3.29}$$

Taking inner product with $u_n(\boldsymbol{\xi}, \cdot)$, one gets

$$\langle u_n(\boldsymbol{\xi}, \cdot), -\mathrm{i}\nabla_{\boldsymbol{x}}\nabla_{\boldsymbol{\xi}}u_n(\boldsymbol{\xi}, \boldsymbol{x})\rangle + \boldsymbol{\xi}\langle u_n(\boldsymbol{\xi}, \cdot), \nabla_{\boldsymbol{\xi}}u_n(\boldsymbol{\xi}, \cdot)\rangle + I/2$$
$$= \nabla_{\boldsymbol{\xi}}E_n(\boldsymbol{\xi})\langle u_n(\boldsymbol{\xi}, \cdot), \nabla_{\boldsymbol{\xi}}u_n(\boldsymbol{\xi}, \boldsymbol{x})\rangle + \tfrac{1}{2}E_n(\boldsymbol{\xi})\langle u_n(\boldsymbol{\xi}, \cdot), \nabla_{\boldsymbol{\xi}}^2 u_n(\boldsymbol{\xi}, \cdot)\rangle. \quad (3.30)$$

These identities (3.28) and (3.30) will be useful later.

We now substitute (3.11) into the Schrödinger equation. For this we first compute the time and space derivatives on $\psi_{\mathrm{FGA},\infty}^{\varepsilon,n}$:

$$\mathrm{i}\varepsilon\partial_t\psi_{\mathrm{FGA},\infty}^{\varepsilon,n} = \frac{1}{(2\pi\varepsilon)^{3d/2}}\iint_{\Omega}\{\mathrm{i}\varepsilon\partial_t b^{\varepsilon} - (\partial_t S_n - \boldsymbol{P}_n \cdot \partial_t \boldsymbol{Q}_n$$
$$+ (\partial_t \boldsymbol{P}_n - \mathrm{i}\partial_t \boldsymbol{Q}_n) \cdot (\boldsymbol{x} - \boldsymbol{Q}_n))b^{\varepsilon}\} \times G_{\boldsymbol{Q}_n,\boldsymbol{P}_n}^{\varepsilon}e^{\mathrm{i}S_n/\varepsilon} \quad (3.31)$$
$$\times \langle G_{\boldsymbol{q},\boldsymbol{p}}^{\varepsilon}u_n(\boldsymbol{p}, \cdot/\varepsilon), \psi_0\rangle \,\mathrm{d}\boldsymbol{q}\,\mathrm{d}\boldsymbol{p}.$$

$$\tfrac{1}{2}\varepsilon^2\Delta\psi_{\mathrm{FGA},\infty}^{\varepsilon,n} = \frac{1}{(2\pi\varepsilon)^{3d/2}}\iint_{\Omega}\left[-\frac{1}{2}(-\mathrm{i}\nabla_{\boldsymbol{X}} + \boldsymbol{P}_n)^2 b^{\varepsilon} - (\nabla_{\boldsymbol{X}}b^{\varepsilon} + \mathrm{i}b^{\varepsilon}\boldsymbol{P}_n) \cdot (\boldsymbol{x} - \boldsymbol{Q}_n) + \right.$$
$$\left. + \frac{1}{2}b^{\varepsilon}|\boldsymbol{x} - \boldsymbol{Q}_n|^2 - \frac{1}{2}\varepsilon b^{\varepsilon}d\right] \times G_{\boldsymbol{Q}_n,\boldsymbol{P}_n}^{\varepsilon}e^{\mathrm{i}S_n/\varepsilon}\langle G_{\boldsymbol{q},\boldsymbol{p}}^{\varepsilon}u_n(\boldsymbol{p}, \cdot/\varepsilon), \psi_0\rangle \,\mathrm{d}\boldsymbol{q}\,\mathrm{d}\boldsymbol{p}.$$
$$(3.32)$$

Hence, after rearranging terms, we arrive at

$$\left(\mathrm{i}\varepsilon\partial_t + \frac{1}{2}\varepsilon^2\Delta - V(\boldsymbol{X}) - U(\boldsymbol{x})\right)\psi_{\mathrm{FGA},\infty}^{\varepsilon,n} =$$
$$= \frac{1}{(2\pi\varepsilon)^{3d/2}}\iint_{\Omega}\left\{\left[-\frac{1}{2}(-\mathrm{i}\nabla_{\boldsymbol{X}} + \boldsymbol{P}_n)^2 - V(\boldsymbol{X}) - U(\boldsymbol{x}) - \partial_t S_n\right]b^{\varepsilon} + \right.$$
$$+ \varepsilon\left(\mathrm{i}\partial_t b^{\varepsilon} - \frac{1}{2}b^{\varepsilon}d\right) - [(\nabla_{\boldsymbol{X}}b^{\varepsilon} + \mathrm{i}b^{\varepsilon}\boldsymbol{P}_n) + (\partial_t \boldsymbol{P}_n - \mathrm{i}\partial_t \boldsymbol{Q}_n)b^{\varepsilon}] \cdot (\boldsymbol{x} - \boldsymbol{Q}_n) +$$
$$\left. + \frac{1}{2}|\boldsymbol{x} - \boldsymbol{Q}_n|^2 b^{\varepsilon} + \boldsymbol{P}_n \cdot \partial_t \boldsymbol{Q}_n b^{\varepsilon}\right\}G_{\boldsymbol{Q}_n,\boldsymbol{P}_n}^{\varepsilon}e^{\mathrm{i}S_n/\varepsilon}\langle G_{\boldsymbol{q},\boldsymbol{p}}^{\varepsilon}u_n(\boldsymbol{p}, \cdot/\varepsilon), \psi_0\rangle \,\mathrm{d}\boldsymbol{q}\,\mathrm{d}\boldsymbol{p}.$$
$$(3.33)$$

Define

$$f_n(t,\boldsymbol{x},\boldsymbol{y},\boldsymbol{q},\boldsymbol{p}) = \left\{\left[-\frac{1}{2}(-\mathrm{i}\nabla_{\boldsymbol{X}}+\boldsymbol{P}_n)^2 - V(\boldsymbol{X}) - U(\boldsymbol{x}) - \partial_t S_n\right]b^\varepsilon +\right.$$

$$+ \varepsilon\big(\mathrm{i}\partial_t b^\varepsilon - \frac{1}{2}b^\varepsilon d\big) - [(\nabla_{\boldsymbol{X}}b^\varepsilon + \mathrm{i}b^\varepsilon \boldsymbol{P}_n) + (\partial_t \boldsymbol{P}_n - \mathrm{i}\partial_t \boldsymbol{Q}_n)b^\varepsilon]\cdot(\boldsymbol{x}-\boldsymbol{Q}_n)+$$

$$\left.+ \frac{1}{2}|\boldsymbol{x}-\boldsymbol{Q}_n|^2 b^\varepsilon + \boldsymbol{P}_n\cdot\partial_t\boldsymbol{Q}_n b^\varepsilon\right\}\bar{u}_n(\boldsymbol{p},\boldsymbol{Y}),$$

(3.34)

then we can write

$$\big(\mathrm{i}\varepsilon\partial_t + \frac{1}{2}\varepsilon^2\Delta - V(\boldsymbol{X}) - U(\boldsymbol{x})\big)\psi_{\mathrm{FGA},\infty}^{\varepsilon,n} =$$

$$= \frac{1}{(2\pi\varepsilon)^{3d/2}}\iint_\Omega\int_{\mathbb{R}^d}f_n(t,\boldsymbol{x},\boldsymbol{y},\boldsymbol{p},\boldsymbol{q})G_{\boldsymbol{Q}_n,\boldsymbol{P}_n}^\varepsilon e^{\mathrm{i}S_n/\varepsilon}\bar{G}_{\boldsymbol{q},\boldsymbol{p}}^\varepsilon(\boldsymbol{y})\psi_0(\boldsymbol{y})\,\mathrm{d}\boldsymbol{y}\,\mathrm{d}\boldsymbol{q}\,\mathrm{d}\boldsymbol{p}. \quad (3.35)$$

Applying Lemma 3.3.2 and adding and subtracting $U(\boldsymbol{Q}_n)$, we get

$$f_n \sim_n \Big(-\frac{1}{2}(-\mathrm{i}\nabla_{\boldsymbol{X}}+\boldsymbol{P}_n)^2 - V(\boldsymbol{X}) - (U(\boldsymbol{x})-U(\boldsymbol{Q}_n)) - \partial_t S_n\Big)b^\varepsilon\bar{u}_n(\boldsymbol{p},\boldsymbol{Y})$$

$$+ \varepsilon\big(\mathrm{i}\partial_t b^\varepsilon - \frac{1}{2}b^\varepsilon d\big)\bar{u}_n(\boldsymbol{p},\boldsymbol{Y})$$

$$+ \varepsilon\partial_{\boldsymbol{z}}\Big([(\nabla_{\boldsymbol{X}}b^\varepsilon + \mathrm{i}b^\varepsilon\boldsymbol{P}_n) + (\partial_t\boldsymbol{P}_n - \mathrm{i}\partial_t\boldsymbol{Q}_n)b^\varepsilon]\,\bar{u}_n(\boldsymbol{p},\boldsymbol{Y})Z_n^{-1}\Big)$$

$$+ \varepsilon\frac{1}{2}b^\varepsilon\,\mathrm{tr}\big[\partial_{\boldsymbol{z}}\boldsymbol{Q}_n Z_n^{-1}\big]\,\bar{u}_n(\boldsymbol{p},\boldsymbol{Y}) + \varepsilon^2\frac{1}{2}\,\mathrm{tr}\big[\partial_{\boldsymbol{z}}\big(\partial_{\boldsymbol{z}}\big(b^\varepsilon\bar{u}_n(\boldsymbol{p},\boldsymbol{Y})Z_n^{-1}\big)Z_n^{-1}\big)\big]$$

$$+ \boldsymbol{P}_n\cdot\partial_t\boldsymbol{Q}_n b^\varepsilon\bar{u}_n(\boldsymbol{p},\boldsymbol{Y}) - U(\boldsymbol{Q}_n)b^\varepsilon\bar{u}_n(\boldsymbol{p},\boldsymbol{Y})$$

(3.36)

We use the Taylor expansion of $U(\boldsymbol{x})$ about $\boldsymbol{Q}_n$ up to order 4 as this will allow us to derive equations for a_0 and a_1. To obtain higher order corrections to the amplitude, one should include more terms in the Taylor series.

$$(U(\boldsymbol{x})-U(\boldsymbol{Q}_n)) = \nabla U(\boldsymbol{Q}_n)(\boldsymbol{x}-\boldsymbol{Q}_n) + \frac{1}{2!}\,\mathrm{tr}\big[\nabla^2 U(\boldsymbol{Q}_n)(\boldsymbol{x}-\boldsymbol{Q}_n)^2\big]+$$

$$\frac{1}{3!}\,\mathrm{tr}\big[\nabla^3 U(\boldsymbol{Q}_n)(\boldsymbol{x}-\boldsymbol{Q}_n)^3\big] + \frac{1}{4!}\,\mathrm{tr}\big[\nabla^4 U(\boldsymbol{Q}_n)(\boldsymbol{x}-\boldsymbol{Q}_n)^4\big] + \left(\sum_{|\alpha|=5}R_\alpha(\boldsymbol{x})(\boldsymbol{x}-\boldsymbol{Q}_n)^\alpha\right)\bigg\}$$

(3.37)

27

with

$$R_\alpha(\boldsymbol{x}) = \frac{|\alpha|}{5!} \int_0^1 (1-\tau)^{|\alpha|-1} \partial_{\boldsymbol{Q}_n}^\alpha U(\boldsymbol{Q}_n + \tau(\boldsymbol{x} - \boldsymbol{Q}_n)) d\tau. \tag{3.38}$$

From now on, let us denote the remainder term in (3.37) by $R(\boldsymbol{x}, \boldsymbol{q}, \boldsymbol{p})$.

Applying Lemma 3.3.2 again to (3.36) together with (3.37), we obtain

$$
\begin{aligned}
f_n \sim_n \Big(&-\frac{1}{2}(-\mathrm{i}\nabla_{\boldsymbol{X}} + \boldsymbol{P}_n)^2 - V(\boldsymbol{X}) - \partial_t S_n \Big) b^\varepsilon \bar{u}_n(\boldsymbol{p}, \boldsymbol{Y}) \\
&+ \boldsymbol{P}_n \cdot \partial_t \boldsymbol{Q}_n b^\varepsilon \bar{u}_n(\boldsymbol{p}, \boldsymbol{Y}) - U(\boldsymbol{Q}_n) b^\varepsilon \bar{u}_n(\boldsymbol{p}, \boldsymbol{Y}) \\
&+ \varepsilon \Big(\mathrm{i}\partial_t b^\varepsilon - \frac{1}{2} b^\varepsilon d \Big) \bar{u}_n(\boldsymbol{p}, \boldsymbol{Y}) + \varepsilon \partial_{\boldsymbol{z}} \left(\nabla U(\boldsymbol{Q}_n) b^\varepsilon \bar{u}_n(\boldsymbol{p}, \boldsymbol{Y}) Z_n^{-1} \right) \\
&+ \varepsilon \partial_{\boldsymbol{z}} \left(\left[(\nabla_{\boldsymbol{X}} b^\varepsilon + \mathrm{i} b^\varepsilon \boldsymbol{P}_n) + (\partial_t \boldsymbol{P}_n - \mathrm{i}\partial_t \boldsymbol{Q}_n) b^\varepsilon \right] \bar{u}_n(\boldsymbol{p}, \boldsymbol{Y}) Z_n^{-1} \right) \\
&+ \varepsilon \frac{1}{2!} \operatorname{tr} \left[\partial_{\boldsymbol{z}} \boldsymbol{Q}_n (I - \nabla^2 U(\boldsymbol{Q}_n)) b^\varepsilon \bar{u}_n(\boldsymbol{p}, \boldsymbol{Y}) Z_n^{-1} \right] \\
&+ \varepsilon^2 \frac{1}{2!} \operatorname{tr} \left[\partial_{\boldsymbol{z}} (\partial_{\boldsymbol{z}} ((I - \nabla^2 U(\boldsymbol{Q}_n)) b^\varepsilon \bar{u}_n(\boldsymbol{p}, \boldsymbol{Y}) Z_n^{-1}) Z_n^{-1}) \right] \\
&+ \varepsilon^2 \frac{2}{3!} \operatorname{tr} \left[\partial_{\boldsymbol{z}} (\partial_{\boldsymbol{z}} \boldsymbol{Q}_n \nabla^3 U(\boldsymbol{Q}_n) b^\varepsilon \bar{u}_n(\boldsymbol{p}, \boldsymbol{Y}) (Z_n^{-1})^2) \right] \\
&+ \varepsilon^2 \frac{1}{3!} \operatorname{tr} \left[\partial_{\boldsymbol{z}} \boldsymbol{Q}_n \partial_{\boldsymbol{z}} (\nabla^3 U(\boldsymbol{Q}_n) b^\varepsilon \bar{u}_n(\boldsymbol{p}, \boldsymbol{Y}) Z_n^{-1}) Z_n^{-1} \right] \\
&- \varepsilon^2 \frac{3}{4!} \operatorname{tr} \left[(\partial_{\boldsymbol{z}} \boldsymbol{Q}_n)^2 \nabla^4 U(\boldsymbol{Q}_n) b^\varepsilon \bar{u}_n(\boldsymbol{p}, \boldsymbol{Y}) (Z_n^{-1})^2 \right] + R(\boldsymbol{x}, \boldsymbol{q}, \boldsymbol{p}) b^\varepsilon \bar{u}_{n,\boldsymbol{p}}(\boldsymbol{Y}).
\end{aligned}
\tag{3.39}
$$

Let us define three operators L_0^n, L_1^n, and L_2^n acting on $\phi = \phi(t, \boldsymbol{x}, \boldsymbol{y}, \boldsymbol{q}, \boldsymbol{p})$ by

$$
\begin{aligned}
L_0^n(\phi) :=& \Big(-\frac{1}{2}(-\mathrm{i}\nabla_{\boldsymbol{X}} + \boldsymbol{P}_n)^2 - V(\boldsymbol{X}) - \partial_t S_n \Big) \phi \\
&+ \boldsymbol{P}_n \cdot \partial_t \boldsymbol{Q}_n \phi - U(\boldsymbol{Q}_n) \phi \\
=& \left(-H_{\boldsymbol{P}_n} + E_n(\boldsymbol{P}_n) \right) \phi,
\end{aligned}
\tag{3.40}
$$

$$
\begin{aligned}
L_1^n(\phi) :=& \Big(\mathrm{i}\partial_t \phi - \frac{1}{2}\phi d \Big) + \partial_{\boldsymbol{z}} \left(\nabla U(\boldsymbol{Q}_n) \phi Z_n^{-1} \right) \\
&+ \partial_{\boldsymbol{z}} \left(\left[(\nabla_{\boldsymbol{X}} \phi + \mathrm{i}\phi \boldsymbol{P}_n) + (\partial_t \boldsymbol{P}_n - \mathrm{i}\partial_t \boldsymbol{Q}_n) \phi \right] Z_n^{-1} \right) \\
&+ \frac{1}{2!} \operatorname{tr} \left[\partial_{\boldsymbol{z}} \boldsymbol{Q}_n (I - \nabla^2 U(\boldsymbol{Q}_n)) \phi Z_n^{-1} \right],
\end{aligned}
\tag{3.41}
$$

28

and

$$L_2^n(\phi) := \frac{1}{2!} \operatorname{tr} \left[\partial_{\boldsymbol{z}}(\partial_{\boldsymbol{z}}((I - \nabla^2 U(\boldsymbol{Q}_n))\phi Z_n^{-1})Z_n^{-1}) \right] \tag{3.42}$$

$$+ \frac{2}{3!} \operatorname{tr} \left[\partial_{\boldsymbol{z}}(\partial_{\boldsymbol{z}}\boldsymbol{Q}_n \nabla^3 U(\boldsymbol{Q}_n)\phi(Z_n^{-1})^2) \right]$$

$$+ \frac{1}{3!} \operatorname{tr} \left[\partial_{\boldsymbol{z}}\boldsymbol{Q}_n \partial_{\boldsymbol{z}}(\nabla^3 U(\boldsymbol{Q}_n)\phi Z_n^{-1})Z_n^{-1} \right]$$

$$- \frac{3}{4!} \operatorname{tr} \left[(\partial_{\boldsymbol{z}}\boldsymbol{Q}_n)^2 \nabla^4 U(\boldsymbol{Q}_n)\phi(Z_n^{-1})^2 \right].$$

We thus arrive at

$$\left(\mathrm{i}\varepsilon\partial_t + \tfrac{1}{2}\varepsilon^2\Delta - V(\boldsymbol{X}) - U(\boldsymbol{x}) \right) \psi_{\mathrm{FGA},\infty}^{\varepsilon,n}$$

$$= \frac{1}{(2\pi\varepsilon)^{3d/2}} \iint_\Omega \int_{\mathbb{R}^d} \{ L_0^n(b^\varepsilon \bar{u}_n(\boldsymbol{p}, \boldsymbol{Y})) + \varepsilon L_1^n(b^\varepsilon \bar{u}_n(\boldsymbol{p}, \boldsymbol{Y}))$$

$$+ \varepsilon^2 L_2^n(b^\varepsilon \bar{u}_n(\boldsymbol{p}, \boldsymbol{Y})) + R(\boldsymbol{x}, \boldsymbol{q}, \boldsymbol{p})b^\varepsilon \bar{u}_n(\boldsymbol{p}, \boldsymbol{Y}) \} G_{\boldsymbol{Q}_n, \boldsymbol{P}_n}^\varepsilon e^{\mathrm{i}S_n/\varepsilon} \bar{G}_{\boldsymbol{q}, \boldsymbol{p}}^\varepsilon(\boldsymbol{y})\psi_0(\boldsymbol{y}) \, \mathrm{d}\boldsymbol{y} \, \mathrm{d}\boldsymbol{q} \, \mathrm{d}\boldsymbol{p}. \quad (3.43)$$

Note that by the choice $b_{n,0} = a_{n,0}u_n(\boldsymbol{P}_n, \boldsymbol{X})$, the $\mathcal{O}(1)$ term in the integrand on the right hand side of (3.43) vanishes as

$$L_0^n(a_{n,0}(t, \boldsymbol{q}, \boldsymbol{p})u_n(\boldsymbol{p}, \boldsymbol{X})) = a_{n,0}(t, \boldsymbol{q}, \boldsymbol{p})\left(-H_{\boldsymbol{P}_n} + E_n(\boldsymbol{P}_n) \right)u_n(\boldsymbol{P}_n, \boldsymbol{X}) = 0 \tag{3.44}$$

for any $a_{n,0}$.

3.3.1 Leading order term $b_{n,0}$

To determine $a_{n,0}$, we set the order $\mathcal{O}(\varepsilon)$ term on the right hand side of (3.43) to zero and get

$$L_0^n(b_{n,1}\bar{u}_n(\boldsymbol{p}, \boldsymbol{Y})) = -L_1^n(b_{n,0}\bar{u}_n(\boldsymbol{p}, \boldsymbol{Y})). \tag{3.45}$$

We multiply the equation by $\bar{u}_n(\boldsymbol{P}_n, \boldsymbol{X})$ and integrate over Γ; this gives

$$\partial_t a_{n,0} = \frac{1}{2}a_{n,0} \operatorname{tr} \left(\partial_{\boldsymbol{z}}\boldsymbol{P}_n(\nabla_{\boldsymbol{P}_n}^2 E_n)Z_n^{-1} \right) - \mathrm{i}a_{n,0}\mathcal{A}(\boldsymbol{P}_n) \cdot \nabla_{\boldsymbol{Q}_n} U$$

$$- \frac{\mathrm{i}}{2}a_{n,0} \operatorname{tr}(\partial_{\boldsymbol{z}}\boldsymbol{Q}_n(\nabla_{\boldsymbol{Q}_n}^2 U)Z_n^{-1}). \tag{3.46}$$

29

Indeed, by integration, we get

$$\int_\Gamma \bar{u}_n(\boldsymbol{P}_n, \boldsymbol{X})\left(-\tfrac{1}{2}(-\mathrm{i}\nabla_{\boldsymbol{X}} + \boldsymbol{P}_n)^2 - V(\boldsymbol{X}) - \partial_t S_n\right)b_1\bar{u}_n(\boldsymbol{p}, \boldsymbol{Y})\,\mathrm{d}\boldsymbol{X}$$

$$+ \int_\Gamma \Big\{ \bar{u}_n(\boldsymbol{P}_n, \boldsymbol{X})\big(\mathrm{i}\partial_t b_0 - \frac{1}{2}b_0 d\big)\bar{u}_n(\boldsymbol{p}, \boldsymbol{Y}) + \bar{u}_n(\boldsymbol{P}_n, \boldsymbol{X})\partial_{\boldsymbol{z}}\left(\nabla U(\boldsymbol{Q}_n)b_0\bar{u}_n(\boldsymbol{p}, \boldsymbol{Y})Z_n^{-1}\right)$$

$$+ \bar{u}_n(\boldsymbol{P}_n, \boldsymbol{X})\partial_{\boldsymbol{z}}\Big([(\nabla_{\boldsymbol{X}} b_0 + \mathrm{i}b_0\boldsymbol{P}_n) + (\partial_t\boldsymbol{P}_n - \mathrm{i}\partial_t\boldsymbol{Q}_n)b_0]\,\bar{u}_n(\boldsymbol{p}, \boldsymbol{Y})Z_n^{-1}\Big)$$

$$+ \bar{u}_n(\boldsymbol{P}_n, \boldsymbol{X})\frac{1}{2!}\operatorname{tr}\left[\partial_{\boldsymbol{z}}\boldsymbol{Q}_n(I - \nabla^2 U(\boldsymbol{Q}_n))b_0\bar{u}_n(\boldsymbol{p}, \boldsymbol{Y})Z_n^{-1}\right]\Big\}\,\mathrm{d}\boldsymbol{X} = 0. \tag{3.47}$$

The perpendicular terms in the b_j's will now drop out and we can simplify this equation to

$$-\left\langle u_n(\boldsymbol{P}_n, \boldsymbol{X}), \partial_{\boldsymbol{z}}\left([\mathrm{i}u_n(\boldsymbol{P}_n, \boldsymbol{X})\nabla_{\boldsymbol{P}_n}E_n - \nabla_{\boldsymbol{X}}u_n(\boldsymbol{P}_n, \boldsymbol{X}) - \mathrm{i}u_n(\boldsymbol{P}_n, \boldsymbol{X})\boldsymbol{P}_n]\times \right.\right.$$

$$\left.\left. a_0\bar{u}_n(\boldsymbol{p}, \boldsymbol{Y})Z_n^{-1}\right)\right\rangle$$

$$+ \left(\mathrm{i}\partial_t a_0 - a_0\mathcal{A}(\boldsymbol{P}_n)\cdot\nabla_{\boldsymbol{Q}_n}U - \frac{d}{2}a_0\right)\bar{u}_n(\boldsymbol{p}, \boldsymbol{Y}) \tag{3.48}$$

$$+ \frac{1}{2}a_0\operatorname{tr}(\partial_{\boldsymbol{z}}\boldsymbol{Q}_n(I - \nabla^2_{\boldsymbol{Q}_n}U)Z_n^{-1})\bar{u}_n(\boldsymbol{p}, \boldsymbol{Y}) = 0.$$

Using (3.28), we observe that

$$\left\langle u_n(\boldsymbol{P}_n, \boldsymbol{X}), [\mathrm{i}u_n(\boldsymbol{P}_n, \boldsymbol{X})\nabla_{\boldsymbol{P}_n}E_n - \nabla_{\boldsymbol{X}}u_n(\boldsymbol{P}_n, \boldsymbol{X}) - \mathrm{i}u_n(\boldsymbol{P}_n, \boldsymbol{X})\boldsymbol{P}_n]\cdot\right.$$

$$\left.\partial_z(a_0\bar{u}_n(\boldsymbol{P}_n, \boldsymbol{Y})Z_n^{-1})\right\rangle = 0. \tag{3.49}$$

Hence, we arrive at

$$a_0\operatorname{tr}\big(\langle u_n(\boldsymbol{P}_n, \boldsymbol{X}), \partial_{\boldsymbol{z}}\cdot[\mathrm{i}u_n(\boldsymbol{P}_n, \boldsymbol{X})\nabla_{\boldsymbol{P}_n}E_n - \nabla_{\boldsymbol{X}}u_n(\boldsymbol{P}_n, \boldsymbol{X}) - \mathrm{i}u_n(\boldsymbol{P}_n, \boldsymbol{X})\boldsymbol{P}_n]\rangle Z_n^{-1}\big)$$

$$+ \left(\mathrm{i}\partial_t a_0 - a_0\mathcal{A}(\boldsymbol{P}_n)\cdot\nabla_{\boldsymbol{Q}_n}U - \frac{d}{2}a_0\right) + \frac{1}{2}a_0\operatorname{tr}\big(\partial_{\boldsymbol{z}}\boldsymbol{Q}_n(I - \nabla^2_{\boldsymbol{Q}_n}U)Z_n^{-1}\big) = 0. \tag{3.50}$$

To further simplify the equation, observe that

$$
\Big\langle u_n(\boldsymbol{P}_n, \boldsymbol{X}), \partial_{\boldsymbol{z}} \cdot [\mathrm{i} u_n(\boldsymbol{P}_n, \boldsymbol{X}) \nabla_{\boldsymbol{P}_n} E_n - \nabla_{\boldsymbol{X}} u_n(\boldsymbol{P}_n, \boldsymbol{X}) - \mathrm{i} u_n(\boldsymbol{P}_n, \boldsymbol{X}) \boldsymbol{P}_n] \Big\rangle
$$

$$
= \mathrm{i} \langle u_n(\boldsymbol{P}_n, \boldsymbol{X}), \partial_{\boldsymbol{z}} u_n(\boldsymbol{P}_n, \boldsymbol{X}) \rangle (\nabla_{\boldsymbol{P}_n} E_n - \boldsymbol{P}_n)
$$

$$
- \langle u_n(\boldsymbol{P}_n, \boldsymbol{X}), \partial_{\boldsymbol{z}} \nabla_{\boldsymbol{X}} u_n(\boldsymbol{P}_n, \boldsymbol{X}) \rangle + \mathrm{i}(\partial_{\boldsymbol{z}} \nabla_{\boldsymbol{P}_n} E_n - \partial_{\boldsymbol{z}} \boldsymbol{P}_n) \tag{3.51}
$$

$$
= \mathrm{i} \partial_{\boldsymbol{z}} \boldsymbol{P}_n \langle u_n(\boldsymbol{P}_n, \boldsymbol{X}), \partial_{\boldsymbol{P}_n} u_n(\boldsymbol{P}_n, \boldsymbol{X}) \rangle (\nabla_{\boldsymbol{P}_n} E_n - \boldsymbol{P}_n)
$$

$$
- \partial_{\boldsymbol{z}} \boldsymbol{P}_n \langle u_n(\boldsymbol{P}_n, \boldsymbol{X}), \nabla_{\boldsymbol{p}} \nabla_{\boldsymbol{X}} u_n(\boldsymbol{P}_n, \boldsymbol{X}) \rangle_\Gamma + \mathrm{i} \partial_{\boldsymbol{z}} \boldsymbol{P}_n (\nabla^2_{\boldsymbol{P}_n} E_n - I)
$$

$$
\overset{(3.30)}{=} \frac{1}{2} \mathrm{i} \partial_{\boldsymbol{z}} \boldsymbol{P}_n (\nabla^2_{\boldsymbol{P}_n} E_n - I).
$$

Putting this into (3.50), we have

$$
\frac{1}{2} \mathrm{i} a_0 \operatorname{tr} \left(\partial_{\boldsymbol{z}} \boldsymbol{P}_n (I - \nabla^2_{\boldsymbol{P}_n} E_n) Z^{-1} \right) + \left(\mathrm{i} \partial_t a_0 - a_0 \mathcal{A}(\boldsymbol{P}_n) \cdot \nabla_{\boldsymbol{Q}_n} U - \frac{d}{2} a_0 \right)
$$

$$
+ \frac{1}{2} a_0 \operatorname{tr}(\partial_{\boldsymbol{z}} \boldsymbol{Q}_n (I - \nabla^2_{\boldsymbol{Q}_n} U) Z_n^{-1})] = 0. \tag{3.52}
$$

We arrive at (3.46) finally by noting that

$$
\frac{1}{2} a \operatorname{tr} \left[\partial_{\boldsymbol{z}} \boldsymbol{Q}_n Z_n^{-1} \right] + \frac{\mathrm{i}}{2} a \operatorname{tr} \left[\partial_{\boldsymbol{z}} \boldsymbol{P}_n Z_n^{-1} \right] = \frac{1}{2} a \operatorname{tr} \left[Z_n Z_n^{-1} \right] = \frac{d}{2} a. \tag{3.53}
$$

3.3.2 Next order term $b_{n,1}$

To characterize $b_{n,1}$, we set the order $\mathcal{O}(\varepsilon^2)$ term in (3.43) to zero, we have

$$
\int_\Gamma \bar{u}_n(\boldsymbol{P}_n, \boldsymbol{X}) \left(L_0^n(b_{n,2} \bar{u}_n(\boldsymbol{p}, \boldsymbol{Y})) + L_1^n(b_{n,1} \bar{u}_n(\boldsymbol{p}, \boldsymbol{Y})) + L_2^n(b_{n,0} \bar{u}_n(\boldsymbol{p}, \boldsymbol{Y})) \right) d\boldsymbol{X} = 0.
$$

$$
\tag{3.54}
$$

Let us first derive the equation for a_1. We start with (3.54) written in expanded form

$$
\int_\Gamma \bar{u}_n(\boldsymbol{P}_n, \boldsymbol{X}) \Big\{ \frac{1}{2!} \operatorname{tr} \big[\partial_{\boldsymbol{z}}(\partial_{\boldsymbol{z}}((I - \nabla^2 U(\boldsymbol{Q}_n)) b_0 \bar{u}_n(\boldsymbol{p}, \boldsymbol{Y}) Z_n^{-1}) Z_n^{-1}) \big]
$$

$$
+ \frac{2}{3!} \operatorname{tr} \big[\partial_{\boldsymbol{z}}(\partial_{\boldsymbol{z}} \boldsymbol{Q}_n \nabla^3 U(\boldsymbol{Q}_n) b_0 \bar{u}_n(\boldsymbol{p}, \boldsymbol{Y})(Z_n^{-1})^2) \big]
$$

$$
+ \frac{1}{3!} \operatorname{tr} \big[\partial_{\boldsymbol{z}} \boldsymbol{Q}_n \partial_{\boldsymbol{z}}(\nabla^3 U(\boldsymbol{Q}_n) b_0 \bar{u}_n(\boldsymbol{p}, \boldsymbol{Y}) Z_n^{-1}) Z_n^{-1} \big]
$$

$$
- \frac{3}{4!} \operatorname{tr} \big[(\partial_{\boldsymbol{z}} \boldsymbol{Q}_n)^2 \nabla^4 U(\boldsymbol{Q}_n) b_0 \bar{u}_n(\boldsymbol{p}, \boldsymbol{Y})(Z_n^{-1})^2 \big] \tag{3.55}
$$

$$
+ \big(\mathrm{i} \partial_t b_1 - \frac{1}{2} b_1 d \big) \bar{u}_n(\boldsymbol{p}, \boldsymbol{Y}) + \partial_{\boldsymbol{z}} \big(\nabla U(\boldsymbol{Q}_n) b_1 \bar{u}_n(\boldsymbol{p}, \boldsymbol{Y}) Z_n^{-1} \big)
$$

$$
+ \partial_{\boldsymbol{z}} \big([(\nabla_{\boldsymbol{X}} b_1 + \mathrm{i} b_1 \boldsymbol{P}_n) + (\partial_t \boldsymbol{P}_n - \mathrm{i} \partial_t \boldsymbol{Q}_n) b_1] \, \bar{u}_n(\boldsymbol{p}, \boldsymbol{Y}) Z_n^{-1} \big)
$$

$$
+ \frac{1}{2!} \operatorname{tr} \big[\partial_{\boldsymbol{z}} \boldsymbol{Q}_n (I - \nabla^2 U(\boldsymbol{Q}_n)) b_1 \bar{u}_n(\boldsymbol{p}, \boldsymbol{Y}) Z_n^{-1} \big]
$$

$$
+ (-H_{\boldsymbol{P}_n} + E(\boldsymbol{P}_n)) b_2 \bar{u}_n(\boldsymbol{p}, \boldsymbol{Y}) \Big\} \, d\boldsymbol{X} = 0.
$$

Making use of the Hamiltonian flow (3.2) and the identity (3.49), we arrive at

$$
- \operatorname{tr} \Big(\langle u_{\boldsymbol{P}_n}, \partial_{\boldsymbol{z}} \cdot [u(\mathrm{i} \nabla E_n(\boldsymbol{P}_n)) - \nabla_{\boldsymbol{X}} u - \mathrm{i} u \boldsymbol{P}_n](a_1) \rangle Z_n^{-1} \Big)
$$

$$
+ \Big(\mathrm{i} \partial_t a_1 - a_1 \mathcal{A}(\boldsymbol{P}_n) \cdot \nabla_{\boldsymbol{Q}_n} U - \frac{d}{2} a_1 \Big) + a_0 \frac{1}{2} \operatorname{tr} \Big(\partial_{\boldsymbol{z}}(\partial_{\boldsymbol{z}}[(I - \nabla^2_{\boldsymbol{Q}_n} U) Z_n^{-1}] Z_n^{-1}) \Big)
$$

$$
+ a_1 \frac{1}{2} \operatorname{tr} \Big(\partial_{\boldsymbol{z}} \boldsymbol{Q}_n (I - \nabla^2_{\boldsymbol{Q}_n} U) Z_n^{-1} \Big) + \frac{2}{3!} a_0 \operatorname{tr} \Big(\partial_{\boldsymbol{z}}(\partial_{\boldsymbol{z}} \boldsymbol{Q}_n \nabla^3_{\boldsymbol{Q}_n} U (Z_n^{-1})^2) \Big)
$$

$$
+ \frac{1}{3!} a_0 \operatorname{tr} \Big(\partial_{\boldsymbol{z}} \boldsymbol{Q}_n \partial_{\boldsymbol{z}}(\nabla^3_{\boldsymbol{Q}_n} U Z_n^{-1}) Z_n^{-1} \Big) - \frac{3}{4!} a_0 \operatorname{tr} \Big((\partial_{\boldsymbol{z}} \boldsymbol{Q}_n)^2 \nabla^4_{\boldsymbol{Q}_n} U (Z_n^{-1})^2 \Big) = 0. \tag{3.56}
$$

Then using (3.51) and (3.53), upon simplification we obtain the equation for $a_{n,1}$

$$
\partial_t a_{n,1} = -\mathrm{i} a_{n,1} \mathcal{A}(\boldsymbol{P}_n) \cdot \nabla_{\boldsymbol{Q}_n} U + \frac{1}{2} a_{n,1} \operatorname{tr} \big(\partial_{\boldsymbol{z}} \boldsymbol{P}_n (\nabla^2_{\boldsymbol{P}_n} E_n) Z_n^{-1} \big)
$$

$$
- \frac{\mathrm{i}}{2} a_{n,1} \operatorname{tr} \Big(\partial_{\boldsymbol{z}} \boldsymbol{Q}_n (\nabla^2_{\boldsymbol{Q}_n} U) Z_n^{-1} \Big) + \frac{\mathrm{i}}{2} a_{n,0} \operatorname{tr} \Big(\partial_{\boldsymbol{z}}(\partial_{\boldsymbol{z}}[(I - \nabla^2_{\boldsymbol{Q}_n} U) Z_n^{-1}] Z_n^{-1}) \Big)
$$

$$
+ \frac{2\mathrm{i}}{3!} a_{n,0} \operatorname{tr} \Big(\partial_{\boldsymbol{z}}(\partial_{\boldsymbol{z}} \boldsymbol{Q}_n \nabla^3_{\boldsymbol{Q}_n} U (Z_n^{-1})^2) \Big) + \frac{\mathrm{i}}{3!} a_{n,0} \operatorname{tr} \Big(\partial_{\boldsymbol{z}} \boldsymbol{Q}_n \partial_{\boldsymbol{z}}(\nabla^3_{\boldsymbol{Q}_n} U Z_n^{-1}) Z_n^{-1} \Big) \tag{3.57}
$$

$$
- \frac{3\mathrm{i}}{4!} a_{n,0} \operatorname{tr} \Big((\partial_{\boldsymbol{z}} \boldsymbol{Q}_n)^2 \nabla^4_{\boldsymbol{Q}_n} U (Z_n^{-1})^2 \Big).
$$

Define the operator $\mathcal{Q} = \operatorname{Id} - \Pi_n$ where Π_n is the projection operator onto the nth

Bloch wave. $b_{n,1}^\perp$ satisfies $\Pi_n b_{n,1}^\perp = \langle u_n(\boldsymbol{P}_n, \boldsymbol{x}), b_{n,1}^\perp \rangle = 0$, and is hence determined by

applying $\mathcal{Q}$ to $L_0^n(b_{n,1}\bar{u}_n(\boldsymbol{p}, \boldsymbol{Y})) = -L_1^n(b_{n,0}\bar{u}_n(\boldsymbol{p}, \boldsymbol{Y}))$. We obtain

$$b_{n,1}^{\perp}\bar{u}_n(\boldsymbol{p}, \boldsymbol{Y}) = -\left(L_0^n\right)^{-1}\mathcal{Q}\left(L_1^n(b_{n,0}\bar{u}_n(\boldsymbol{p}, \boldsymbol{Y}))\right). \tag{3.58}$$

Note that the inverse of the operator L_0^n can be defined on its range.

Thus, we have obtained the equations for $a_{n,0}$ (3.46), $a_{n,1}$ (3.57), and $b_{n,1}^{\perp}$ (3.58). This can be continued to higher orders.

Chapter 4

Proof of the first order convergence in the L^2 sense

We will now proof that $\psi_{\mathrm{FGA}}^{\varepsilon}$ is indeed an asymptotic solution to equation (1.9). More specifically, we will prove that $\psi_{\mathrm{FGA}}^{\varepsilon}$ converges to the exact solution in the L^2 sense as ε goes to 0. We will show that the rate of convergence is $\mathcal{O}(\varepsilon)$.

4.1   Strategy of the proof

To prove theorem 3.2.1, one needs to insert $\psi_{\mathrm{FGA},\infty}^{\varepsilon,n}$ into equation 1.9 and obtain an equation for the remainder. Our goal is to bound this remainder in the L^2 sense. To do this we will need to make the following assumptions:

• the nth Bloch band should not intersect any other Bloch band. This will be needed to bound $b_n^{\varepsilon,1}$.

• The Hamiltonian $h_n(\boldsymbol{q}, \boldsymbol{p})$ is sub-quadratic. This is needed to bound the gradients $\nabla^i U(\boldsymbol{Q}_n)$ for $i \geqslant 2$.

• $V_\Gamma(\boldsymbol{x})$ is smooth. This assumption will allow us to bound other terms that appear in

the remainder.

4.2 Estimates for the Hamiltonian flows

To bound the error for $t > 0$, we estimate quantities associated with the Hamiltonian flow $h_n(\boldsymbol{q}, \boldsymbol{p})$ for each n.

The following notation is useful in the proof. For $u \in \mathcal{C}^\infty(\Omega, \mathbb{C})$, we define for $k \in \mathbb{N}$,

$$M_k[u] = \max_{|\alpha_q| + |\alpha_p| \leqslant k} \sup_{(\boldsymbol{q}, \boldsymbol{p}) \in \Omega} \left| \partial_{\boldsymbol{q}}^{\alpha_q} \partial_{\boldsymbol{p}}^{\alpha_p} u(\boldsymbol{q}, \boldsymbol{p}) \right| \tag{4.1}$$

where α_q and α_p are multiindex corresponding to $\boldsymbol{q}$ and $\boldsymbol{p}$, respectively.

Definition 4.2.1. (Canonical Transformation) Let $\kappa_n : \mathbb{R}^{2d} \to \mathbb{R}^{2d}$ be a differentiable map $\kappa_n(\boldsymbol{q}, \boldsymbol{p}) = (\boldsymbol{Q}_n(\boldsymbol{q}, \boldsymbol{p}), \boldsymbol{P}_n(\boldsymbol{q}, \boldsymbol{p}))$ and denote the Jacobian matrix as

$$(F_n) = \begin{pmatrix} (\partial_{\boldsymbol{q}} \boldsymbol{Q}_n)^T(\boldsymbol{q}, \boldsymbol{p}) & (\partial_{\boldsymbol{p}} \boldsymbol{Q}_n)^T(\boldsymbol{q}, \boldsymbol{p}) \\ (\partial_{\boldsymbol{q}} \boldsymbol{P}_n)^T(\boldsymbol{q}, \boldsymbol{p}) & (\partial_{\boldsymbol{p}} \boldsymbol{P}_n)^T(\boldsymbol{q}, \boldsymbol{p}) \end{pmatrix}. \tag{4.2}$$

We say κ_n is a *canonical transformation* if F_n is symplectic for any $(\boldsymbol{q}, \boldsymbol{p}) \in \mathbb{R}^{2d}$, i.e.

$$(F_n)^T \begin{pmatrix} 0 & \mathrm{Id}_d \\ -\mathrm{Id}_d & 0 \end{pmatrix} F_n = \begin{pmatrix} 0 & \mathrm{Id}_d \\ -\mathrm{Id}_d & 0 \end{pmatrix}. \tag{4.3}$$

It is easy to check by the definition that the map $\kappa_n(t) : \mathbb{R}^{2d} \to \mathbb{R}^{2d}$ defined by $(\boldsymbol{q}, \boldsymbol{p}) \to (\boldsymbol{Q}_n(t, \boldsymbol{q}, \boldsymbol{p}), \boldsymbol{P}_n(t, \boldsymbol{q}, \boldsymbol{p}))$ solving (3.2) is a canonical transformation.

Proposition 4.2.2. *We have for all $k \geqslant 0$*

$$\sup_{t \in [0,T]} M_k \left[F_n(t) \right] < \infty \qquad \sup_{t \in [0,T]} M_k \left[\frac{\mathrm{d}}{\mathrm{d}t} F_n(t) \right] < \infty. \tag{4.4}$$

35

Proof: Differentiating $F_n(t, \boldsymbol{q}, \boldsymbol{p})$ with respect to t gives

$$\frac{\mathrm{d}}{\mathrm{d}t} F_n(t, \boldsymbol{q}, \boldsymbol{p}) = \begin{pmatrix} \partial_{\boldsymbol{P}} \partial_{\boldsymbol{Q}} h_n & \partial_{\boldsymbol{P}} \partial_{\boldsymbol{P}} h_n \\ -\partial_{\boldsymbol{Q}} \partial_{\boldsymbol{Q}} h_n & -\partial_{\boldsymbol{Q}} \partial_{\boldsymbol{P}} h_n \end{pmatrix} F_n(t, \boldsymbol{q}, \boldsymbol{p}). \tag{4.5}$$

By our assumption that U is subquadratic on $\mathbb{R}^d$ and since $E_n \in \mathcal{C}^\infty(\Gamma^*)$, there exists a constant C independent of $(\boldsymbol{q}, \boldsymbol{p})$ such that

$$\frac{\mathrm{d}}{\mathrm{d}t} |F_n(t, \boldsymbol{q}, \boldsymbol{p})| = \left| \begin{pmatrix} \partial_{\boldsymbol{P}} \partial_{\boldsymbol{Q}} h_n & \partial_{\boldsymbol{P}} \partial_{\boldsymbol{P}} h_n \\ -\partial_{\boldsymbol{Q}} \partial_{\boldsymbol{Q}} h_n & -\partial_{\boldsymbol{Q}} \partial_{\boldsymbol{P}} h_n \end{pmatrix} \right| |F_n(t, \boldsymbol{q}, \boldsymbol{p})| \leqslant C |F_n(t, \boldsymbol{q}, \boldsymbol{p})| \tag{4.6}$$

with $|F_n(0)| = |\mathrm{Id}_{2d}|$. By an application of Gronwall's inequality, we obtain

$$|F_n(t)| \leqslant e^{C|t|}. \tag{4.7}$$

Differentiating (4.5) with respect to $(\boldsymbol{q}, \boldsymbol{p})$ yields

$$\frac{\mathrm{d}}{\mathrm{d}t} \partial_{\boldsymbol{q}}^{\alpha_{\boldsymbol{q}}} \partial_{\boldsymbol{p}}^{\alpha_{\boldsymbol{p}}} F_n(t, \boldsymbol{q}, \boldsymbol{p}) = \sum_{\beta_{\boldsymbol{q}} \leqslant \alpha_{\boldsymbol{q}}, \beta_{\boldsymbol{p}} \leqslant \alpha_{\boldsymbol{p}}} \binom{\alpha_{\boldsymbol{q}}}{\beta_{\boldsymbol{q}}} \binom{\alpha_{\boldsymbol{p}}}{\beta_{\boldsymbol{p}}} \partial_{\boldsymbol{q}}^{\beta_{\boldsymbol{q}}} \partial_{\boldsymbol{p}}^{\beta_{\boldsymbol{p}}} \begin{pmatrix} \partial_{\boldsymbol{P}} \partial_{\boldsymbol{Q}} h_n & \partial_{\boldsymbol{P}} \partial_{\boldsymbol{P}} h_n \\ -\partial_{\boldsymbol{Q}} \partial_{\boldsymbol{Q}} h_n & -\partial_{\boldsymbol{Q}} \partial_{\boldsymbol{P}} h_n \end{pmatrix} \times$$

$$\times \partial_{\boldsymbol{q}}^{\alpha_{\boldsymbol{q}} - \beta_{\boldsymbol{q}}} \partial_{\boldsymbol{p}}^{\alpha_{\boldsymbol{p}} - \beta_{\boldsymbol{p}}} F_n(t, \boldsymbol{q}, \boldsymbol{p}). \tag{4.8}$$

Our estimate now follows by induction.

Recall that the matrix $Z_n(t, \boldsymbol{q}, \boldsymbol{p})$ is defined by

$$Z_n(t, \boldsymbol{q}, \boldsymbol{p}) := \partial_{\boldsymbol{z}} \left(\boldsymbol{Q}_n(t, \boldsymbol{q}, \boldsymbol{p}) + \mathrm{i} \boldsymbol{P}_n(t, \boldsymbol{q}, \boldsymbol{p}) \right) = \left(\partial_{\boldsymbol{q}} - \mathrm{i} \partial_{\boldsymbol{p}} \right) \left(\boldsymbol{Q}_n(t, \boldsymbol{q}, \boldsymbol{p}) + \mathrm{i} \boldsymbol{P}_n(t, \boldsymbol{q}, \boldsymbol{p}) \right). \tag{4.9}$$

Proposition 4.2.3. *$Z_n(t, \boldsymbol{q}, \boldsymbol{p})$ is invertible for $(\boldsymbol{q}, \boldsymbol{p}) \in \Omega$. Moreover, for each $k \in \mathbb{N}$,*

$$M_k \left[\left(Z_n(t) \right)^{-1} \right] < \infty. \tag{4.10}$$

(see proposition 3.5, [10])

36

Proof: $Z_n(t, \boldsymbol{q}, \boldsymbol{p})$ inherits the property that $M_k(Z_n(t, \boldsymbol{q}, \boldsymbol{p})) < \infty$ from the same estimate for $F_n(t, \boldsymbol{q}, \boldsymbol{p})$. Moreover, we have

$$
\begin{aligned}
Z_n(Z_n)^*(t, \boldsymbol{q}, \boldsymbol{p}) &= \begin{pmatrix} \mathrm{i\,Id}_d & \mathrm{Id}_d \end{pmatrix} (F_n)^T(t, \boldsymbol{q}, \boldsymbol{p}) \begin{pmatrix} \mathrm{Id}_d & -\mathrm{i\,Id}_d \\ \mathrm{i\,Id}_d & \mathrm{Id}_d \end{pmatrix} F_n(t, \boldsymbol{q}, \boldsymbol{p}) \begin{pmatrix} -\mathrm{i\,Id}_d \\ \mathrm{Id}_d \end{pmatrix} \\
&= \begin{pmatrix} \mathrm{i\,Id}_d & \mathrm{Id}_d \end{pmatrix} \left((F_n)^T(F_n) \right)(t, \boldsymbol{q}, \boldsymbol{p}) \begin{pmatrix} -\mathrm{i\,Id}_d \\ \mathrm{Id}_d \end{pmatrix} \\
&\quad + \begin{pmatrix} \mathrm{i\,Id}_d & \mathrm{Id}_d \end{pmatrix} (F_n)^T(t, \boldsymbol{q}, \boldsymbol{p}) \begin{pmatrix} 0 & -\mathrm{i\,Id}_d \\ \mathrm{i\,Id}_d & 0 \end{pmatrix} F_n(t, \boldsymbol{q}, \boldsymbol{p}) \begin{pmatrix} -\mathrm{i\,Id}_d \\ \mathrm{Id}_d \end{pmatrix} \\
&= \begin{pmatrix} \mathrm{i\,Id}_d & \mathrm{Id}_d \end{pmatrix} \left((F_n)^T F_n \right)(t, \boldsymbol{q}, \boldsymbol{p}) \begin{pmatrix} -\mathrm{i\,Id}_d \\ \mathrm{Id}_d \end{pmatrix} + 2\,\mathrm{Id}_d.
\end{aligned}
$$

$$(4.11)$$

This calculation shows that, since $(F_n(t))^T F_n(t)$ is semi-positive definite, for any $\boldsymbol{v} \in \mathbb{C}^{2d}$,

$$
\boldsymbol{v}^* Z_n(t)(Z_n(t))^* \boldsymbol{v} \geqslant 2|\boldsymbol{v}|^2. \tag{4.12}
$$

Therefore $Z_n(t, \boldsymbol{q}, \boldsymbol{p})$ is invertible and $\det\!\big(Z_n(t)\big)$ is uniformly bounded away from 0 for all $\boldsymbol{q}$ and $\boldsymbol{p}$, so by representing $(Z_n)^{-1}(t, \boldsymbol{q}, \boldsymbol{p})$ by minors, $M_k\!\big((Z_n)^{-1}(t, \boldsymbol{q}, \boldsymbol{p})\big) < \infty$, as $M_k(Z_n(t, \boldsymbol{q}, \boldsymbol{p}))$ is.

4.3   Estimates for the Bloch waves and amplitudes

Proposition 4.3.1. *For each $k \in \mathbb{N}$,*

$$
\sup_{t \in [0,T]} M_k \left[u_n(\boldsymbol{P}_n, \boldsymbol{x}) \right] < \infty. \tag{4.13}
$$

Proof: $u_n(\boldsymbol{P}_n, \boldsymbol{x})$ is smooth on the compact set $\Gamma^* \times \Gamma$ since the n-th band is separated from the rest of the spectrum (see e.g., [22]). Thus $u_n(\boldsymbol{P}_n, \boldsymbol{x})$ is uniformly

bounded on $\Gamma^* \times \Gamma$ and hence $\Gamma^* \times \mathbb{R}^d$ due to periodicity. We also see from Proposition 4.2.2 that the derivatives of $u_n(\boldsymbol{P}_n, \boldsymbol{x})$ are also bounded. Thus, $M_k[u_n(\boldsymbol{P}_n, \boldsymbol{x})] < \infty$ for any finite time t.

Let us summarize estimates for the amplitude equations derived in chapter 6.

Proposition 4.3.2. *For each $k \in \mathbb{N}$, the amplitudes $a_{n,0}$ and $a_{n,1}$, given by (3.46) and (3.57) satisfy*

$$\sup_{t\in[0,T]} M_k[a_{n,0}] < \infty, \qquad and \qquad \sup_{t\in[0,T]} M_k[a_{n,1}] < \infty. \tag{4.14}$$

Proof: By (4.2.2), (4.2.3) and (4.3.1), we see that the right hand side of (3.46) and (3.57) are bounded by some constants independent of $\boldsymbol{q}$ and $\boldsymbol{p}$ times $a_{n,0}$ and $a_{n,1}$, respectively. An application of Gronwall's inequality yields the result.

Proposition 4.3.3. *For each $k \in \mathbb{N}$ we have that*

$$\sup_{t\in[0,T]} M_k[b_{n,1}^{\perp}\bar{u}_n(\boldsymbol{P}_n, \boldsymbol{Y})] < \infty. \tag{4.15}$$

Proof: The equation for $b_{n,1}^{\perp}$ is given by equation (3.58). We thus obtain a bound by using the spectrum of L_0^n. We can write

$$(L_0^n)^{-1}(\Phi) = \sum_{m\neq n} \frac{\langle u_m(\boldsymbol{P}_m, \cdot), \Phi(\cdot, \boldsymbol{Y}, \boldsymbol{q}, \boldsymbol{p})\rangle_{L^2(\Gamma)} \, u_m(\boldsymbol{P}_m, \boldsymbol{X})}{E_n(\boldsymbol{P}_n) - E_m(\boldsymbol{P}_m)}. \tag{4.16}$$

Let $g = \min_{\boldsymbol{\xi}\in[-\pi,\pi]^d}\{|E_n(\boldsymbol{\xi}) - E_{n-1}(\boldsymbol{\xi})|, |E_n(\boldsymbol{\xi}) - E_{n+1}(\boldsymbol{\xi})|\}$. Then for each $k \in \mathbb{N}$, we obtain

$$
\begin{aligned}
M_k[b_{n,1}^{\perp}\bar{u}_n(\boldsymbol{P}_n, \boldsymbol{Y})] &\leqslant M_k\left[\frac{1}{g}\sum_{m\neq n}\langle u_m(\boldsymbol{P}_m, \cdot), b_{n,0}(t, \cdot, \boldsymbol{q}, \boldsymbol{p})\bar{u}_n(\boldsymbol{p}, \boldsymbol{Y})\rangle_{L^2(\Gamma)} u_n(\boldsymbol{P}_n, \boldsymbol{X})\right] \\
&= M_k\left[\frac{\bar{u}_n(\boldsymbol{p}, \boldsymbol{Y})}{g}\sum_{m\neq n} a_{n,0}(t, \boldsymbol{q}, \boldsymbol{p})\langle u_m(\boldsymbol{P}_m, \cdot), u_n(\boldsymbol{P}_n, \cdot)\rangle_{L^2(\Gamma)} u_n(\boldsymbol{P}_n, \boldsymbol{X})\right].
\end{aligned}
$$
$$\tag{4.17}$$

Hence, by Propositions 4.3.1 and 4.3.2, it suffices to control

$$M_k\left[\sum_{m\neq n}\langle u_m(\boldsymbol{P}_m, \boldsymbol{X}), u_n(\boldsymbol{P}_n, \boldsymbol{X})\rangle_{L^2(\Gamma)}\right]. \tag{4.18}$$

Since $\int_\Gamma |u_n(\boldsymbol{\xi}, \boldsymbol{x})|^2 d\boldsymbol{x} = 1$, Bessel's inequality implies that the above is finite.

4.4 Proof of theorem 3.2.1

We will need the following estimate,

Lemma 4.4.1. *Suppose $H(\varepsilon)$ is a family of self-adjoint operators for $\varepsilon > 0$. Suppose $\psi(t,\varepsilon)$ belongs to the domain of $H(\varepsilon)$, is continuously differentiable in t and approximately solves the Schrodinger equation in the sense that*

$$\mathrm{i}\varepsilon\frac{\partial\psi}{\partial t}(t,\varepsilon) = H(\varepsilon)\psi(t,\varepsilon) + \zeta(t,\varepsilon), \tag{4.19}$$

where $\zeta(t,\varepsilon)$ satisfies

$$\|\zeta(t,\varepsilon)\| \leqslant \mu(t,\varepsilon). \tag{4.20}$$

Then,

$$e^{-\mathrm{i}tH(\varepsilon)/\varepsilon}\psi(0,\varepsilon) - \psi(t,\varepsilon) \leqslant \varepsilon^{-1}\int_0^t \mu(s,\varepsilon)ds. \tag{4.21}$$

This lemma can be proved using the fundamental theorem of calculus, for brevity we refer the reader to [23]Lemma 2.8 for details.

Moreover, for the Fourier integral operator, we have

Lemma 4.4.2. *If, for fixed $\boldsymbol{x}, \boldsymbol{y} \in \mathbb{R}^d$, $u(\boldsymbol{x},\boldsymbol{y},\boldsymbol{q},\boldsymbol{p}) \in L^\infty(\Omega;\mathbb{C})$, for each $n \in \mathbb{N}$ and any t, $\mathcal{I}^\varepsilon(u)$ can be extended to a linear bounded operator on $L^2(\mathbb{R}^d,\mathbb{C})$, and we have*

$$\|\mathcal{I}(u)\|_{\mathscr{L}(L^2(\mathbb{R}^d;\mathbb{C}))} \leqslant 2^{-d/2}\|u\|_{L^\infty(\mathbb{R}^{2d};\mathbb{C})}. \tag{4.22}$$

Proof: The proof of lemma 4.4.2 is essentially the same as Proposition 3.7 in [10] and thus is omitted here.

We are now ready to prove Theorem 3.2.1.

Proof: [Proof of Theorem 3.2.1] Computing $\mathrm{i}\varepsilon\dfrac{\partial}{\partial t} + \dfrac{1}{2}\varepsilon^2\nabla^2 - V(\boldsymbol{X}) - U(\boldsymbol{x})$ applied to $\mathcal{I}^\varepsilon\left(b_n^{\varepsilon,1}(t,\boldsymbol{X},\boldsymbol{q},\boldsymbol{p})\bar{u}_n(\boldsymbol{p},\boldsymbol{Y})\right)$, we obtain

$$\left(\mathrm{i}\varepsilon\frac{\mathrm{d}}{\mathrm{d}t} + \frac{1}{2}\varepsilon^2\nabla^2 - V(\boldsymbol{X}) - U(\boldsymbol{x})\right)\mathcal{I}^\varepsilon\left(b_n^{\varepsilon,1}\bar{u}_n(\boldsymbol{p},\boldsymbol{Y})\right) = \mathcal{I}^\varepsilon\left(\sum_{j=0}^1 \varepsilon^j v_{n,j}\right) + \varepsilon^2\mathcal{I}^\varepsilon\left(v_{n,2}^\varepsilon\right). \tag{4.23}$$

The expressions for $v_{n,0}$, $v_{n,1}$, and $v_{n,2}$ follows from (3.43) by expanding b^ε and the linearity of L_0^n, L_1^n, and L_2^n. By equations (3.44) and (3.45), $v_{n,0}$ and $v_{n,1}$ vanish. The remaining term

$$v_{n,2}^\varepsilon = L_2^n(b_n^{\varepsilon,1}\bar{u}_n(\boldsymbol{p}, \boldsymbol{Y})) + R(\boldsymbol{x}, \boldsymbol{q}, \boldsymbol{p})b_n^{\varepsilon,1}\bar{u}_n(\boldsymbol{p}, \boldsymbol{Y}). \tag{4.24}$$

satisfies $M_k[v_{n,2}^\varepsilon] < \infty$ by Propositions 4.2.3, 4.3.2, and 4.3.3. Finally, applying Lemma 4.4.2 and Lemma 4.4.1 we obtain the inequality in Theorem 3.2.1.

Chapter 5

FGA algorithm and numerical results

5.1 Deriving a guage-invariant algorithm

Recall from chapter 5, that the eigenfunction $u_n(\boldsymbol{\xi}, \boldsymbol{x})$ of (2.3) is defined up to a unit complex number $e^{i\phi(\boldsymbol{\xi})}$. This is known as gauge freedom and it is problematic numerically as different choices of the gauge $\phi(\boldsymbol{\xi})$ may lead to different numerical results for the Berry phase term $\mathcal{A}_n(\boldsymbol{\xi}) = \langle u_n(\boldsymbol{\xi}, \boldsymbol{x}) | i\nabla_{\boldsymbol{\xi}} u_n(\boldsymbol{\xi}, \boldsymbol{x}) \rangle$, and hence $\psi_{\text{FGA}}^{\varepsilon}$ will not be well defined. We modify our ansatz $\psi_{\text{FGA}}^{\varepsilon}$ so that direct numerical computation of the Berry phase is avoided.

To separate the dependence of a_n on $\mathcal{A}_n$ in the evolution equation (3.6) we use a standard differential equations technique know as the method of integrating factors. We define $S_n^{\mathcal{A}}$ the phase contribution due to the Berry phase term

$$S_n^{\mathcal{A}}(t, \boldsymbol{q}, \boldsymbol{p}) = \int_0^t \mathcal{A}_n(\boldsymbol{P}_n) \cdot \nabla U(\boldsymbol{Q}_n) \, \mathrm{d}s. \tag{5.1}$$

41

and let

$$b_n(t, \boldsymbol{q}, \boldsymbol{p}) = a_n(t, \boldsymbol{q}, \boldsymbol{p}) \exp(\mathrm{i} S_n^{\mathcal{A}}(t, \boldsymbol{q}, \boldsymbol{p})). \tag{5.2}$$

We note that the exponential term of equation (5.2) is the integrating factor. Multiplying equation (3.6) by the integrating factor and simplifying, we deduce that b_n solves,

$$\frac{\mathrm{d}b_n}{\mathrm{d}t} = \frac{1}{2} b_n \operatorname{tr}\left(\partial_{\boldsymbol{z}} \boldsymbol{P}_n \nabla^2 E_n(\boldsymbol{P}_n) Z_n^{-1}\right) - \frac{\mathrm{i}}{2} b_n \operatorname{tr}\left(\partial_{\boldsymbol{z}} \boldsymbol{Q}_n \nabla^2 U(\boldsymbol{Q}_n) Z_n^{-1}\right), \tag{5.3}$$

with initial condition $b_n(0, \boldsymbol{q}, \boldsymbol{p}) = 2^{d/2}$. The evolution equation (5.3) for b_n is *manifestly gauge-invariant*, as all terms are independent of the gauge choice. Using the amplitude function b_n, the frozen Gaussian approximation (equation (3.8)) can be rewritten as

$$\psi_{\mathrm{FGA}}^{\varepsilon}(t, \boldsymbol{x}) = \frac{1}{(2\pi\varepsilon)^{3d/2}} \sum_{n=1}^{\infty} \int_{\Gamma^*} \int_{\mathbb{R}^d} b_n(t, \boldsymbol{q}, \boldsymbol{p}) u_n\left(\boldsymbol{P}_n, \boldsymbol{x}/\varepsilon\right) G_{\boldsymbol{Q}_n, \boldsymbol{P}_n}^{\varepsilon}(\boldsymbol{x}) e^{\mathrm{i} S_n(t, \boldsymbol{q}, \boldsymbol{p})/\varepsilon - \mathrm{i} S_n^{\mathcal{A}}(t, \boldsymbol{q}, \boldsymbol{p})}$$

$$\times \langle G_{\boldsymbol{q}, \boldsymbol{p}}^{\varepsilon} u_n(\boldsymbol{p}, \cdot/\varepsilon) | \psi_0 \rangle \, \mathrm{d}\boldsymbol{q} \, \mathrm{d}\boldsymbol{p}. \tag{5.4}$$

The gauge-dependent term in (5.4) thus reads

$$u_n(\boldsymbol{P}_n, \boldsymbol{x}/\varepsilon) e^{-\mathrm{i} S_n^{\boldsymbol{A}}(t, \boldsymbol{q}, \boldsymbol{p})} \overline{u}_n(\boldsymbol{p}, \boldsymbol{y}/\varepsilon). \tag{5.5}$$

Our goal is hence to design a gauge-invariant time integrator for (5.1) such that the term (5.5) becomes independent of the gauge. Observe that, by the Hamiltonian flow (3.2),

$$S_n^{\mathcal{A}}(t, \boldsymbol{q}, \boldsymbol{p}) = -\int_0^t \mathcal{A}(\boldsymbol{P}_n) \cdot \mathrm{d}\boldsymbol{P}_n(s). \tag{5.6}$$

Let $0 = t_0 < t_1 < \cdots < t_K = t$ be a time discretization, we have

$$\exp(-\mathrm{i} S_n^{\mathcal{A}}) = \exp\left(\mathrm{i} \int_0^t \mathcal{A}(\boldsymbol{P}_n) \cdot \mathrm{d}\boldsymbol{P}_n(s)\right) = \prod_{k=1}^K \exp\left(\mathrm{i} \int_{t_{k-1}}^{t_k} \mathcal{A}(\boldsymbol{P}_n) \cdot \mathrm{d}\boldsymbol{P}_n(s)\right). \tag{5.7}$$

Let us assume that we have chosen a gauge where $u_n(\boldsymbol{\xi}, \cdot)$ is smooth in $\boldsymbol{\xi} \in \Gamma^*$. Note that since our final formula is gauge-independent, the choice of the gauge here is only for the

derivation. Using the Taylor approximation, we obtain

$$
\mathrm{i} \int_{t_{k-1}}^{t_k} \mathcal{A}(\boldsymbol{P}_n) \cdot \mathrm{d}\boldsymbol{P}_n(s) = -\mathrm{i}\,\mathfrak{Im}\left\{\langle u_n(\boldsymbol{P}_n(t_{k-1}), \cdot) | \nabla u_n(\boldsymbol{P}_n(t_{k-1}), \cdot)\rangle \cdot \Delta\boldsymbol{P}_{k,n}\right\}
$$

$$
+ \mathcal{O}(\Delta\boldsymbol{P}_{k,n})^2
$$

$$
= \mathrm{i}\,\mathfrak{Im}\left\{1 - \langle u_n(\boldsymbol{P}_n(t_{k-1}), \cdot) | u_n(\boldsymbol{P}_n(t_k), \cdot)\rangle\right\} + \mathcal{O}(\Delta\boldsymbol{P}_{k,n})^2
$$

$$
= \mathrm{i}\,\mathfrak{Im}\{\ln\langle u_n(\boldsymbol{P}_n(t_k), \cdot) | u_n(\boldsymbol{P}_n(t_{k-1}), \cdot)\rangle\} + \mathcal{O}(\Delta\boldsymbol{P}_{k,n})^2,
$$

(5.8)

where $\Delta\boldsymbol{P}_{k,n} = \boldsymbol{P}_n(t_k) - \boldsymbol{P}_n(t_{k-1})$. The first approximation was obtained by using a left Riemann sum. The next approximation is the forward difference approximation for the derivative. The last approximation is the Taylor series for $\ln \boldsymbol{z}$ around $\boldsymbol{z} = 1$. Therefore, exponentiating, we get

$$
\exp\left(\mathrm{i} \int_{t_{k-1}}^{t_k} \mathcal{A}(\boldsymbol{P}_n) \cdot \mathrm{d}\boldsymbol{P}_n(s)\right) = \frac{\langle u_n(\boldsymbol{P}_n(t_k), \cdot) | u_n(\boldsymbol{P}_n(t_{k-1}), \cdot)\rangle}{\left|\langle u_n(\boldsymbol{P}_n(t_k), \cdot) | u_n(\boldsymbol{P}_n(t_{k-1}), \cdot)\rangle\right|} + \mathcal{O}(\Delta\boldsymbol{P}_{k,n})^2. \quad (5.9)
$$

Substituting the last equation in the right hand side of (5.7) gives an approximation to $\exp(-\mathrm{i}S_n^{\mathcal{A}})$ with and error $\mathcal{O}(\Delta\boldsymbol{P}_n)$ with $\Delta\boldsymbol{P}_n = \max_k |\Delta\boldsymbol{P}_{k,n}|$. This then gives the approximation to (5.5) as

$$
u_n(\boldsymbol{P}_n, \boldsymbol{x}/\varepsilon) e^{-\mathrm{i}S_n^{\boldsymbol{A}}(t,\boldsymbol{q},\boldsymbol{p})} \overline{u}_n(\boldsymbol{p}, \boldsymbol{y}/\varepsilon) \approx F_n(t, \boldsymbol{q}, \boldsymbol{p}, \boldsymbol{x}, \boldsymbol{y}) :=
$$

$$
:= \left|u_n(\boldsymbol{P}_n(t_K), \boldsymbol{x}/\varepsilon)\right\rangle \prod_{k=1}^{K} \frac{\langle u_n(\boldsymbol{P}_n(t_k), \cdot) | u_n(\boldsymbol{P}_n(t_{k-1}), \cdot)\rangle}{\left|\langle u_n(\boldsymbol{P}_n(t_k), \cdot) | u_n(\boldsymbol{P}_n(t_{k-1}), \cdot)\rangle\right|} \langle u_n(\boldsymbol{P}_n(t_0), \boldsymbol{y}/\varepsilon)\right| + \mathcal{O}(\Delta\boldsymbol{P}_n).
$$

(5.10)

The right hand side of (5.10) is manifestly gauge-invariant, as the phase term in $|u_n(\boldsymbol{P}_n(t_k), \cdot)\rangle$ will cancel with that of $\langle u_n(\boldsymbol{P}_n(t_k), \cdot)|$, for $k = 0, \ldots, K$.

Therefore, in summary, we arrive at a gauge-invariant reformulation of $\psi_{\mathrm{FGA}}^{\varepsilon}$ as

$$
\psi_{\mathrm{FGA}}^{\varepsilon}(t, \boldsymbol{x}) \approx \frac{1}{(2\pi\varepsilon)^{3d/2}} \sum_{n=1}^{\infty} \int_{\Gamma^*} \int_{\mathbb{R}^d} b_n(t, \boldsymbol{q}, \boldsymbol{p}) F_n(t, \boldsymbol{q}, \boldsymbol{p}, \boldsymbol{x}, \boldsymbol{y}) G_{\boldsymbol{Q}_n, \boldsymbol{P}_n}^{\varepsilon}(\boldsymbol{x})
$$

$$
\times e^{\mathrm{i}S_n(t,\boldsymbol{q},\boldsymbol{p})/\varepsilon} \langle G_{\boldsymbol{q},\boldsymbol{p}}^{\varepsilon} | \psi_0\rangle \, \mathrm{d}\boldsymbol{q} \, \mathrm{d}\boldsymbol{p}, \quad (5.11)
$$

43

where F_n is given by (5.10), and the evolution of $(\boldsymbol{Q}_n, \boldsymbol{P}_n)$ follows the Hamiltonian dynamics

$$\begin{cases} \dfrac{d\boldsymbol{Q}_n}{dt} = \nabla E_n(\boldsymbol{P}_n), \\ \dfrac{d\boldsymbol{P}_n}{dt} = -\nabla U(\boldsymbol{Q}_n), \end{cases} \qquad (5.12)$$

with initial condition $\boldsymbol{Q}_n(0, \boldsymbol{q}, \boldsymbol{p}) = \boldsymbol{q}$ and $\boldsymbol{P}_n(0, \boldsymbol{q}, \boldsymbol{p}) = \boldsymbol{p}$.

The action S_n solves

$$\frac{dS_n}{dt} = \boldsymbol{P}_n \cdot \nabla_{\boldsymbol{P}} h_n(\boldsymbol{Q}_n, \boldsymbol{P}_n) - h_n(\boldsymbol{Q}_n, \boldsymbol{P}_n), \qquad (5.13)$$

with initial condition $S_n(0, \boldsymbol{q}, \boldsymbol{p}) = 0$, and the amplitude b_n follows the evolution

$$\frac{db_n}{dt} = \frac{1}{2} b_n \operatorname{tr} \left(\partial_z \boldsymbol{P}_n \nabla^2 E_n(\boldsymbol{P}_n) Z_n^{-1} \right) - \frac{\mathrm{i}}{2} b_n \operatorname{tr} \left(\partial_z \boldsymbol{Q}_n \nabla^2 U_n(\boldsymbol{Q}_n) Z_n^{-1} \right), \qquad (5.14)$$

with initial condition $b_n(0, \boldsymbol{q}, \boldsymbol{p}) = 2^{d/2}$.

5.2 Computing Bloch energy bands and Bloch waves in one-dimension

As a prerequisite for implementing equation (5.11) numerically, we will need to compute the eigenvalues and eigenfunctions of (2.4). We restrict our computations to 1-dimension as computation of true solutions to (1.9) with high accuracy is extremely time-consuming in high dimensions, and thus it is difficult for us to confirm numerically the asymptotic convergence order with the pollution of non-negligible numerical errors. Also, band-crossing is quite common in high dimensional cases (e.g., in honeycomb lattice), which requires more techniques than the scope of this thesis, and we will leave the numerical study of high dimensional examples as future work. We also note that the calculations in this section can be easily generalized to higher dimensions by vectorizing all the appropriate variables.

Define the Fourier transform of $u_n(\xi, x)$ as

$$\hat{u}_n(\xi, \eta) = \frac{1}{2\pi} \int_\Gamma u_n(\xi, x) e^{-ix\eta} \, dx. \tag{5.15}$$

Taking the Fourier transform of (2.4) one obtains

$$\frac{(\eta + \xi)^2}{2} \hat{u}_n(\xi, \eta) + \widehat{V_\Gamma}(\eta) * \widehat{u_n}(\xi, \eta) = E_n(\xi) \hat{u}_n(\xi, \eta), \tag{5.16}$$

where "$*$" stands for the operation of convolution.

Truncating the Fourier grid to $\{-\Lambda, \cdots, \Lambda - 1\} \subset \mathbb{Z}$ gives

$$H_\xi(\Lambda) \begin{pmatrix} \hat{u}_n(\xi, -\Lambda) \\ \hat{u}_n(\xi, 1 - \Lambda) \\ \vdots \\ \hat{u}_n(\xi, \Lambda - 1) \end{pmatrix} = E_n(\xi) \begin{pmatrix} \hat{u}_n(\xi, -\Lambda) \\ \hat{u}_n(\xi, 1 - \Lambda) \\ \vdots \\ \hat{u}_n(\xi, \Lambda - 1) \end{pmatrix} \tag{5.17}$$

where $H_\xi(\Lambda)$ is the $2\Lambda \times 2\Lambda$ matrix given by

$$H_\xi(\Lambda) = \begin{pmatrix} \frac{(-\Lambda + \xi)^2}{2} + \hat{V}_\Gamma(0) & \hat{V}_\Gamma(-1) & \cdots & \hat{V}_\Gamma(1 - 2\Lambda) \\ \hat{V}_\Gamma(1) & \frac{(-\Lambda + 1 + \xi)^2}{2} + \hat{V}_\Gamma(0) & \cdots & \hat{V}_\Gamma(2 - 2\Lambda) \\ \cdots & \cdots & \ddots & \cdots \\ \hat{V}_\Gamma(2\Lambda - 1) & \hat{V}(2\Lambda - 2) & \cdots & \frac{(\Lambda - 1 + \xi)^2}{2} + \hat{V}_\Gamma(0) \end{pmatrix}. \tag{5.18}$$

After diagonalizing the matrix, the eigenfunction in the physical domain is then obtained via inverse Fourier transform

$$u_n(\xi, x) \approx \sum_{y=-\Lambda}^{\Lambda-1} \hat{u}_n(\xi, \eta) e^{i\eta x}. \tag{5.19}$$

Example 5.2.1. *In this example, we compute Bloch eigenvalues and eigenfunctions with potential $V_\Gamma(x) = \exp\left(-25x^2\right)$. The extension of $V_\Gamma(x)$ periodically with respect to Γ is not analytic on the boundary of Γ. However, this lack of smoothness presents a negligible*

45
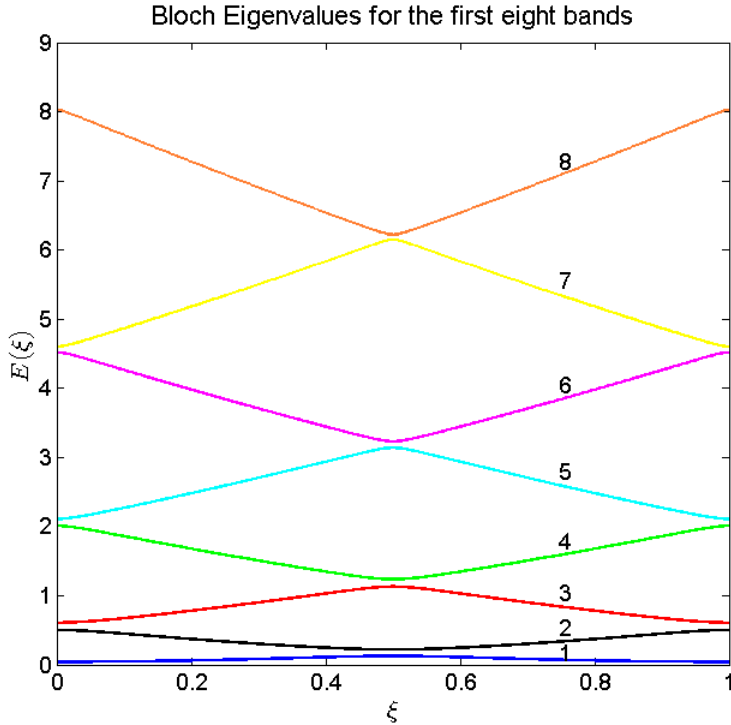
Figure 5.1: Energy eigenvalues for the one-dimensional lattice potential $V(x) = \exp\left(-25x^2\right)$

problem numerically as $V_\Gamma(x)$ decays rapidly. Figure 5.1 shows the energy eigenvalues $E_n(\xi)$ for $\xi \in [0,1)$. The plot shows the first 8 bands where the bottom curve corresponds to $n = 1$ (lowest band) and the top curve represents $n = 8$ (highest band). Figure 5.2 shows the modules of the corresponding Bloch eigenfunctions for the first 4 bands. Notice that while these surfaces are continuous and periodic, the next two figures (5.3 and 5.4) of the real and imaginary parts of the Bloch eigenfunctions are not. This is due to the arbitrary gauge freedom in the diagonalization.

Remark. 1. In the numerical computation of $E(\xi)$, the corresponding eigenfunctions and their derivatives near the points $\xi = 0$ and $\xi = 0.5$ (and $\xi = 1$ by periodicity) is tricky, since the Bloch bands are close to each other near these points (see Figure 5.1). For this reason, our grid for the ξ variable will not contain these points. In other words, we shift

46
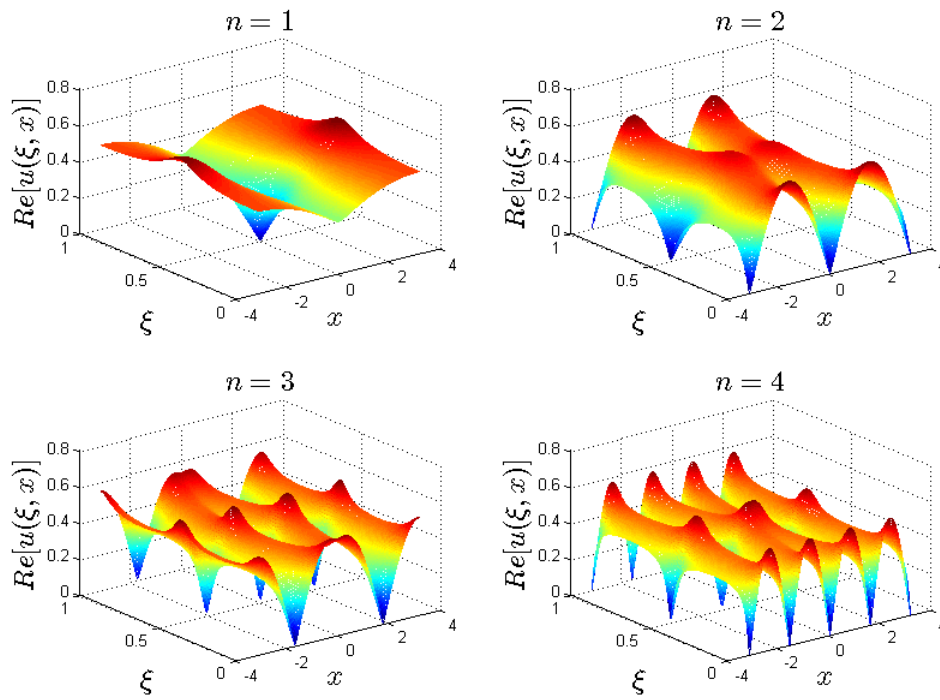
Figure 5.2: Module of eigenfunctions for the one-dimensional lattice potential $V(x) = \exp\left(-25x^2\right)$. We display absolute value of the first 4 lowest energy eigenfunctions.
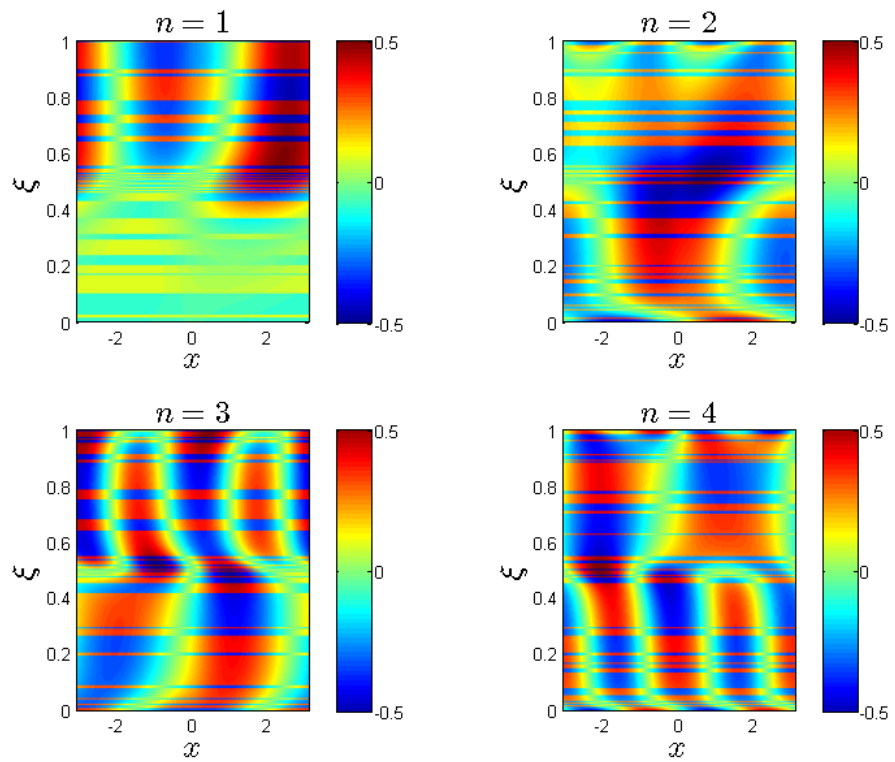
Figure 5.3: Real part of the eigenfunctions for the one-dimensional lattice potential $V(x) = \exp\left(-25x^2\right)$. We display the real parts for the first 4 lowest energy eigenfunctions. We use 100 data points for the $\boldsymbol{\xi}$ variable.
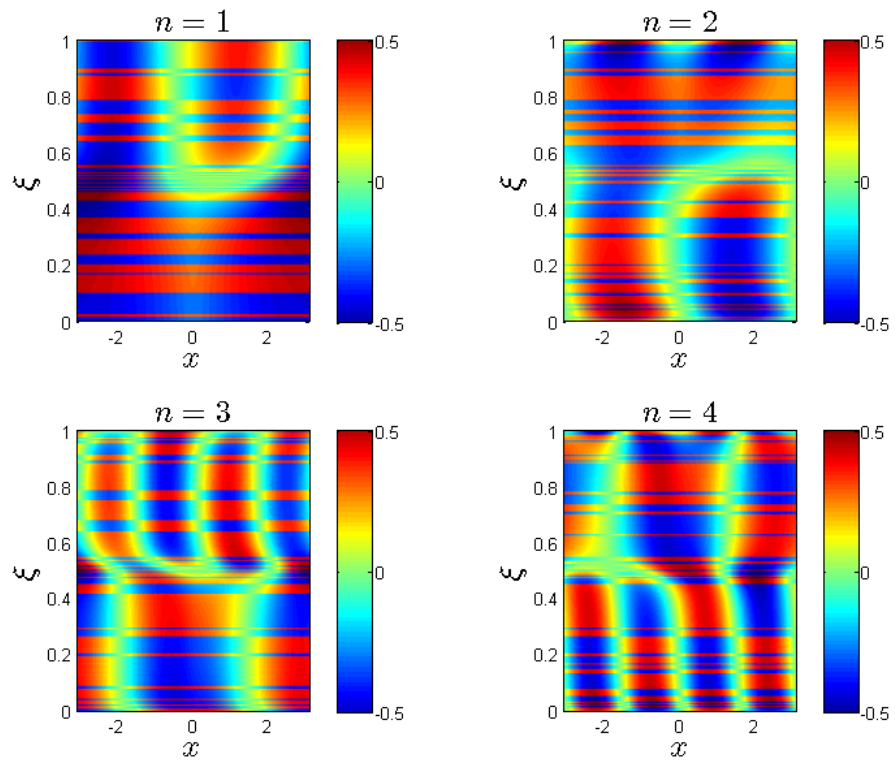
Figure 5.4: Imaginary part of the eigenfunctions for the one-dimensional lattice potential $V(x) = \exp\left(-25x^2\right)$. We display the imaginary parts for the first 4 lowest energy eigenfunctions. We use 100 data points for the $\boldsymbol{\xi}$ variable.

the grids in the first Brillouin zone to avoid these high symmetry points.

2. One can apply the same technique to derive an algorithm for computing Bloch eigenvalues and eigenfunctions in higher dimensions. The main issue with this algorithm is that the numerical cost increases drastically for $d > 1$. In the case where the periodic potential has the form $V_\Gamma(\boldsymbol{x}) = \sum_{j=1}^{d} V_j(x_j)$ with $V_j(x_j + 2\pi) = V(x_j)$, computation of Bloch bands can be treated for each coordinate x_j separately. For some common potentials, data for the energy eigenvalues has already been produced (see remark 2.1 in [24]).

5.2.1 Description of the gauge-invariant algorithm

We assume that the initial data $\psi_0(x)$ has compact support or that it decays sufficiently fast as $|x| \to \infty$, and hence, we only need to use a finite number of mesh points in physical space.

For a mesh size δx and starting point $x^0 \in \mathbb{R}$, the grid is specified as

$$x^m = x^0 + (m - 1)\delta x, \tag{5.20}$$

for $m = 1, \cdots, N_x$, where N_x is the number of the spatial grid in one dimension.

We present the algorithm in five steps below.

Step 1. Compute the Bloch eigenvalues $E_n(\xi)$ and eigenfunctions $u_n(\xi, x)$ of (2.4), according to the algorithm described in Section 5.2.

Remark. For our one dimensional examples in Section 5.3, we choose a mesh for (ξ, x) such that $\delta\xi = (1 - 2\rho)/199$ with $\xi^0 = -1/2 + \rho$ and $N_\xi = 200$; and $\delta x = 2\pi/804$ with $x^0 = -\pi$ and $N_x = 805$ for some $0 < \rho \ll 1$. ρ was included to avoid putting mesh points at high symmetry points in the first Brillouin zone. This number of grid points is enough to ensure that the eigenvalues and eigenfunctions are computed with sufficient accuracy for our numerical tests.

50

Step 2. Compute $(Q_n(t, q, p), P_n(t, q, p), S_n(t, q, p), b_n(t, q, p))$ in (5.12), (5.13), and (5.14).

To integrate the ODEs for (Q_n, P_n, S_n, b_n), we use a symplectic fourth order Runge-Kutta method. Coefficients for the Butcher tableau can be found in [25]. We will choose a mesh for $(q, p) \in \Omega$ and (Q_n, P_n) takes initial value at the grid points. That is,

$$Q_n(0, q, p) = q^I = q^0 + I\delta q \tag{5.21}$$

$$P_n(0, q, p) = p^J = p^0 + J\delta p \tag{5.22}$$

where $I \in 1, \cdots, N_I$ and $J \in 1, \cdots, N_J$. Notice that to represent the initial condition $\psi_{\text{FGA}}^\varepsilon(0, x)$ one only needs the mesh points q^I near x. To be more precise, as the standard deviation of the semiclassical Gaussian functions in (2.21) is $\sqrt{\varepsilon}$ so one only needs the mesh points q^I contributing significantly to $\psi_{\text{FGA}}^\varepsilon(0, x)$ satisfy $|x - q^I| \leqslant \mathcal{O}(\sqrt{\varepsilon})$. This implies that one can put a finite number of mesh points for q-coordinate and not on all of $\mathbb{R}$. The mesh size for q^I and p^J is chosen to be $\mathcal{O}(\sqrt{\varepsilon})$, which resolves the oscillation of the initial condition.

Step 3. Compute the windowed Bloch transformation of the initial condition $\langle u_n(p, \cdot/\varepsilon)G_{q,p}^\varepsilon | \psi_0 \rangle$. For the sake of convenience, denote this term by $w_n^\varepsilon(q, p)$. Let

$$y^K = y^0 + (K - 1)\delta y \tag{5.23}$$

be a discrete mesh of y where $K = 1, \cdots, N_y$. Then,

$$w_n^\varepsilon(q^I, p^J) \approx \sum_{K=1}^{N_y} \bar{G}_{q^I, p^J}^\varepsilon(y^K)\bar{u}(p^J, y^K/\varepsilon)\psi_0(y^K)r_\theta\left(|y^K - q^I|\right)\delta y, \tag{5.24}$$

with r_θ a cut-off function such that $r_\theta = 1$ in the ball of radius $\theta > 0$ centered at the origin and $r_\theta = 0$ outside the ball.

The mesh y^K should approximately cover the support of the initial condition $\psi_0(y)$. As can be seen by the form of w_n^ε, the size of N_y will depend on ε. The mesh should be fine enough to accurately capture $\bar{u}_n(p, y/\varepsilon)\bar{G}_{q,p}^\varepsilon(y)\psi_0(y)$ for all bands n.

51

Remark. One can reduce the computation time of $w_n^\varepsilon(q^I, p^J)$ by incorporating the periodicity of $u_n(\xi, x)$ with respect to x. As can be seen by Figure 5.2, $u_n(\xi, x)$ tends to become more oscillatory as n increases. Thus, the mesh of y^K should be adapted so that it depends on n.

Step 4. Denote the product term in (5.10) by

$$\widetilde{F}_n(t, q, p) := \prod_{k=1}^{K} \frac{\langle u(P_n(t_k), \cdot), u(P_n(t_{k-1}), \cdot) \rangle}{|\langle u(P_n(t_k), \cdot), u(P_n(t_{k-1}), \cdot) \rangle|}, \tag{5.25}$$

and note that

$$F_n(t, q, p, x, y) = |u_n(P_n(t_K), x/\varepsilon) \rangle \widetilde{F}_n(t, q, p) \langle u_n(P_n(t_0), y/\varepsilon)|.$$

At this point we now have the required data to compute $\widetilde{F}_n$. Discretize $\widetilde{F}_n$ using the same mesh from the previous steps to obtain $\widetilde{F}_n(t, q^I, p^J)$. Here, $t_0 = 0 < t_1 < t_2 < \cdots < t_K = t$ is the temporal mesh used in Step 2.

Step 5. Reconstruct the solution using (5.11)

$$\psi_{\text{FGA}}^\varepsilon(t, x^L) \approx \sum_{n=1}^{N} \sum_I \sum_J \Big(b_n(t, q^I, p^J) \bar{u}_n\big(P_n(t, q^I, p^J), x^L/\varepsilon\big) G_{Q_n, P_n}^\varepsilon(x^L) e^{S_n(t, q^I, p^J)/\varepsilon}$$

$$\times \widetilde{F}_n(t, q^I, p^J) \widetilde{\psi}_n^\varepsilon(q^I, p^J) r_\theta \big(|x^L - Q_n^{I,J}|\big)\Big) \delta q \delta p, \tag{5.26}$$

where Q_n and P_n are evaluated at (t, q^I, p^J), and r_θ is a cutoff function as described in Step 3 and N is the maximum number of Bloch bands used.

Remark. The error arising from the gauge-invariant algorithm described above is

$$\mathcal{O}(\varepsilon + \frac{\delta t^4}{\varepsilon} + \max_n \Delta \boldsymbol{P}_n) + ||\psi_0^\varepsilon - \sum_{n=1}^{N} \prod_n^{\mathcal{W}, \varepsilon} \psi_0^\varepsilon||_{L^2}. \tag{5.27}$$

5.3 Verification of the convergence rate of FGA using numerical examples

In this section, we show the numerical performance of gauge invariant frozen Gaussian approximation (GIFGA) by several one dimensional examples, which also confirm the first order asymptotic convergence analyzed in Chapter 4.

Initial decomposition.

In the first two examples, we test the initial decomposition of GIFGA described in Section 2.2. We compute $\psi_{\text{FGA}}^\varepsilon$ at $t = 0$ via equation (3.8). As we cannot numerically sum to infinity, we choose to use at most 8 bands in all of our examples. Expressed differently, the solution will be concentrated on the first 8 bands. Because of the need for $\mathcal{O}(\sqrt{\varepsilon})$ mesh size for both coordinates (q^I, p^J) of phase space, we choose approximately $2/\sqrt{\varepsilon}$ number of grid points for each unit interval.

Example 5.3.1. *In this example, we check the initial decomposition by choosing $\psi_0 = A(x)\exp\big(iS(x)/\varepsilon\big)$ with $A(x) = \exp\left(-50x^2\right)\cos((x-0.5)/\varepsilon)$ and $S(x) = 0.3(x-0.5) + 0.1\sin(x-0.5)$, and the lattice potential $V_\Gamma = \cos(x)$. We record the data in Table 5.1.*

Example 5.3.2. *In this example, we check the initial decomposition by choosing $\psi_0 = A(x)\exp\big(iS(x)/\varepsilon\big)$ with $A(x) = \exp\left(-50x^2\right)$ and $S(x) = 0.3 + 0.1\sin(x-0.5)$, and the lattice potential to be $V_\Gamma = \exp(-25x^2)$. We record the data in Table 5.2.*

Tables 5.1, and 5.2 show that FGA indeed matches the initial condition more closely as N increases. Furthermore, we have essentially the same L^2 error for each ε. This provides numerical verification of the independence of ε of the initial decomposition.

Remark. Let us note that from equations (2.4) and (2.3), the convergence rate should depend on the form of the lattice potential $V_\Gamma(x)$. Also, by equation (2.14), the convergence

$\varepsilon = 1/64$	Error $||\psi_0 - \psi_{\mathrm{FGA}}^\varepsilon||_{L^2}$
$N = 1$	0.13260
$N = 2$	0.11328
$N = 4$	0.033126
$N = 8$	7.2587e-05
$\varepsilon = 1/128$	Error $||\psi_0 - \psi_{\mathrm{FGA}}^\varepsilon||_{L^2}$
$N = 1$	0.15361
$N = 2$	0.096905
$N = 4$	0.031652
$N = 8$	7.0574e-05
$\varepsilon = 1/256$	Error $||\psi_0 - \psi_{\mathrm{FGA}}^\varepsilon||_{L^2}$
$N = 1$	0.14165
$N = 2$	0.1063
$N = 4$	0.032405
$N = 8$	6.9192e-05
$\varepsilon = 1/512$	Error $||\psi_0 - \psi_{\mathrm{FGA}}^\varepsilon||_{L^2}$
$N = 1$	0.15885
$N = 2$	0.09276
$N = 4$	0.031263
$N = 8$	6.8701e-05

Table 5.1: L^2 error of $\psi_0(x) - \psi_{\mathrm{FGA}}^\varepsilon(0, x)$ for Example 5.3.1. We display various values of ε and sum over N Bloch bands in $\psi_{\mathrm{FGA}}^\varepsilon$.

$\varepsilon = 1/64$	Error $||\psi_0 - \psi_{\text{FGA}}^\varepsilon||_{L^2}$
$N = 1$	0.035736
$N = 2$	0.02463
$N = 4$	0.0075756
$N = 8$	0.0018796

$\varepsilon = 1/128$	Error $||\psi_0 - \psi_{\text{FGA}}^\varepsilon||_{L^2}$
$N = 1$	0.031445
$N = 2$	0.024814
$N = 4$	0.007579
$N = 8$	0.0018579

$\varepsilon = 1/256$	Error $||\psi_0 - \psi_{\text{FGA}}^\varepsilon||_{L^2}$
$N = 1$	0.030633
$N = 2$	0.024967
$N = 4$	0.0076045
$N = 8$	0.0018698

$\varepsilon = 1/512$	Error $||\psi_0 - \psi_{\text{FGA}}^\varepsilon||_{L^2}$
$N = 1$	0.030375
$N = 2$	0.025078
$N = 4$	0.0076103
$N = 8$	0.0018769

Table 5.2: L^2 error of $\psi_0(x) - \psi_{\text{FGA}}^\varepsilon(0, x)$ for Example 5.3.2. We display various values of ε and sum over N Bloch bands in $\psi_{\text{FGA}}^\varepsilon$.
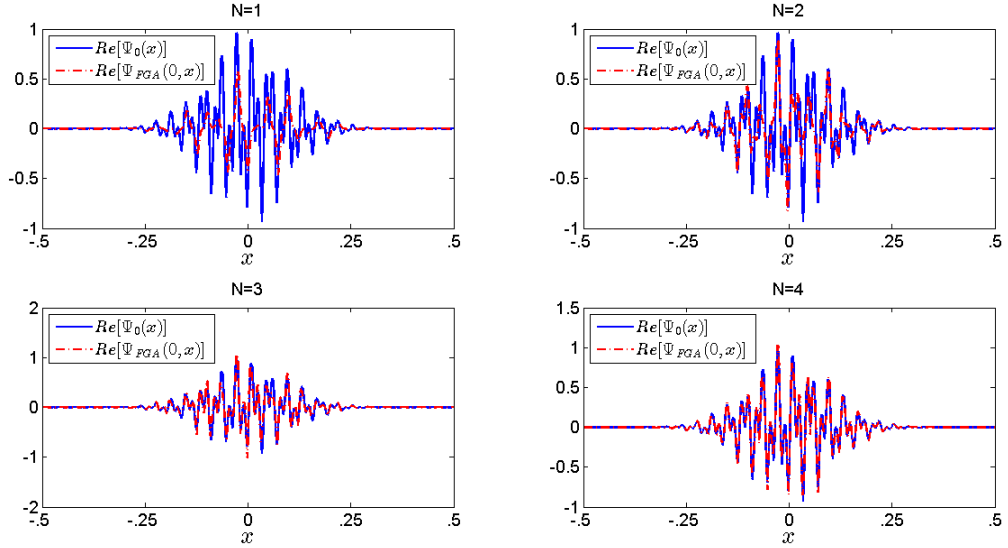
Figure 5.5: Initial decomposition for example 5.3.1. The real part of $\psi_0(x)$ and $\psi_{\text{FGA}}^{\varepsilon}(0, x)$ are shown for $\varepsilon = 1/256$. The summation in $\psi_{\text{FGA}}^{\varepsilon}(0, x)$ is over the first 4 lowest energy bands.

rate also depends on the form of the initial condition. We see from Examples 5.3.1, and 5.3.2 that the cosine lattice potential seem to produce faster convergence with respect to the number of bands used. Different initial conditions may also converge faster as N increases. Example 5.3.4 uses an initial condition projected onto the first band. Choosing such initial condition has the advantage of needing only to compute $\psi_{\text{FGA}}^{\varepsilon}$ over one band, i.e. $\psi_{\text{FGA}}^{\varepsilon, n}$.

By examining the L^2 errors or the convergence rates, one could determine the minimum number of bands to sum over to achieve required accuracy. In Example 5.3.1, it shows that upon summing over $N = 4$ bands, the initial decomposition starts to resemble the initial condition.

Verification of the convergence rate of FGA.

First, we choose to test the convergence rate of (3.8) with external potential $U(x) = 0$ in Examples 5.3.3 and 5.3.4. With this choice of potential, there is no need for a gauge-
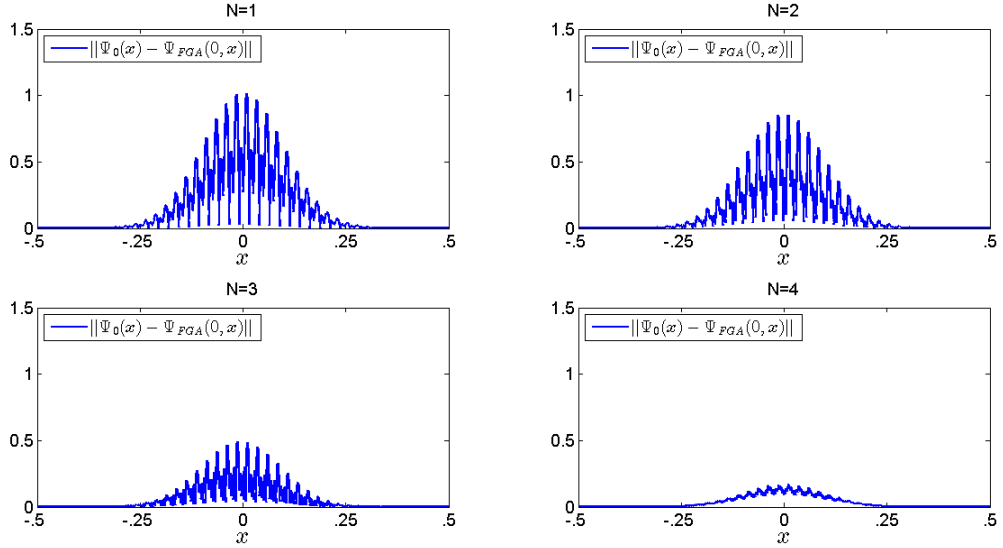
Figure 5.6: The plot of $||\psi_0(x) - \psi^\varepsilon_{\mathrm{FGA}}(0,x)||_{l^2}$ for figure 5.5 is displayed here.

invariant algorithm. One can optimize the algorithm described in Section 5.2.1 by setting $\tilde{F}(t,q,p) = 1$ in (5.25) in Step 4. Thus, for Examples 5.3.3 and 5.3.4, numerical errors coming from $\tilde{F}(t,q,p)$ will be absent. Examples 5.3.5 and 5.3.6 have nonzero external potential so there will be some numerical errors introduced by $\tilde{F}(t,q,p)$. We continue using $2/\sqrt{\varepsilon}$ mesh points per unit interval in q and p and sum up to eight bands (except for Example 5.3.4). We choose a time step of size $\Delta t = T/150$. The exact solution to equation (1.9) will be computed using the Strang-splitting spectral method [4]. For all of our examples, the Strang-splitting spectral method did not need a mesh finer than $\Delta x = 1/2^{16}$ and $\Delta t = 1/2^{12}$.

Example 5.3.3. *In this example we choose the initial condition to be*
$\psi_0 = A(x)\exp\big(\mathrm{i}S(x)/\varepsilon\big)$ *with* $A(x) = \exp\big(-50x^2\big)$ *and* $S(x) = 0.3 + 0.1\sin(x - 0.5)$.
The exact solution is computed using the Strang-Splitting spectral method. This is done at time $T = 0.35$. *The lattice potential used is* $V_\Gamma(x) = \cos(x)$. *We record the data in Table 5.3. The convergence order of the data in table 5.3 is 1.0366. We display plots of*

	Error $\|\psi_{Spec} - \psi_{\mathrm{FGA}}^{\varepsilon}\|_{l^2}$	Rate of Convergence
$\varepsilon = 1/8$	0.09112	
$\varepsilon = 1/16$	0.048907	0.8977
$\varepsilon = 1/32$	0.022603	1.1135
$\varepsilon = 1/64$	0.010555	1.0986

Table 5.3: L^2 error of $\psi_{Spec}(0.35, x) - \psi_{\mathrm{FGA}}^{\varepsilon}(0.35, x)$ for various values of ε. The summation in $\psi_{\mathrm{FGA}}^{\varepsilon}$ is over the first 8 lowest energy bands.

	Error $\|\psi_{Spec} - \psi_{FGA}^{\varepsilon}\|_{l^2}$	Rate of convergence
$\varepsilon = 1/64$	0.0269	
$\varepsilon = 1/128$	0.0144	0.9015
$\varepsilon = 1/256$	0.0069	1.0614

Table 5.4: L^2 error of $\psi_{Spec}(0.35, x) - \psi_{FGA}^{\varepsilon}(0.35, x)$ for initial condition projected onto the first Bloch band.

the solution for $\varepsilon = 1/8, 1/16, 1/32$ and $1/64$ in Figures 5.7, 5.8, 5.9, and 5.10.

In the next example, we will choose initial condition projected onto one Bloch band. With this choice of initial condition, there will be no initial error.

Example 5.3.4. In this example we will choose an initial condition $\Pi_{n=1}^{\mathcal{W},\varepsilon}\psi_0(x)$ given by (2.15) with $\psi_0(x) = A(x)\exp(\mathrm{i}S(x)/\varepsilon)$ where $A(x) = \exp(-50x^2)$ and $S(x) = 0.3x + 0.1\sin(x - 0.5)$ with lattice potential $\exp(-20x^2)$ and external potential $U(x) = 0$. We compute the solution at time $T = 0.35$ using the Strang-Splitting spectral method and GIFGA. The L^2 errors are recorded in Table 5.4. The convergence order is 0.9814. We display plots of the solution for $\varepsilon = 1/64, 1/128$ and $1/256$ in Figures 5.11, 5.12, and 5.13.
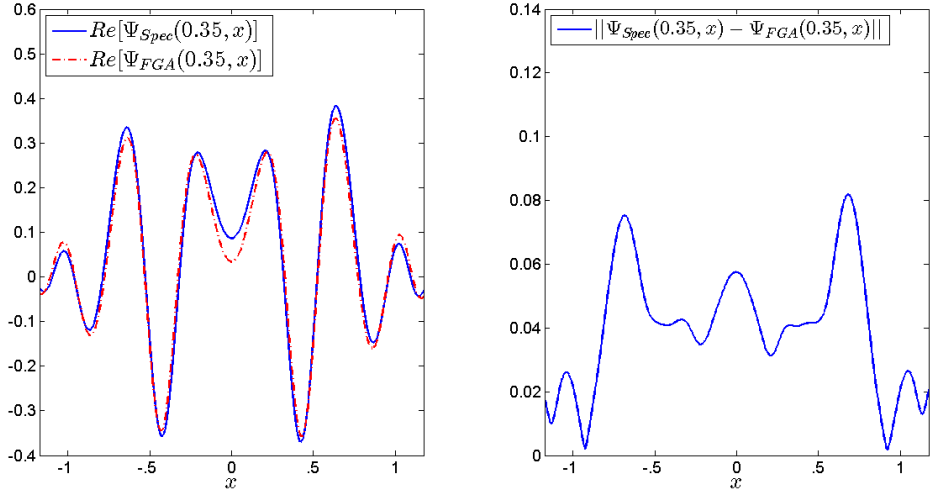
Figure 5.7: Example 5.3.3 plot of real parts of $\psi^{\varepsilon}_{\mathrm{FGA}}(0.35, x)$ and $\psi_{Spec}(0.35, x)$ along side with the L^2 error for $\varepsilon = 1/8$.
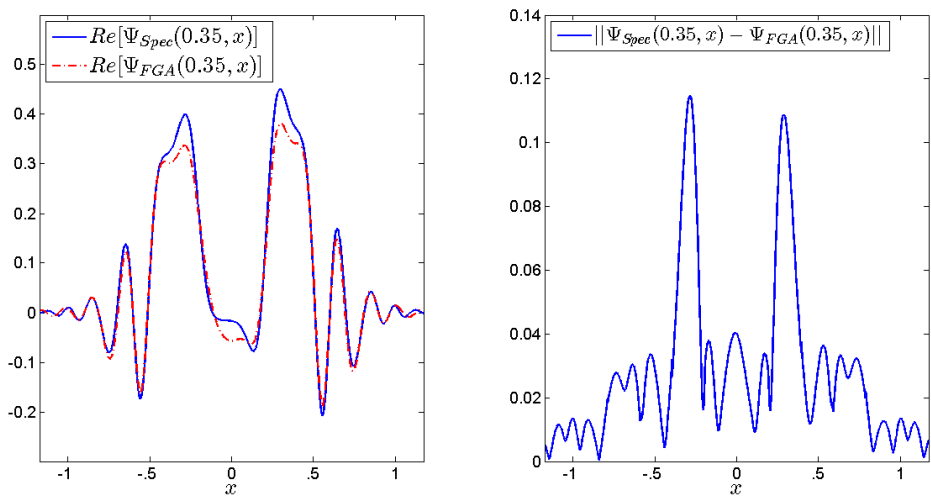
Figure 5.8: Example 5.3.3 plot of real parts of $\psi^{\varepsilon}_{\mathrm{FGA}}(0.35, x)$ and $\psi_{Spec}(0.35, x)$ along side with the L^2 error for $\varepsilon = 1/16$.
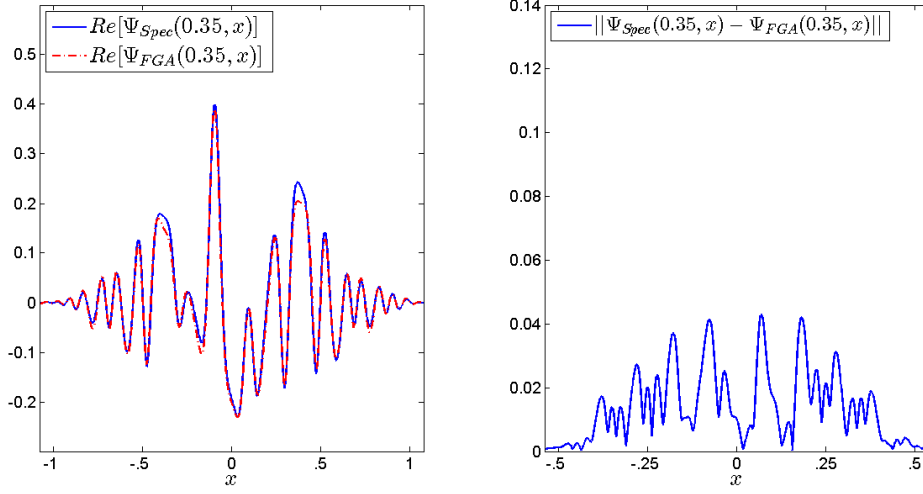
Figure 5.9: Example 5.3.3 plot of real parts of $\psi^{\varepsilon}_{\mathrm{FGA}}(0.35, x)$ and $\psi_{Spec}(0.35, x)$ along side with the L^2 error for $\varepsilon = 1/32$.
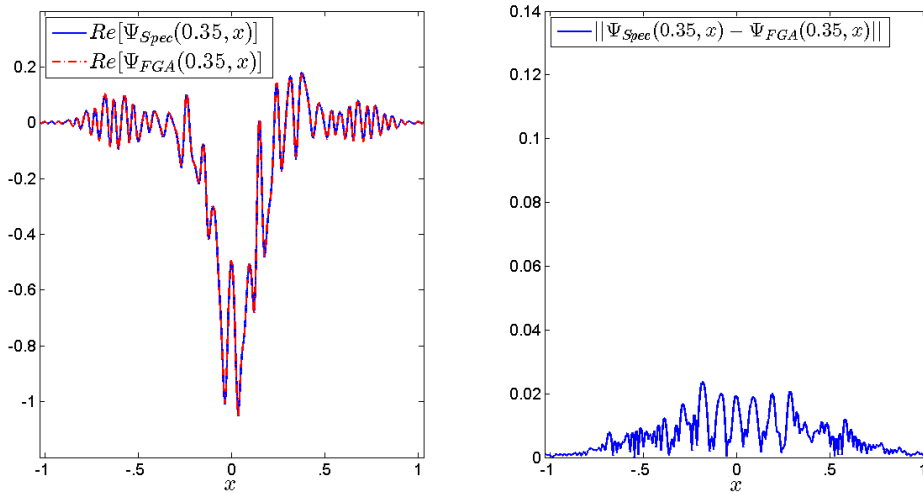
Figure 5.10: Example 5.3.3 plot of real parts of $\psi^{\varepsilon}_{\mathrm{FGA}}(0.35, x)$ and $\psi_{Spec}(0.35, x)$ along side with the L^2 error for $\varepsilon = 1/64$.
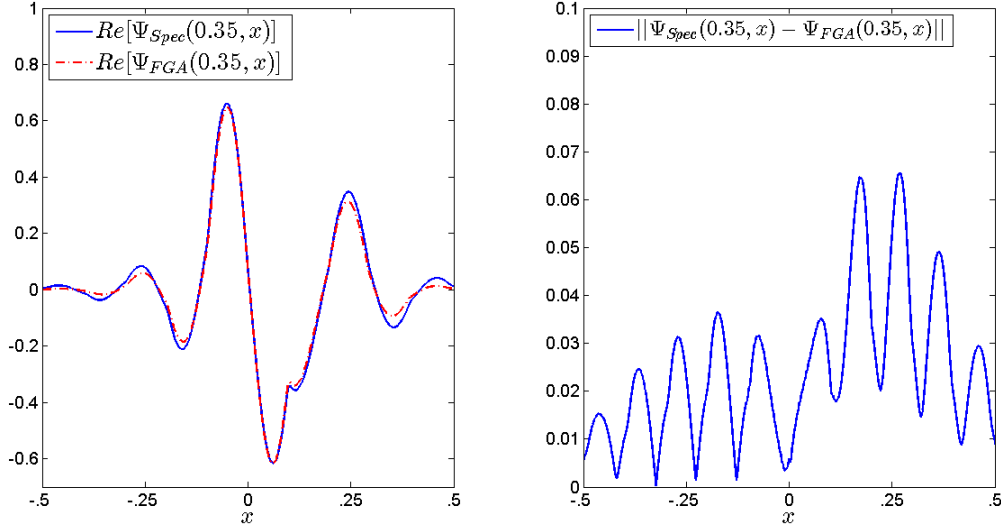
Figure 5.11: Example 5.3.4 plot of the real part of $\psi_{Spec}(0.35, x)$ and $\psi^\varepsilon_{FGA}(0.35, x)$ alongside with the L^2 error of $\psi_{Spec}(0.35, x) - \psi^\varepsilon_{FGA}(0.35, x)$ for example 5.3.4. We use $\varepsilon = 1/64$.
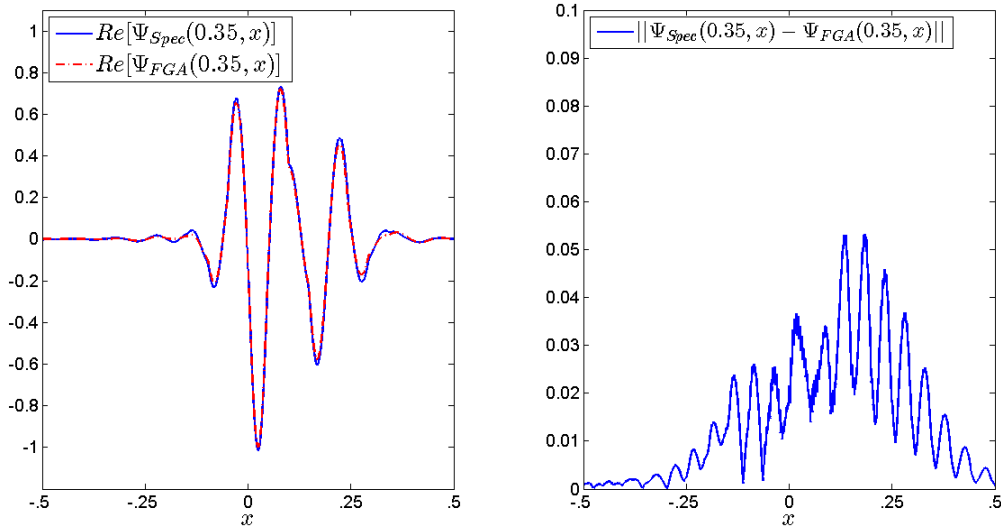
Figure 5.12: Example 5.3.4 plot of the real part of $\psi_{Spec}(0.35, x)$ and $\psi^\varepsilon_{FGA}(0.35, x)$ alongside with the L^2 error of $\psi_{Spec}(0.35, x) - \psi^\varepsilon_{FGA}(0.35, x)$ for example 5.3.4. We use $\varepsilon = 1/128$.
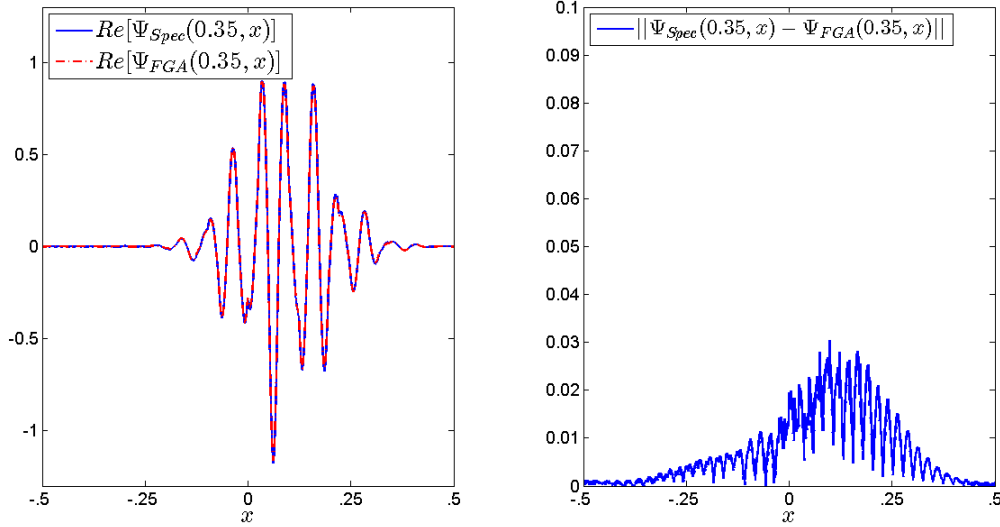
Figure 5.13: Example 5.3.4 plot of the real part of $\psi_{Spec}(0.35, x)$ and $\psi_{FGA}^\varepsilon(0.35, x)$ alongside with the L^2 error of $\psi_{Spec}(0.35, x) - \psi_{FGA}^\varepsilon(0.35, x)$ for example 5.3.4. We use $\varepsilon = 1/256$.

Example 5.3.5. *In this example we choose the initial condition to be* $\psi_0 = A(x) \exp\big(\mathrm{i}S(x)/\varepsilon\big)$ *with* $A(x) = \exp\big(-50x^2\big)\cos((x-0.5)/\varepsilon)$ *and* $S(x) = 0.3(x-0.5) + 0.1\sin(x-0.5)$. *The exact solution is computed using the Strang-splitting spectral method. This is done at time* $T = 0.2$. *The potential used is* $V_\Gamma(x) = \exp(-25x^2)$ *with external potential* $U(x) = \dfrac{1}{2}x^2$. *Our results are shown in Table 5.5. The convergence order of the data in table 5.5 is* 0.9488. *We display plots of the solution for* $\varepsilon = 1/128, 1/256$ *and* $1/512$ *in Figures 5.14, 5.15, and 5.16.*

Example 5.3.6. *In this example we choose the same initial condition as in Example 5.3.5. All of the same parameters as in Example 5.3.5 will also be used. The exact solution is again computed using the Strang Splitting spectral method at time* $T = 0.2$. *The only difference is that we change the external potential to* $U(x) = \cos(x)$. *The convergence order of the data in Table 5.6 is* 0.8439. *We display plots of the solution for* $\varepsilon = 1/128, 1/256$ *and* $1/512$ *in Figures 5.17, 5.18, and 5.19.*

	Error $||\psi_{Spec} - \psi_{FGA}||_{l^2}$	Rate of Convergence
$\varepsilon = 1/64$	0.059576	
$\varepsilon = 1/128$	0.038811	.61826
$\varepsilon = 1/256$	0.015225	1.3500
$\varepsilon = 1/512$	0.0082833	0.8782

Table 5.5: L^2 error of $\psi_{Spec}(0.2, x) - \psi^\varepsilon_{FGA}(0.2, x)$ for various values of ε. The summation in ψ^ε_{FGA} is over the first 8 lowest energy bands.
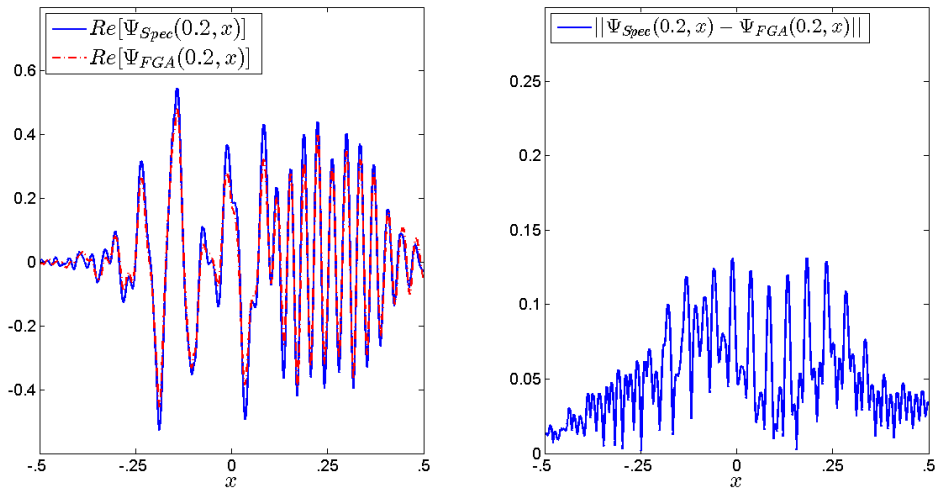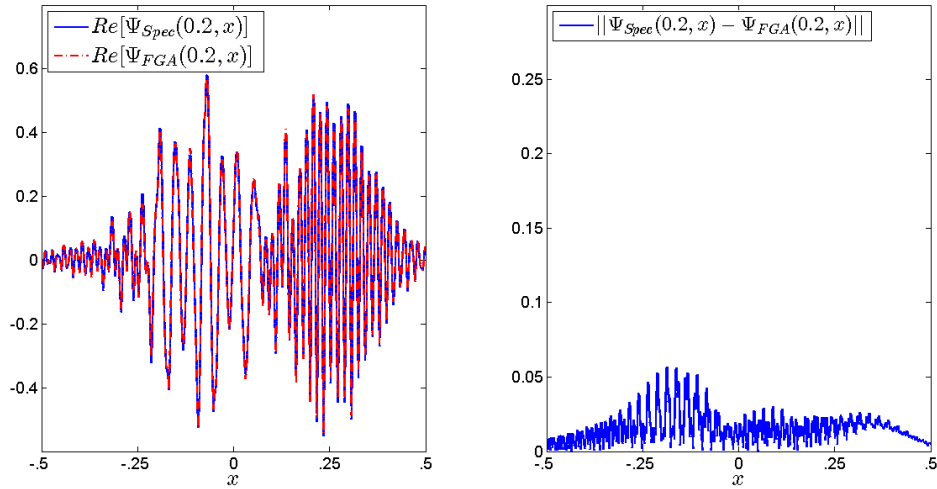

Figure 5.14: Example 5.3.5 plot of the real parts of $\psi^\varepsilon_{FGA}(0.2, x)$ and $\psi_{Spec}(0.2, x)$ along side with the L^2 error for $\varepsilon = 1/128$.

	Error $||\psi_{Spec} - \psi^\varepsilon_{FGA}||_{l^2}$	Rate of Convergence
$\varepsilon = 1/128$	0.039714	
$\varepsilon = 1/256$	0.019057	1.0593
$\varepsilon = 1/512$	0.012327	0.6285

Table 5.6: L^2 error of $\psi_{Spec}(0.2, x) - \psi^\varepsilon_{FGA}(0.2, x)$ for various values of ε. The summation in ψ^ε_{FGA} is over the first 8 lowest energy bands.

Figure 5.15: Example 5.3.5 plot of the real parts of $\psi_{FGA}^{\varepsilon}(0.2, x)$ and $\psi_{Spec}(0.2, x)$ along side with the L^2 error for $\varepsilon = 1/256$.
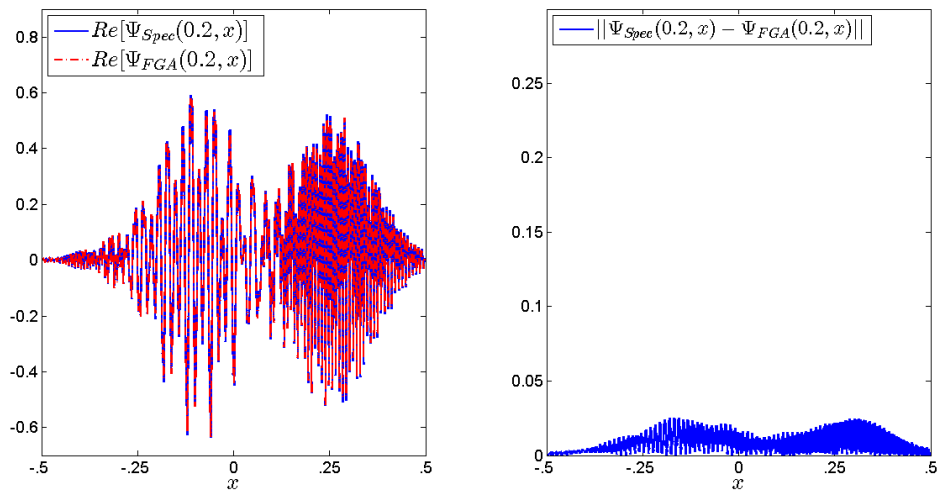
Figure 5.16: Example 5.3.5 plot of the real parts of $\psi_{FGA}^{\varepsilon}(0.2, x)$ and $\psi_{Spec}(0.2, x)$ along side with the L^2 error for $\varepsilon = 1/512$.

64
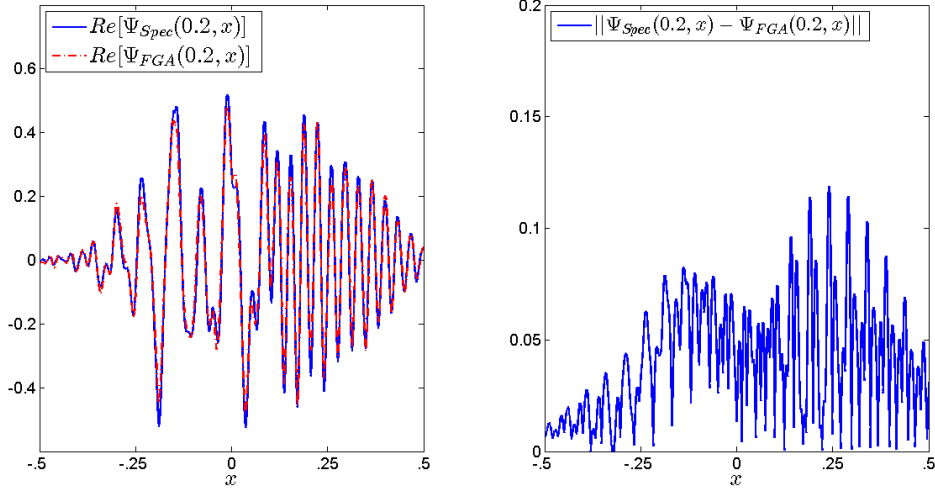
Figure 5.17: Plot of real parts of $\psi_{FGA}^{\varepsilon}(0.2, x)$ and $\psi_{Spec}(0.2, x)$ along side with the L^2 error for $\varepsilon = 1/128$.
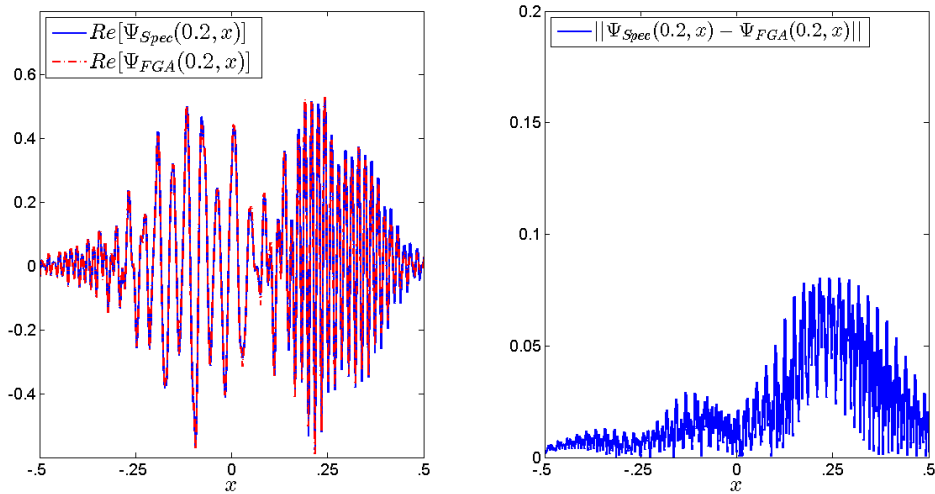
Figure 5.18: Plot of real parts of $\psi_{FGA}^{\varepsilon}(0.2, x)$ and $\psi_{Spec}(0.2, x)$ along side with the L^2 error for $\varepsilon = 1/256$.
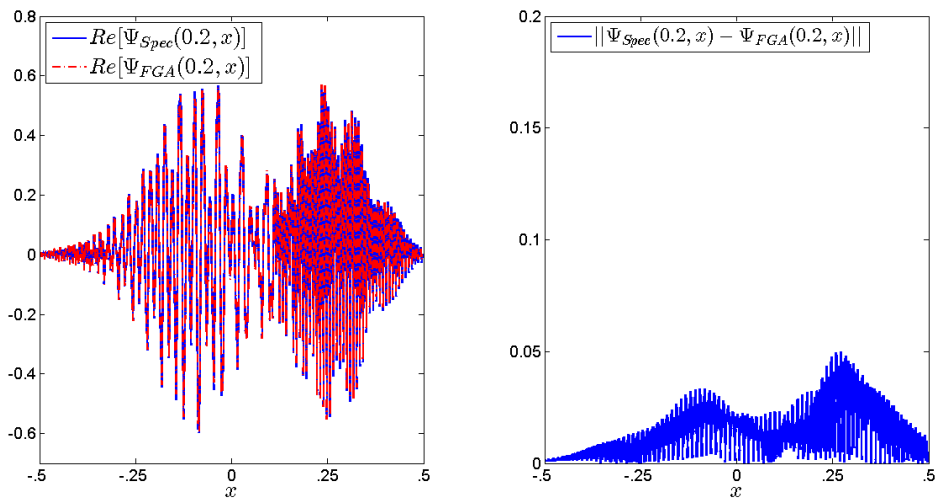
Figure 5.19: Plot of real parts of $\psi^{\varepsilon}_{FGA}(0.2, x)$ and $\psi_{Spec}(0.2, x)$ along side with the L^2 error for $\varepsilon = 1/512$.

Chapter 6

Artificial boundary conditions for the nonlinear Schrödinger equation

6.1 The nonlinear Schrödinger equation and artificial boundary conditions

We start this chapter with a brief introduction to the nonlinear Schrödinger equation (NLS),

$$i\varepsilon\partial_t\psi^\varepsilon = -\frac{\varepsilon^2}{2}\Delta\psi^\varepsilon + V(\boldsymbol{x})\psi^\varepsilon + f(|\psi^\varepsilon|^2)\psi^\varepsilon, \tag{6.1}$$

where $i = \sqrt{-1}$ is the imaginary unit, $\psi(x,t)$ is a complex-valued solution to equation (6.1), and f is a real-valued smooth function. $V(x)$ represents a smooth external potential. The constant ε ($0 < \varepsilon \ll 1$) is described in terms of physical constants by equation (1.5). The initial condition $\psi_0^\varepsilon(\boldsymbol{x})$ will be in $L^2(\mathbb{R}^d)$. As before, we will also consider the case of periodic potentials so that equation (6.1) becomes,

$$i\varepsilon\partial_t\psi^\varepsilon = -\frac{\varepsilon^2}{2}\Delta\psi^\varepsilon + V_\Gamma(\boldsymbol{x})\psi^\varepsilon + U(\boldsymbol{x})\psi^\varepsilon + f(|\psi^\varepsilon|^2)\psi^\varepsilon, \tag{6.2}$$

where $V_\Gamma(\boldsymbol{x})$ is periodic with respect to $\Gamma = [0,1)^d$. From now on, we will work in one-spatial dimension. Higher dimensional generalizations is straight forward.

Artificial boundary conditions.

The purpose of constructing artificial boundary conditions is to approximate the solution to a whole-space problem, to that restricted to a bounded domain. The main idea is to construct boundaries to absorb waves arriving at artificial boundaries. One way to achieve this is to follow Kuska's method for absorbing boundary conditions (see [26]). We will now describe this method. Rewrite the NLS (6.1) in the operator form

$$i\varepsilon \partial_t \psi^\varepsilon = \mathcal{L}\psi^\varepsilon + \mathcal{N}\psi^\varepsilon, \tag{6.3}$$

where $\mathcal{L} = -\varepsilon^2 \Delta \psi^\varepsilon$, and $\mathcal{N} = (V(x) + f(|\psi^\varepsilon|^2))\psi^\varepsilon$. Let us approximate $\mathcal{L}$ by $\mathcal{L}^n$ where n will be related to the convergence of the Padé expansion to be described later. Thus, equation (6.3) becomes,

$$i\varepsilon \partial_t \psi^\varepsilon = \mathcal{L}^n \psi^\varepsilon + \mathcal{N}\psi^\varepsilon. \tag{6.4}$$

To derive $\mathcal{L}^n$, we will assume that the boundary is transparent to plane waves

$$\psi(x,t) = \exp\left(-i(\omega t - \xi x)\right), \tag{6.5}$$

where ω is the frequency and ξ is the wave number. Inserting this plane wave into the Schrödinger equation with zero potential yields $\varepsilon^2 \xi^2 = 2\varepsilon\omega$, or

$$\varepsilon\xi = \pm\sqrt{2\varepsilon\omega}. \tag{6.6}$$

The $+$ sign corresponds to right-moving waves and the $-$ sign to waves left-moving waves. Now we use the padé expansion about ω_0 for $\sqrt{\cdot}$ to third order,

$$\sqrt{2\varepsilon\omega} \approx \sqrt{\omega_0}\frac{\omega_0 + 6\varepsilon\omega}{3\omega_0 + 2\varepsilon\omega}. \tag{6.7}$$

Denote $k_0 = \sqrt{\omega_0}$ and substitute (6.7) into (6.6) to get

$$\varepsilon\xi = \pm k_0 \frac{k_0^2 + 6\varepsilon\omega}{3k_0^2 + 2\varepsilon\omega}. \tag{6.8}$$

Next, we use the dual relation

$$\xi \Leftrightarrow -\mathrm{i}\partial_x \qquad \omega \Leftrightarrow \mathrm{i}\partial_t \tag{6.9}$$

to rewrite equation (6.8) as

$$-2\varepsilon^2 \psi_{xt} \pm 6\mathrm{i}\varepsilon k_0 \psi_t + 3\mathrm{i}\varepsilon k_0^2 \psi_x \pm k_0^3 \psi = 0, \tag{6.10}$$

which further simplifies to

$$\mathrm{i}\varepsilon\partial_t\psi = -(2\mathrm{i}\varepsilon\partial_x \pm 6k_0)^{-1}(3\mathrm{i}\varepsilon k_0^2\partial_x \pm k_0^3)\psi := \mathcal{L}^3\psi. \tag{6.11}$$

Now we substitute equation (6.11) into equation (6.4),

$$-2\varepsilon^2\partial_{x,t}\psi \pm 6\mathrm{i}\varepsilon k_0\partial_x\psi + 3\mathrm{i}\varepsilon k_0^2\partial_x\psi \pm k_0^3\psi = [V(x) + f(|\psi|^2)](2\mathrm{i}\varepsilon\psi_x \pm 6k_0\psi). \tag{6.12}$$

We now summarize the boundary strategy discussed above,

$$\begin{cases} \mathrm{i}\varepsilon\partial_t\psi = -\dfrac{\varepsilon^2}{2}\partial_x^2\psi + V(x)\psi + f(|\psi|^2)\psi, & x_l < x < x_r,\ 0 < t \leqslant T \\[2mm] \text{equation (6.12)}, & \text{with } x_l \Leftrightarrow - \text{ and } x_r \Leftrightarrow + \\[2mm] \psi(x,0) = \psi_0(x), & x_l \leqslant x \leqslant x_r \end{cases} \tag{6.13}$$

See [99],[97] for related work.

6.2 Time-splitting FGA method for the NLS

First-order time-splitting FGA method.

Because the Fourier integral operator, equation (2.19), is limited to solving linear problems, to solve nonlinear problems, we inevitably must split the NLS into its linear

69

and nonlinear parts. Following the Strang-splitting spectral method in chapter 4, we
discretize time $0 = t_0 < t_1 < t_2 < \cdots < t_N = t_{final}$ and split (6.2) in two parts,

$$i\varepsilon\partial_t\psi^\varepsilon = -\frac{\varepsilon^2}{2}\Delta\psi^\varepsilon + V_\Gamma(x)\psi^\varepsilon + U(\boldsymbol{x})\psi^\varepsilon, \tag{6.14}$$

and

$$i\varepsilon\partial_t\psi^\varepsilon = f\left(|\Psi^\varepsilon|^2\right)\psi^\varepsilon. \tag{6.15}$$

The linear Schrödinger equation, (6.14), can be solved numerically using a direct method
like the Strang-splitting spectral method. However, due to the high computational cost
of direct methods, we will apply the FGA to solve equation (6.14).

We may approximate (6.15) at time t_{n+1} by

$$\psi^\varepsilon(t_{n+1}, x) \approx \exp\left(-\frac{i}{\varepsilon}f(|\psi^\varepsilon_{\text{FGA}}(t_{n+1}, x)|^2\delta t)\right)\psi^\varepsilon_{\text{FGA}}(t_{n+1}, x). \tag{6.16}$$

Iterating the above algorithm using N_t number of time steps starting at time $t = 0$ and
ending at some time $t = T$ with $\delta t = \dfrac{T}{N_t}$ will give us an approximate solution $\psi^\varepsilon(T, x)$
to the NLS equation (6.2).

Remark. The exact solution to equation (6.15) is

$$\exp\left(-\frac{i}{\varepsilon}\int_{t_n}^{t_{n+1}} f(|\psi_{\text{FGA}}(s, x)|^2)\right)\psi_{\text{FGA}}(t_{n+1}, \boldsymbol{x}), \tag{6.17}$$

but for small time step, we may approximate the evaluation of the integral as in equation
(6.16).

Accuracy. Assume the numerical integrator used for solving (5.12) is of order p
with the time step δt, as noted in equation (5.27), the error of computing (6.14) is
$\mathcal{O}\left(\varepsilon + \frac{(\delta t)^p}{\varepsilon} + \max_n \Delta\boldsymbol{P}_n\right) + ||\sum_{n=1}^N \prod_n^{\mathcal{W},\varepsilon} \psi_0^\varepsilon||_{L^2}$. The error of computing (6.16) and
total splitting error is both $\mathcal{O}(\delta t)$. Therefore, the total accuracy is of
$\mathcal{O}\left(\varepsilon + \delta t + \frac{(\delta t)^p}{\varepsilon} + \max_n \Delta\boldsymbol{P}_n\right) + ||\sum_{n=1}^N \prod_n^{\mathcal{W},\varepsilon} \psi_0^\varepsilon||_{L^2}$.

If equation (6.1) does not contain a periodic potential, one can improve the accuracy by using the FGA method described in chapter 4. In this case, the accuracy will be $\mathcal{O}\left(\varepsilon + \delta t + \frac{(\delta t)^p}{\varepsilon}\right)$.

Complexity of first-order NLS algorithm. Typically, the time-splitting method requires δt to be $\mathcal{O}\left(\varepsilon\right)$, or $N_t = \mathcal{O}(1/\varepsilon)$ so that equation (6.15) is computed accurately. We also need $\delta x = \mathcal{O}\left(\varepsilon\right)$, or $N_x = \mathcal{O}(1/\varepsilon)$. Thus the total complexity is N_t times the complexity of computing the solution to equation (6.14).

FGA-Based Strang-splitting.

We can increase the accuracy to second order in time by splitting equation (6.2) in three parts. Given a time discretization, $0 = t_0 < t_1 < t_2 < \cdots < t_N = t_{final}$ we can describe the approximate solution by the following algorithm:

$$i\varepsilon\partial_t\psi^\varepsilon = f(|\psi^\varepsilon|^2)\psi^\varepsilon, \tag{6.18}$$

$$i\varepsilon\partial_t\psi^\varepsilon = -\frac{\varepsilon^2}{2}\Delta\psi^\varepsilon + (V_\Gamma(\boldsymbol{x}) + U(\boldsymbol{x}))\,\psi^\varepsilon, \tag{6.19}$$

$$i\varepsilon\partial_t\psi^\varepsilon = f(|\psi^\varepsilon|^2)\psi^\varepsilon, \tag{6.20}$$

and solving equation (6.18) and (6.20) on half a time step and equation (6.19) on one time step. More explicitly, the solution at time t_{n+1} is given by

$$\psi^\varepsilon(t_{n+1}, \boldsymbol{x}) = \exp\left(-\frac{i}{2\varepsilon}f(|\psi^\varepsilon|^2)\delta t\right)\psi^*(t_{n+1}, \boldsymbol{x}) \tag{6.21}$$

where $\psi^*(t_{n+1}, \boldsymbol{x})$ is the FGA solution to equation (6.19) with initial condition

$$\exp\left(-\frac{i}{2\varepsilon}f(|\psi^\varepsilon|^2)\delta t\right)\psi^\varepsilon(t_n, \boldsymbol{x}). \tag{6.22}$$

71

Alternative. Note that the option of splitting the operators on the right-hand-side of (6.2) is not unique, and another possibility is to split (6.2) as

$$i\varepsilon\partial_t\psi^\varepsilon = -\frac{\varepsilon^2}{2}\Delta\psi^\varepsilon, \tag{6.23}$$

and

$$i\varepsilon\partial_t\psi^\varepsilon = (V_\Gamma(\boldsymbol{x}) + U(\boldsymbol{x}))\psi^\varepsilon + f\left(|\psi|^2\right)\psi^\varepsilon. \tag{6.24}$$

One can get the FGA solution at time t_{n+1} to (6.23) by using (1.53) with initial condition $\psi(t_n, x)$. The solution to (6.24) can be approximated by

$$\psi(t_{n+1}, \boldsymbol{x}) \approx \exp\left(-\frac{i}{\varepsilon}\delta t\left(V_\Gamma(\boldsymbol{x}) + U(\boldsymbol{x}) + f(|\psi_{\text{FGA}}(t_{n+1}, x)|^2)\right)\right)\psi_{\text{FGA}}(t_{n+1}, \boldsymbol{x}). \tag{6.25}$$

Iterating the above two equations using N_t number of time steps starting at time $t_0 = 0$ and ending at some time $t_N = T$ with $\delta t = \dfrac{T}{N}$ will still give us an approximate solution $\psi(T, x)$ to (6.1). The disadvantage in using this method is that we don't take full advantage of ψ_{FGA} to save computational cost for highly oscillatory periodic potentials.

Boundary strategy for the FGA in one-dimension.

In this subsection, we briefly describe FGA-based artificial boundary conditions for the linear Schrödinger equation (1.4) (or (1.9)), and we will introduce how to generalize it to the nonlinear Schrödinger equation.

The key idea in deriving equation (6.13) is to make the boundaries transparent to plane waves. Motivated by this observation, we propose to delete Gaussian functions, whose trajectory is determined by the Hamiltonian flow, that fall outside the boundary.

Let us assume that ψ_0 is compactly supported in Ω_0 and suppose that we are only interested in the solution to (6.14) on a domain $\Omega_1 = (x_l, x_r)$. In order to accurately compute the weight function

$$\langle G_{\boldsymbol{q},\boldsymbol{p}}^\varepsilon(\cdot)u_n(\boldsymbol{p}, \cdot), \psi_0^\varepsilon\rangle \tag{6.26}$$

of equation (3.5), we will need to define our phase space grid in $\boldsymbol{q}$-space to cover $\Omega_0 + \mathcal{O}(\sqrt{\varepsilon})$. The second term is included because the width of the semiclassical Gaussian is $\sqrt{\varepsilon}$ and Gaussian functions whose centers are within a few $\sqrt{\varepsilon}$ distance of Ω_0 will contribute a non-negligible portion of equation (6.26).

We will therefore place $N_q = \mathcal{O}(1/\sqrt{\varepsilon})$ Gaussian functions on the support Ω_0 of ψ_0. If one desires the solution for all $x \in \Omega_1$, we will need to retain the Gaussian functions centered at $Q(T, q, p)$ whose distance to Ω_1 is less than $\mathcal{O}(\sqrt{\varepsilon})$. In summary, for sufficient accuracy, our boundary strategy needs to satisfy:

1. Retain the Gaussians centered at q located a distance less than $\mathcal{O}(\sqrt{\varepsilon})$ of Ω_0.

2. Retain the Gaussians centered at $Q(T, q, p)$ located a distance less than $\mathcal{O}(\sqrt{\varepsilon})$ of Ω_1.

Example 6.2.1. *We show the accuracy our boundary strategy in this example. We use $\Omega_0 = (-1, 1)$ and $\Omega_1 = (-1, 0)$ with the initial condition*
$\psi_0(x) = \exp\left(-50(x - 1/2)^2\right) + \exp\left(-50(x + 1/2)^2\right)$ and potential $V(x) = \exp(-0.2x^2)$. We remove the Gaussians that are further than $2\sqrt{\varepsilon}$ away from the domains. We solve this at time $t = 0.25$, and plot $\mathfrak{Re}\psi_{FGA}^{\varepsilon}(0.25, x)$ against $\mathfrak{Re}\psi(0.25, x)$ in figure 6.1. Notice that $\mathfrak{Re}\psi_{FGA}^{\varepsilon}$ closely matches the exact solution in Ω_1, as it should.

one-dimensional FGA-based Strang-splitting Algorithm.

Suppose we are interested in the solution $\psi^{\varepsilon}(x, T)$ on the domain $[a, b]$. Let $\Delta x = (b - a)/M$ be the spatial mesh size and $\Delta t = T/N$ be the temporal mesh size, where M and N are positive integers of order ε^{-1}. Set up the mesh

$$x_j = a + j\Delta x, \qquad t_n = nk, \qquad j = 0, 1, 2, \cdots, M, \qquad n = 0, 1, 2, \cdots, N. \quad (6.27)$$
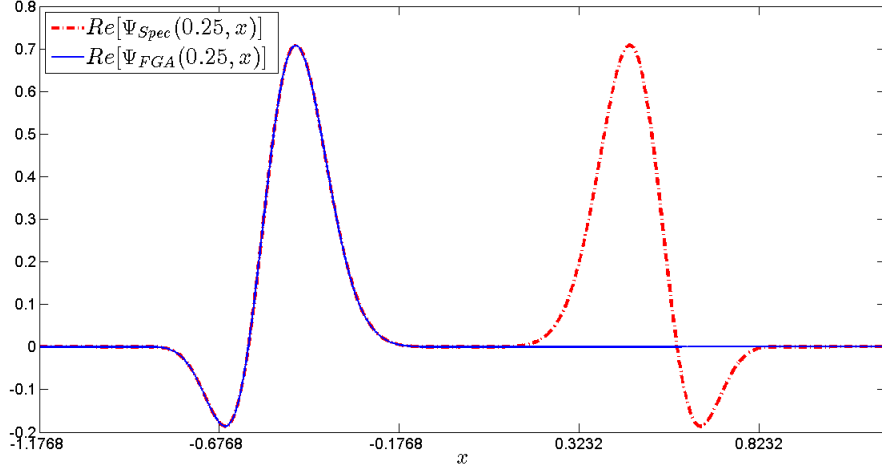
Figure 6.1: Plot of real parts of $\psi_{FGA}^{\varepsilon}(0.25, x)$ and $\psi_{Spec}(0.25, x)$.

Also define the domain $\mathcal{D} = [a, b]$ for which we will apply the boundary strategy. Let $\psi_j^{n,\varepsilon}$ be the approximation $\psi^{\varepsilon}(x_j, t_n)$. Obtaining an approximate solution from time $t = t_n$ to time $t = t_{n+1}$ can be done as follows:

Compute the temporary variable $U_j^{*,\varepsilon}$,

$$U_j^{*,\varepsilon} = e^{-\frac{i}{2\varepsilon} f\left(|U_j^{n,\varepsilon}|^2 \Delta t\right)} U_j^{n,\varepsilon}, \qquad j = 0, 1, 2, \cdots, M. \tag{6.28}$$

Apply the frozen Gaussian approximation from time t_n to time t_{n+1} with initial condition $U^{*,\varepsilon}$.

$$U_j^{**,\varepsilon} = \mathcal{I}^{\varepsilon}\left(U^{*,\varepsilon}\right), \qquad j = 0, 1, 2, \cdots, M. \tag{6.29}$$

Here, the notation $\mathcal{I}^{\varepsilon}\left(\phi\right)$ denotes the FGA solution with initial data ϕ. It is at this step where we remove Gaussian functions whose distance to $\mathcal{D}$ is greater than $\mathcal{O}(\sqrt{\varepsilon})$. The numerical solution at the next time step is approximated by,

$$U_j^{n+1,\varepsilon} = e^{-\frac{i}{2\varepsilon} f\left(|U_j^{*,\varepsilon}|^2 \Delta t\right)} U_j^{**,\varepsilon}, \qquad j = 0, 1, 2, \cdots, M. \tag{6.30}$$

Finally, we iterate the above three equations until we reach the desired time.

Table 6.1: l_2 and l_∞ error of $\|\psi_{Spec}(0.4, \boldsymbol{x}) - \widetilde{\psi}^\varepsilon_{FGA}(0.4, \boldsymbol{x})\|$ of example 6.3.1 on different computational domains for $\varepsilon = 1/128$.

$\mathcal{D} = [x_l, x_r]$	[-1,1]	[-1.5,1.5]	[-2,2]	[-2.5,2.5]
l_2 **Error**	$4.6858 \cdot 10^{-3}$	$4.6868 \cdot 10^{-3}$	$4.6862 \cdot 10^{-3}$	$4.6861 \cdot 10^{-3}$
l_∞ **Error**	$7.2755 \cdot 10^{-3}$	$7.2767 \cdot 10^{-3}$	$7.2760 \cdot 10^{-3}$	$7.2756 \cdot 10^{-3}$

6.3 Numerical examples

Example 6.3.1. *(1d Schrödinger) We choose the initial condition, potential function, and nonlinearity to be*

$$\psi_0(x) = \exp(-25x^2), \quad V(x) = \exp(-0.2x^2), \quad f(x) = x, \tag{6.31}$$

respectively. We will test the performance of the FGA-based second-order time-splitting algorithm for $\varepsilon \ll 1$ and on different computational domains.

Table 6.1 compares l_2 and l_∞ errors between the exact solution (computed using the time-splitting spectral method) and that of the FGA-based algorithm. We omit Gaussians not within $2\sqrt{\varepsilon}$ of the domain $\mathcal{D}$ for different choices of domains for $\varepsilon = 1/128$. Table 6.2 compares the performance of the FGA-based Strang-splitting as ε varies. To satisfy the required complexity of the FGA, we use approximately $2\varepsilon^{-\frac{1}{2}}$ number of Gaussians per unit interval in phase space. The mesh size δt used for the time-splitting is $\delta t = T\varepsilon$ with $\delta x = \frac{1}{4}\varepsilon$. The l_2 and l_∞ error did not significantly change as the support of the solution is mostly contained in $[-1, 1]$ (see figure 6.2).

Example 6.3.2. *(1d Schrödinger) We choose the initial condition, potential function, and nonlinearity as*

$$\psi_0(x) = \exp(-25x^2 + i(x^2 + 3x)/\varepsilon), \quad V(x) = \exp(-0.2x^2), \quad f(x) = x \tag{6.32}$$

Figure 6.2: Real and Imaginary parts of $\psi_{Exact}(0.4, \boldsymbol{x})$ $\psi^{\varepsilon}_{FGA}(0.4, \boldsymbol{x})$ and l_∞ error of example 6.3.1 using $\varepsilon = 1/128$.
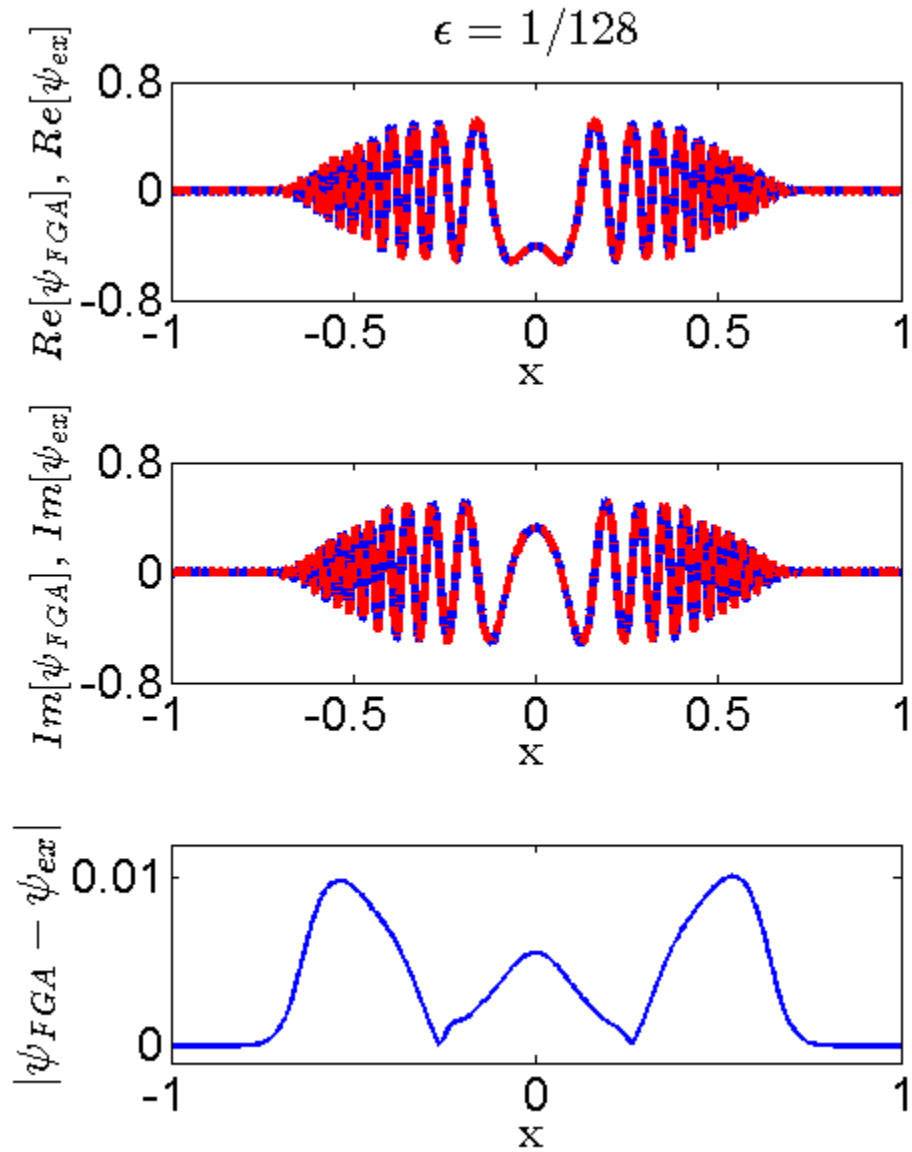
Table 6.2: l_2 and l_∞ error of $||\psi_{Spec}(0.4, \boldsymbol{x}) - \widetilde{\psi}^\varepsilon_{FGA}(0.4, \boldsymbol{x})||$ of example 6.3.1 using different values of ε.

ε	$\varepsilon = 1/64$	$\varepsilon = 1/128$	$\varepsilon = 1/256$
l_2 **Error**	$4.3820 \cdot 10^{-3}$	$4.6868 \cdot 10^{-3}$	$6.5000 \cdot 10^{-3}$
l_∞ **Error**	$6.3271 \cdot 10^{-3}$	$7.2767 \cdot 10^{-3}$	$9.4334 \cdot 10^{-3}$

Table 6.3: l_2 and l_∞ error of $|\psi_{Spec}(0.4, \boldsymbol{x}) - \widetilde{\psi}^\varepsilon_{FGA}(0.4, \boldsymbol{x})|$.

Gaussians per unit interval	$1/\sqrt{\varepsilon}$	$2/\sqrt{\varepsilon}$	$4/\sqrt{\varepsilon}$
$\varepsilon = 1/16, l_2$	Null	$6.4143 \cdot 10^{-3}$	$6.4348 \cdot 10^{-3}$
$\varepsilon = 1/16, l_\infty$	Null	$6.9843 \cdot 10^{-3}$	$7.0998 \cdot 10^{-3}$
$\varepsilon = 1/64, l_2$	Null	$2.6039 \cdot 10^{-2}$	$2.6055 \cdot 10^{-2}$
$\varepsilon = 1/64, l_\infty$	Null	$3.6233 \cdot 10^{-2}$	$3.6155 \cdot 10^{-2}$

In table 6.3, we compute the solution to example 6.3.2 using the Strang-splitting FGA algorithm and compare it with the exact solution. We use the same mesh size as in example 6.3.1. Figure 6.3 displays the error between the real and imaginary parts. We choose $\mathcal{D} = [-2, 2]$. We also compute the l_2 and l_∞ error as the number of Gaussians increases for $\varepsilon = 1/16$ and $\varepsilon = 1/64$. Table 6.3 summarizes our results. We see that using $\varepsilon^{-\frac{1}{2}}$ number of Gaussians is too few, and that there is no significant improvement in accuracy by using more than $2\varepsilon^{-\frac{1}{2}}$ per unit interval.

Our last example contains a highly oscillatory periodic potential, thus we will use the Bloch-based FGA to approximate equation (6.19).

Example 6.3.3. *(1d Schrödinger with periodic potential) We choose the initial condition and nonlinearity as*
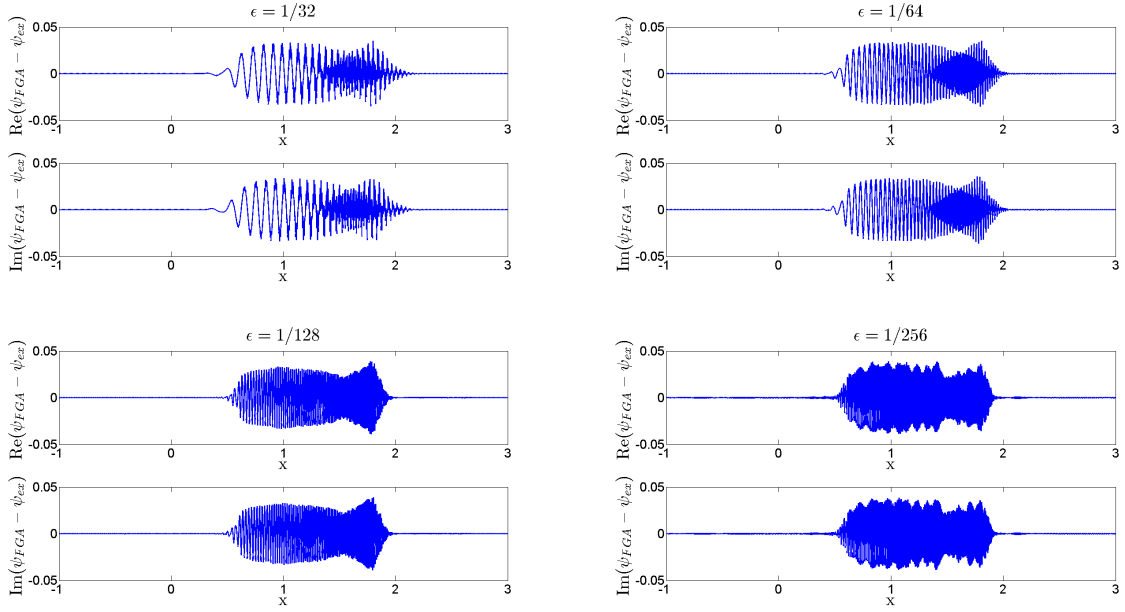
$$\psi_0(x) = \exp(-25x^2), \quad f(x) = x. \tag{6.33}$$

Figure 6.3: Plot of $\mathfrak{Re}[\psi_{ex}] - \mathfrak{Re}[\psi_{FGA}]$ and $\mathfrak{Im}[\psi_{ex}] - \mathfrak{Im}[\psi_{FGA}]$ for $\varepsilon = 1/32, 1/64, 1/128,$ and $1/256$ for example 6.3.2

We take the potential to be $V(x/\varepsilon)$ where $V(x) = \exp(-x^2)$ is extended periodically with respect to the lattice $[-\pi, \pi)$. Note that this extension is not analytic on $-\pi$ and π but due to the rapid decay of the exponential function, this poses no problem numerically. Figure 6.4 displays the FGA-based solution vs the exact solution for $\varepsilon = 1/16$.
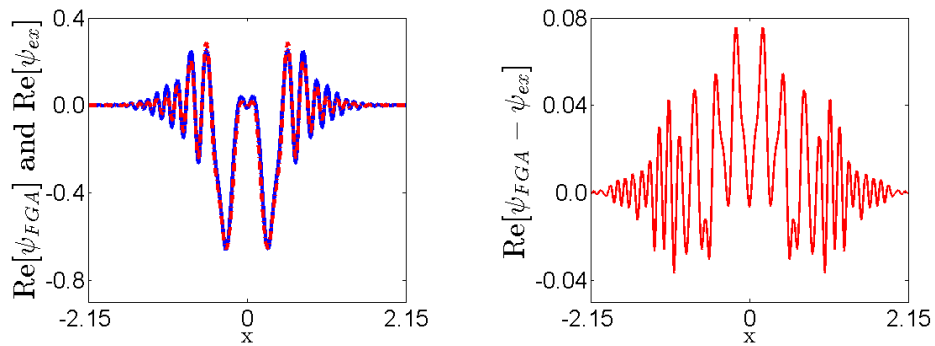
Figure 6.4: Plot of $\mathfrak{Re}[\psi_{ex}]$ and $\mathfrak{Re}[\psi_{FGA}]$ and $\mathfrak{Re}[\psi_{ex} - \psi_{FGA}]$ for $\varepsilon = 1/16$ for example 6.3.3

6.4 Concluding Remarks

In this thesis, we developed the Bloch-decomposition based FGA for the linear Schrödinger equation with periodic potentials in the semiclassical regime. We prove that the convergence of our method satisfies the inequality,

$$||\psi_{Exact}(t, \boldsymbol{x}) - \psi_{\mathrm{FGA}}(t, \boldsymbol{x})||_{L^2} \leqslant \mathcal{O}(\varepsilon). \tag{6.34}$$

The method we have presented is invariant with respect to the gauge choice and thus avoids the difficulty of numerically computing the Berry phase. By splitting the NLS operator into its linear and nonlinear parts, we are able to apply the FGA to the NLS. To compute the solution of the NLS on an unbounded domain, we propose the boundary strategy of removing Gaussians whose distance is greater than $\mathcal{O}(\sqrt{\varepsilon})$ of the domain. We produce several numerical examples confirming our methods.

Bibliography

[1] W. Bao, D. Jaksch, and P. Markowich, *Numerical solution of the gross-pitaevskii equation for the bose-einstein condensation, J. Comput. Phys.* **187** (2003) 318–342.

[2] P. Markowich, P. Pietra, and C. Pohl, *Numerical approximation of quadratic observable of Schrödinger equation-type equations in the semiclassical limit, Numer. Math.* **81** (1999) 595–630.

[3] P. Markowich, P. Pietra, C. Pohl, and H. Stimming, *A Wigner-measure analysis of the Dufort-Frankel scheme for the Schrödinger equation, SIAM J. Numer. Anal.* **40** (2000) 1281–1310.

[4] W. Bao, S. Jin, and P. Markowich, *On time-splitting spectral approximations for the Schrödinger equation in the semiclassical regime, J. Comput. Phys.* **175** (2002) 487–524.

[5] A. Bensoussan, J. Lions, and G. Papanicolaou, *Asymptotic Analysis for Periodic Structures.* North-Holland Publishing Co., Amsterdam-New York, 1978.

[6] G. Panati, H. Spohn, and S. Teufel, *Effective dynamics for Bloch electrons: Peierls substitution and beyond, Comm. Math. Phys.* **242** (2003) 547–578.

[7] G. Panati, H. Spohn, and S. Teufel, *Motions of electrons in adiabatically perturbed periodic structures*, 2006.

[8] M. Popov, *A new method of computation of wave fields using Gaussian beams, Wave Motion* **4** (1982) 85–97.

[9] J. Lu and X. Yang, *Convergence of frozen Gaussian approximation for high frequency wave propagation, Comm. Pure Appl. Math.* **65** (2012) 759–789.

[10] J. Lu and X. Yang, *Frozen Gaussian approximation for high frequency wave propagation, Commun. Math. Sci.* **9** (2011) 663–683.

[11] S. Jin, H. Wu, and X. Yang, *Gaussian beam methods for the Schrödinger equation in the semi-classical regime: Lagrangian and Eulerian formulations, Commun. Math. Sci.* **6** (2008) 995–1020.

[12] N. Tanushev, J. Qian, and J. Ralston, *Mountain waves and Gaussian beams*, *Multiscale Model. Simul.* **6** (2007) 688–709.

[13] N. Tanushev, *Superpositions and higher order Gaussian beams*, *Commun. Math. Sci.* **6** (2008) 449–475.

[14] J. Lu and X. Yang, *Frozen Gaussian approximation for general linear strictly hyperbolic system: Formulation and Eulerian methods*, *Multiscale Model. Simul.* **10** (2012) 451–472.

[15] Z. Huang, S. Jin, P. Markowich, and C. Sparber, *A bloch decomposition-based split-step pseudospectral method for quantum dynamics with periodic potentials*, *SIAM J. Sci. Comput.* **29** (2007) 515–538.

[16] R. Carles, P. Markowich, and C. Sparber, *Semiclassical asymptotics for weakly nonlinear bloch waves*, . arXiv:math-ph/0401053v4.

[17] S. Jin, H. Wu, X. Yang, and Z. Huang, *Bloch decomposition-based Gaussian beam method for the Schrödinger equation with periodic potentials*, *J. Comput. Phys.* **229** (2010) 4869–4883.

[18] C. Wilcox, *Theory of bloch waves*, *J. Anal. Math.* **33** (1978) 146–167.

[19] R. D. King-Smith and D. Vanderbilt, *Theory of polarization of crystalline solids*, *Phys. Rev. B* **47** (Jan, 1993) 1651–1654.

[20] R. Delgadillo, J. Lu, and X. Yang, *Frozen gaussian approximation for high frequency wave propagation in periodic media*, 2014. preprint.

[21] T. Swart and V. Rousse, *A mathematical justification of the Herman-Kluk propagator*, *Commun. Math. Phys.* **286** (2009) 725–750.

[22] M. Reed and B. Simon, *Methods of Modern Mathematical Physics, Vol IV*. Academic Press, New York, 1980.

[23] G. A. Hagedorn, *Raising and lowering operators for semiclassical wave packets*, *Annals of Physics* **269** (2002) 77–104.

[24] Z. Huang, S. Jin, P. Markowich, and C. Sparber, *A Bloch decomposition-based split-step pseudospectral method for quantum dynamics with periodic potentials*, *SIAM J. Sci. Comput.* **29** (2007) 515–538.

[25] G. Sun, *A simple way constructing symplectic Runge-Kutta methods*, *Math. Comp.* **18** (2000) 61–68.

[26] J.-P. Kuska., *Absorbing boundary conditions for the schrodinger equation on finite intervals*, *Phys. Rev B* **46** (1992) 5000–5003.

[27] D. Vanderbilt and R. D. King-Smith, *Electric polarization as a bulk quantity and its relation to surface charge*, Phys. Rev. B **48** (Aug, 1993) 4442–4455.

[28] B. Engquist and O. Runborg, *Computational high frequency wave propagation*, Acta Numer. **12** (2003) 181–266.

[29] P. Bechouche, N. Mauser, and F. Poupaud, *Semiclassical limit for the Schrödinger-Poisson equation in a crystal*, Comm. Pure Appl. Math. **54** (2001) 851–890.

[30] E. Faou, V. Gradinaru, and C. Lubich, *Computing semiclassical quantum dynamics with Hagedorn wavepackets*, Commun. Math. Phys. **31** (2009) 3027–3041.

[31] G. A. Hagedorn, *Semiclassical quantum mechanics I: $\hbar \to 0$ limit for coherent states*, Commun. Math. Phys. **71** (1980) 77–93.

[32] E. Heller, *Frozen Gaussians: A very simple semiclassical approximation*, J. Chem. Phys. **75** (1981) 2923–2931.

[33] E. Heller, *Guided gaussian wave packets*, Acc. Chem. Res. **39** (2006) 127–134.

[34] M. Herman and E. Kluk, *A semiclassical justification for the use of non-spreading wavepackets in dynamics calculations*, Chem. Phys. **91** (1984) 27–34.

[35] S. Jin, H. Wu, and X. Yang, *A numerical study of the Gaussian beam methods for one-dimensional Schrödinger-Poisson equations*, J. Comput. Math. **28** (2010) 261–272.

[36] S. Jin, H. Wu, and X. Yang, *Semi-Eulerian and high order Gaussian beam methods for the Schrödinger equation in the semiclassical regime*, Commun. Comput. Phys. **9** (2011) 668–687.

[37] M. Dimassi, J. Guillot, and J. Ralston, *Gaussian beam construction for adiabatic pertubations*, Math. Phys. Anal. Geom. **9** (2006) 187–201.

[38] K. Kay, *Integral expressions for the semi-classical time-dependent propagator*, J. Chem. Phys. **100** (1994) 4377–4392.

[39] K. Kay, *The Herman-Kluk approximation: Derivation and semiclassical corrections*, Chem. Phys. **322** (2006) 3–12.

[40] S. Leung and J. Qian, *Eulerian Gaussian beams for Schrödinger equations in the semi-classical regime*, J. Comput. Phys. **228** (2009) 2951–2977.

[41] S. Leung, J. Qian, and R. Burridge, *Eulerian Gaussian beams for high-frequency wave propagation*, Geophysics **72** (2007) 61–76.

[42] H. Liu and J. Ralston, *Recovery of high frequency wave fields for the acoustic wave equation, Multiscale Model. Simul.* **8** (2009) 428–444.

[43] H. Liu and J. Ralston, *Recovery of high frequency wave fields from phase space based measurements, Multiscale Model. Simul.* **8** (2010) 622–644.

[44] M. Motamed and O. Runborg, *Taylor expansion and discretization errors in Gaussian beam superposition, Wave Motion* **47** (2010) 421–439.

[45] J. Qian and L. Ying, *Fast Gaussian wavepacket transforms and Gaussian beams for the Schrödinger equation, J. Comput. Phys.* **229** (2010) 7848–7873.

[46] J. Qian and L. Ying, *Fast multiscale Gaussian wavepacket transforms and multiscale Gaussian beams for the wave equation, Multiscale Model. Simul.* **8** (2010) 1803–1837.

[47] J. Ralston, *Gaussian beams and the propagation of singularities, Studies in PDEs, MAA Stud. Math.* **23** (1982) 206–248.

[48] O. Runborg, *Mathematical models and numerical methods for high frequency waves, Commun. Comput. Phys.* **2** (2007) 827–880.

[49] S. Jin, H. Liu, S. Osher, and R. Tsai, *Computing multi-valued physical observables for high frequency lmit of symmetric hyperbolic systems, J. Comput. Phys.* **210** (2005) 497–518.

[50] S. Jin and S. Osher, *A level set method for the computation of multivalued solutions to quasi-linear hyperbolic Pdes and Hamilton-Jacobi equations, Commun. Math. Sci.* **1** (2003) 575–591.

[51] D. Hawken, J. Gottlieb, and J. Hansen, *Review of some adaptive node-movement techniques in finite-element and finite-difference solutions of partial differential equations, J. Comput. Phys.* **95** (1991) 254–302.

[52] D. Robert, *On the Herman-Kluk semiclassical approximation, Rev. Math. Phys.* **22** (2010) 1123–1145.

[53] S. Bougacha, J. Akian, and R. Alexandre, *Gaussian beams summation for the wave equation in a convex domain, Commun. Math. Sci.* **7** (2009) 973–1008.

[54] M. Combescure and D. Robert, *Semiclassical spreading of quantum wave packets and applications near unstable fixed points of the classical flow, Asympt. Anal.* **14** (1997) 377–404.

[55] V. Cerveny, M. Popov, and I. Psencik, *Computation of wave fields in inhomogeneous media – Gaussian beam approach, Geophys. J. Roy. Astr. Soc.* **70** (1982) 109–128.

[56] S. Gray, *Efficient traveltime calculations for Kirchhoff migration, Geophysics* **51** (1986) 1685–1688.

[57] G. McMechan and G. Fuis, *Ray equation migration of wide-angle reflections from Southern Alaska, J. Geophys. Res.* **92** (1987) 407–420.

[58] T. Keho and W. Beydoun, *Paraxial ray Kirchhoff migration, Geophysics* **53** (1988) 1540–1546.

[59] N. Hill, *Gaussian beam migration, Geophysics* **55** (1990) 1416–1428.

[60] N. Hill, *Prestack Gaussian-beam depth migration, Geophysics* **66** (2001) 1240–1250.

[61] T. Alkhalifah, *Gaussian beam depth migration for anisotropic media, Geophysics* **60** (1995) 1474–1484.

[62] S. Gray, *Gaussian beam migration of common-shot records, Geophysics* **70** (2005) S71–S77.

[63] M. Popov, N. Semtchenok, P. Popov, and A. Verdel, *Depth migration by the gaussian beam summation method, Geophysics* **75** (2010) S81–S93.

[64] S. Jin and X. Liao, *A Hamiltonian-preserving scheme for high frequency elastic waves in heterogeneous media, J. Hyperbolic Differ. Equ.* **3** (2006) 741–777.

[65] S. Jin, X. Liao, and X. Yang, *Computation of interface reflection and regular or diffuse transmission of the planar symmetric radiative transfer equation with isotropic scattering and its diffusion limit, SIAM J. Sci. Comput.* **30** (2008) 1992–2017.

[66] S. Jin, P. Markowich, and C. Sparber, *Mathematical and computational methods for semiclassical Schrödinger equations, Acta Numer.* **20** (2011) 211–289.

[67] S. Jin and X. Wen, *Hamiltonian-preserving schemes for the Liouville equation with discontinuous potentials, Commun. Math. Sci.* **3** (2005) 285–315.

[68] S. Jin and X. Wen, *Hamiltonian-preserving schemes for the Liouville equation of geometrical optics with discontinuous local wave speeds, J. Comput. Phys.* **214** (2006) 672–697.

[69] S. Jin and X. Wen, *Hamiltonian-preserving schemes for the Liouville equation of geometrical optics with partial transmissions and reflections, SIAM J. Numer. Anal.* **44** (2006) 1801–1828.

[70] S. Jin and X. Wen, *Computation of transmissions and reflections in geometrical optics the reduced Liouville equation, Wave Motion* **43** (2006) 667–688.

[71] D. Wei, S. Jin, R. Tsai, and X. Yang, *A level set method for the semiclassical limit of the Schrödinger equation with discontinuous potentials*, J. Comput. Phys **229** (2010) 7440–7455.

[72] W. Weiss and G. Hagedorn, *Reflection and transmission of high freuency pulses at an interface*, Transport Theory Statist. Phys. **14** (1985) 539–565.

[73] D. Yin and C. Zheng, *Gaussian beam formulations and interface conditions for the one-dimensional linear Schrödinger equation*, Wave Motion **48** (2011) 310–324.

[74] D. Peng, B. Merriman, S. Osher, H. Zhao, and M. Kang, *A PDE based fast local level set method*, J. Comput. Phys. **155** (1999) 410–438.

[75] X. Wen, *High order numerical quadratures to one dimensional delta function integrals*, SIAM J. Sci. Comput. **30** (2008) 1825–1846.

[76] W. E, J. Lu, and X. Yang, *Asymptotic analysis of the quantum dynamics in crystals: The Bloch-Wigner transform, Bloch dynamics and Berry phase*, Acta Math. Appl. Sin. Engl. Ser. **29** (2013) 465–476.

[77] H. Liu, O. Runborg, and N. Tanushev, *Error estimates for Gaussian beam superpositions*, Math. Comp. **82** (2013) 919–952.

[78] V. Rousse and T. Swart, *Global L^2-boundedness theorems for semiclassical Fourier integral operators with complex phase*, 2007. arXiv:0710.4200.

[79] N. Tanushev, R. Tsai, S. Fomel, and B. Engquist, *Gaussian beam decomposition for seismic migration*, 2011. ICES Report: 11-08.

[80] S. Jin, D. Wei, and D. Yin, *Gaussian beam methods for the Schrödinger equation with discontinuous potentials*, 2012. preprint.

[81] L. Jefferis and S. Jin, *A Gaussian beam method for high frequency solution of symmetric hyperbolic systems with polarized waves*, 2014. preprint.

[82] R. Delgadillo, J. Lu, and X. Yang, "Gauge-invariant frozen Gaussian approximation method for the Schrödinger equation with periodic potentials." in preparation.

[83] H. Wu, Z. Huang, S. Jin, and D. Yin, *Gaussian beam methods for the Dirac equation in the semi-classical regime*, 2012. preprint.

[84] M. Motamed and O. Runborg, "A wavefront Gaussian beam method for high-frequency wave propagation." WAVES 2007, University of Reading, UK, July 2007.

[85] Z. Huang, S. Jin, P. Markowich, and C. Sparber, *Numerical simulation of the nonlinear Schrödinger equation with multi-dimensional periodic potentials*, *Multiscale Model. Simul.* **7** (2008) 539–564.

[86] Z. Huang, S. Jin, P. Markowich, and C. Sparber, *On the Bloch decomposition based spectral method for wave propagation in periodic media*, *Wave Motion* **46** (2009) 15–28.

[87] R. Carles, *Wkb analysis for the nonlinear schrodinger equation and instability results*, . arXiv:math/0702318v1.

[88] R. LeVeque, *Numerical methods for conservation laws*. Birkhäuser Verlag, Basel, 1992.

[89] A. Martinez, *An introduction to semiclassical and microlocal analysis*. Springer-Verlag, New York, 2002.

[90] M. Taylor, *Pseudodifferential operators*. Princeton University Press, Princeton, NJ, 1981.

[91] L. Hörmander, *The Analysis of Linear Partial Differential Operators I, Distribution Theory and Fourier Analysis*. Springer Verlag, New York, 1983.

[92] G. Folland, *Harmonic analysis in phase space*. Annals of Mathematics Studies, no. 122. Princeton University Press, Princeton, 1989.

[93] V. Cerveny, *Seismic ray theory*. Cambridge University Press, Cambridge, 2001.

[94] E. J. Heller, *Cellular dynamics: a new semiclassical approach to timedependent quantum mechanics*, *J. Chem. Phys.* **94** (1991) 2723–2729.

[95] S. Jin, H. Wu, and Z. Huang, *A hybrid phase-flow method for hamiltonian systems with discontinuous hamiltonians*, *SIAM J. Sci. Comput.* **31** (2008) 1303–1321.

[96] J. Ralston, *Gaussian beams and the propagation of singularities, Studies in PDEs, MAA Stud. Math.* **23** (1982) 206–248.

[97] X. Yang and J. Zhang, *Computation of the schrödinger equation in the semiclassical regime on unbounded domain*, *SIAM J. Numer. Anal.* **52** (2014) 808–831.

[98] J. Zhang, Z. Sun, X. Wu, and D. Wang, *Analysis of high-order absorbing boundary conditions for the schrödinger equation*, *Commun. Comput. Phys.* **10** (2011) 742–766.

[99] B. Engquist and A. Majda, *Radiation boundary conditions for acoustic and elastic wave calculations*, *Comm. Pure Appl. Math.* **32** (1979) 314–358.

[100] G. Strang, *On the construction and comparison of difference schemes, SIAM J. Numer. Anal.* **5** (1968) 506–517.